



**MONTCLAIR STATE**  
UNIVERSITY

Montclair State University  
**Montclair State University Digital  
Commons**

---

Theses, Dissertations and Culminating Projects

---

8-2016

## **An Assessment of Antarctic Ice Sheet Dynamics from a Pliocene Polar Paleoclimate Archive**

Melissa A. Hansen  
*Montclair State University*

Follow this and additional works at: <https://digitalcommons.montclair.edu/etd>



Part of the [Environmental Sciences Commons](#)

---

### **Recommended Citation**

Hansen, Melissa A., "An Assessment of Antarctic Ice Sheet Dynamics from a Pliocene Polar Paleoclimate Archive" (2016). *Theses, Dissertations and Culminating Projects*. 32.  
<https://digitalcommons.montclair.edu/etd/32>

This Dissertation is brought to you for free and open access by Montclair State University Digital Commons. It has been accepted for inclusion in Theses, Dissertations and Culminating Projects by an authorized administrator of Montclair State University Digital Commons. For more information, please contact [digitalcommons@montclair.edu](mailto:digitalcommons@montclair.edu).

AN ASSESSMENT OF ANTARCTIC ICE SHEET DYNAMICS FROM A PLIOCENE  
POLAR PALEOCLIMATE ARCHIVE

A DISSERTATION

Submitted to the Faculty of  
Montclair State University in partial fulfillment  
of the requirements  
for the degree of Doctor of Philosophy

by

MELISSA A. HANSEN

Montclair State University

Upper Montclair, NJ

2016

Dissertation Chair: Dr. Sandra Passchier

Copyright © 2016 by *Melissa A. Hansen*. All rights reserved.

MONTCLAIR STATE UNIVERSITY  
THE GRADUATE SCHOOL  
DISSERTATION APPROVAL

We hereby approve the Dissertation  
AN ASSESSMENT OF ANTARCTIC ICE SHEET DYNAMICS FROM A PLIOCENE  
POLAR PALEOCLIMATE ARCHIVE

of

Melissa A. Hansen


Candidate for the Degree:

Doctor of Philosophy

Dissertation Committee:

Department of Earth &  
Environmental Studies



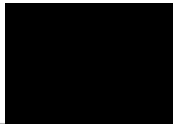
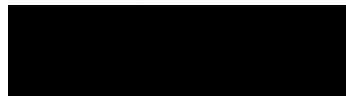
Certified by:



Dr. Joan C. Ficke  
Dean of The Graduate School

Date

7/19/16

  
Dr. Sandra Passchier  
Dissertation Chair  
Dr. Stefanie Brachfeld  
Dr. Clement Alo  
Dr. Trevor Williams

## ABSTRACT

### AN ASSESSMENT OF ANTARCTIC ICE SHEET DYNAMICS FROM A PLIOCENE POLAR PALEOCLIMATE ARCHIVE

by Melissa A. Hansen

The potential impact of East Antarctic Ice Sheet (EAIS) response to warming over the next century is of major concern, particularly due to its influence on sea level rise. Efforts to understand its impact are limited due to the restrictions of short-term modeling, as well as the assumption that all ice behaves similarly across the EAIS, meriting the need for further study over longer time periods. The early Pliocene (5.33-2.58 Ma) is the most suitable period of time in which to assess EAIS dynamics because of its similarity to modern tectonic configuration and similar CO<sub>2</sub> estimates (~400 ppm). Due to a paucity of records, the present study expands on the existing knowledge of ice sheet dynamics by providing a reconstruction of ice-rafting history in a previously unstudied sector of the EAIS. The aim of this study is to evaluate the behavior of the Wilkes Land ice sheet and whether its response is part of a continental response or on a smaller, local scale. A high-resolution record of ice-rafting history in the Wilkes Land region from IODP Site U1359 was used to (1) identify periods of advance and retreat during the early Pliocene, (2) determine the orbital variations within the ice-rafting record, (3) assess the effects of warming on the interaction between the ice sheet and Southern Ocean during the Pliocene Climatic Optimum and (4) evaluate the behavior of the EAIS during early Pliocene warmth through regional correlation. A time series analysis to assess the orbital variations of the ice sheet determined a transition from obliquity forced to precession

forced variability of ice-rafting ~4.6 Ma. Concurrently, geochemical analysis revealed enhanced downwelling may have lead to greater venting of CO<sub>2</sub> during deglaciation, accompanied by higher productivity in response to increased iron-bearing dust fertilization. A regional correlation shows that the ice sheet was susceptible to warming during the Pliocene Climatic Optimum, as opposed to the later mid-Pliocene Warm Period, where the ice sheet remained in a retreated position.

## ACKNOWLEDGEMENTS

I would like to thank my advisor and mentor Dr. Sandra Passchier for her support and guidance. I would also like to thank my committee members for their valuable input and interesting questions (Drs. Brachfeld, Alo, and Williams).

The first three years of this research was supported financially by an NSF grant awarded to Dr. Passchier. I am also thankful to Montclair State University for the continued financial support through graduate assistantships, analytical facilities, and the help of Christie from the Center for Writing Excellence for proofreading dissertation chapters. Thank you to Stacy Pinto for her help in formatting this dissertation. A special thanks to Daniel Ciarletta and Jessica Rosenberg for their company and assistance in the laboratory.

To the colleagues who became friends—Jason Darley, Dan Hauptvogel, Dan Ciarletta, Jessica Rosenberg, Vicky Sekkas, Jennifer Light, April Kelly, and many others. To those students I helped mentor in the laboratory, I thank you for seeking my advice and helping me to discover how much I enjoy mentoring. To Dean Robert Prezant, Associate Dean Jinan Jaber, and the College of Science and Mathematics (CSAM) Ambassadors for allowing me to not only represent the college during special events, but to share my experiences and research with the next generation of scientists.

To my fitness coach Kendall Green and ‘FitFam’ for their encouragement and support. Always ‘Be Strong’ and ‘Stay with the Fight!’. To the Earth and Environmental Studies (EAES) graduate office gym crew, aka Swoll Squad, and ‘coach’ Taylor Wiczerak.

Thank you to my family for their patience, support, and love. To my best friend and ‘big brother’ Nick Figler. Lastly but not least, to my boyfriend Andrew Temples, who has offered encouragement and praise, kept me grounded, and reminded me to laugh and enjoy the good times.



DEDICATION

*To my loving and ever supportive parents, Chris and Donna, and my siblings, Stephanie  
and Daniel*

*Gone but never forgotten*

*Destiny Marie Jazikoff*

*September 22, 1987 – May 24, 2016*

## TABLE OF CONTENTS

ABSTRACT.....	IV
CHAPTER 1 .....	1
INTRODUCTION .....	1
1.1 Introduction.....	1
1.2 Site Location .....	6
1.2.1 Wilkes Land.....	6
1.3 Thesis Aims & Objectives .....	8
1.4 Organization of Thesis.....	9
1.5 References.....	12
THRESHOLD BEHAVIOR OF A MARINE-BASED SECTOR OF THE EAST ANTARCTIC ICE SHEET IN RESPONSE TO EARLY PLIOCENE OCEAN WARMING.....	17
Abstract.....	17
2.1 Introduction.....	19
2.2 Materials and Methods.....	22
2.2.1 Study Site .....	22
2.2.2 Age Model .....	23
2.2.3 Biogenic Opal .....	24
2.2.4 Ice-Rafted Debris .....	25
2.2.5 Microtextural Analysis.....	26
2.2.6 Time Series Analysis .....	27
2.3 Results.....	30
2.3.1 Biogenic Opal .....	30
2.3.2 Particle Size Distributions and IRD MAR.....	30
2.3.3 Quartz Grain Surface Textures .....	31
2.3.4 Time Series Analysis .....	34
2.4 Discussion.....	37
2.4.1 Sedimentation at Site U1359 .....	37
2.4.2 Iceberg Calving Mechanisms and Climate Forcings .....	40
2.5 Conclusions.....	45
2.6 References.....	47
VENTILATION OF THE SOUTHERN OCEAN DURING THE PLIOCENE CLIMATIC OPTIMUM .....	57
Abstract.....	57
5.1 Introduction.....	58
5.2 Geochemical Variations in U1359B .....	60
3.2.1 Paleoredox Conditions .....	61
3.2.1 Paleoproductivity Bloom .....	64

5.3	Nutrient Pathways and Utilization in the Southern Ocean .....	66
5.4	Conclusion .....	70
5.5	References Cited .....	72
THE BEHAVIOR OF THE EAST ANTARCTIC ICE SHEET DURING PERIODS OF EARLY PLIOCENE WARMTH: EVIDENCE FROM POLAR PALEOCLIMATE ARCHIVES.....		81
	Abstract.....	81
4.1	Introduction.....	83
4.2	Ice sheet behavior during the early Pliocene .....	88
4.2.1	Pliocene Climatic Optimum (~4.5 – 4.0 Ma) .....	91
4.2.2	Mid-Pliocene Warm Period (~3.3 – 3.0 Ma) .....	97
4.3	Retreat of Wilkes Land ice sheet .....	98
4.4	Discussion and Implications .....	100
4.5	Conclusions.....	103
4.6	References.....	105
SUMMARY AND FUTURE OUTLOOK .....		114
5.1	Summary.....	114
5.2	Environmental Implications.....	117
5.3	Concluding Remarks.....	118
LIST OF APPENDICES.....		119
APPENDIX A.....		120
APPENDIX B .....		126
APPENDIX C .....		191

## LIST OF TABLES

Table 2-1. Age tie points in Ma for Site U1359 .....	24
Table 2-2. Early Pliocene sea surface temperatures .....	40
Table 4-1. Location of sites used for this study, age model used, and the references to the original works. ....	90

## LIST OF FIGURES

Figure 1-1. Map of Antarctica showing the location of IODP Site U1359 (star) on the Wilkes Land continental rise in relation to shelf site U1358 and adjacent rise site U1361 (dots). Antarctica land cover shown in white and ice shelves shown in blue was acquired from the Antarctica Digital Database (ADD Consortium, 2000). The graticule was acquired from Natural Earth Data.....	2
Figure 2-1. Location of Antarctic Wilkes Land continental rise Sites U1359 and U1361, continental shelf Site U1358 near Mertz Glacier and Prydz Bay continental rise Site 1165.....	21
Figure 2-2. Distribution of opal, ice-rafted debris (IRD) mass accumulation rates (MAR), sand percentage, gravel (clast abundance), terrigenous silt and clay percentage and sorting of fine fraction at Site U1359 (Encompasses both Hole A and B). Data for Site U1359 are shown on the depth scale for Hole U1359A (mbsf-A) to allow correlation to the lithological log of Hole U1359A. The lithology log for Hole U1359A is based on the data recorded on the shipboard Visual Core Description sheets and smear-slide observations [Expedition 318 Scientists, 2011] augmented with postcruise observations of high-resolution line-scan images. Magnetostratigraphy log after Tauxe et al. [2012]. .....	30
Figure 2-3. (A) IRD MAR distribution highlighting three main intervals of variability and sample selection (B) Abundances of each grain type for each sample identified on mbsf-A depth scale (C) Selected micrographs from the SEM Secondary Electron detector showing glacial texture types 1-3 [per <i>Damiani et al.</i> , 2006] found on sample grains. Fresh mechanical textures indicating glacial type 1 present on micrograph (top) and varying degrees of silica precipitation indicative of glacial type 2 (middle) and type 3 (bottom). .....	34
Figure 2-4. Morlet powered wavelet spectrum of Site U1359 (A) evenly spaced IRD MAR (B) Detrended (Log10) IRD MAR and (C) Mean monthly summer insolation at 65°S [ <i>Laskar et al.</i> , 2004], highlighting orbital signal intensities over time. The 95% confidence contour was derived using chi-square distribution [ <i>Torrence and Compo</i> , 1998].....	35
Figure 2-5. (A) Early Pliocene sea surface temperatures based on values compiled in Table 2 [ <i>McKay et al.</i> 2012; <i>Whitehead and Bohaty</i> , 2003; and <i>Escutia et al.</i> 2009]. Site U1359 IRD MAR band-pass filtered periodicities of (B) precession, (C) obliquity and (D) eccentricity with (E) <i>Laskar et al.</i> [2004] eccentricity cycle (400-kyr and 100-kyr) and (F) IRD MAR.....	36
Figure 3-1. The location of Mertz Glacier (MG) in Wilkes Land, Antarctica with continental rise Sites U1359 and U1361, shelf Site U1358, and Prydz Bay continental rise site 1165. The position of the Antarctic Polar Front (PF), southern boundary for the Antarctic Circumpolar Current (ACC) and southern limit of upwelling circumpolar deep water (UCDW) based on Orsi et al. (1995). .....	61
Figure 3-2. Data for Hole U1359B are shown on mbsf-A scale to allow correlation to lithological log for Hole U1359A. Distribution of (A) Opal (B) ice-rafted debris (IRD) mass accumulation rates (MAR), and (C) Gravel (Clast Abundance) after	

Hansen et al. (2015). (D) Magnetostratigraphy log after Tauxe et al. (2012). (E – I) Detailed summary of IRD MAR and chemical ratios during the early Pliocene for section dated between ~4.7-4.3 Ma. ....	64
Figure 3-3. Barite particles identified using EDS mapping tool highlighting elements Barium (red) and Sulfur (green) (A). Enlarged image of barite grain (highlighted in red box) (B). SEM micrograph of sedimentary barite (C) and EDS spectra (D).....	65
Figure 4-1. Location of Antarctic drill core sites discussed within text. DVDP (tan) = Dry Valley Drilling Project, DSDP (brown) = Deep Sea Drilling Project, ODP (gold) = Ocean Drilling Program, and IODP (yellow) = Integrated Ocean Drilling Program. BEDMAP V2 showing bed topography from Fretwell et al. (2013). ....	88
Figure 4-2. Regional comparison of Pliocene polar paleoclimate archives. Age boundaries are based on the Gradstein et al. (2012) time scale. Sea surface temperatures are compiled from (1) McKay et al. (2012); Whitehead and Bohaty (2003); and Escutia et al. (2009). References: (2) Passchier, (2011); (3) Grützner et al. (2005), Passchier. (2011); (4) Whitehead et al. (2001); (5) Naish et al. (2009), McKay et al. (2012); (6) Ishman and Rieck (1992), McKelvey (1981); (7) Pyne et al. (1985), Barrett and Hambrey (1992); (8) Hansen et al. (2015), Rosenberg, (2014); (9) Expedition 318 Scientists (2011) .....	94

## LIST OF ABBREVIATIONS

AIS	Antarctic Ice Sheet
ANDRILL	Antarctic Geologic Drilling
CIROS	Cenozoic Investigation of the Western Ross Sea
DSDP	Deep Sea Drilling Program
DVDP	Dry Valleys Drilling Project
EAIS	East Antarctic Ice Sheet
IODP	Integrated Oceanic Drilling Program
IPCC	Intergovernmental Panel on Climate Change
IRD MAR	Ice-Rafted Debris Mass Accumulation Rates
MIS	Marine Isotopic Stage
MPWP	mid-Pliocene Warm Period (3.3 – 3.0 Ma)
ODP	Ocean Drilling Program
PCO	Pliocene climatic optimum (~4.5 – 4.0 Ma)
WAIS	West Antarctic Ice Sheet

## CHAPTER 1

### Introduction

#### 1.1 Introduction

Since its inception, the Antarctic cryosphere has played a vital role in the Earth's climate system due to its effects on global sea level, ocean circulation and heat transport, marine productivity, and planetary albedo. With the current rise of greenhouse gases and resulting increase in global temperatures, studies of ice sheets and their potential impacts in a warming world are essential. More importantly, the Intergovernmental Panel on Climate Change (IPCC) projects further greenhouse gas increases and  $\sim 1.5$  to  $>2^{\circ}\text{C}$  of additional temperature rise by the end of this century (IPCC, 2013; See Appendix A). Estimating the ice sheet's contribution to sea level as climate warms is made difficult due to a longer equilibrium-response timescale as compared to the atmosphere and ocean (Golledge et al., 2015). The uncertainty in future sea level contribution raises an important question for its potential impact on low lying coastal regions. Our current understanding of the cryosphere's response to future warming is limited due to the restrictive nature of decadal scale modeling making it difficult to establish whether the ice sheets are currently responding to warming or if a delay in response exists. Climate models need validation through sediment records that reflect climate fluctuations over long timescales and may provide constraints for future predictions about East Antarctic Ice Sheet (EAIS) stability in a warming world.

The purpose of this research is to generate a high-resolution record of ice sheet behavior in the Wilkes Land region (Figure 1-1) during the warm early Pliocene. The



geologic records in combination with climate modeling may provide a more in depth look of how the ice sheets behave under warmer conditions. Current CO<sub>2</sub> levels are ~400 ppm and have not been experienced since the early Pliocene (5.33-2.58 Ma) when the EAIS may have been subject to major fluctuations, and raises the concern for the possibility of it becoming unstable within the next century (Escutia et al., 2005).

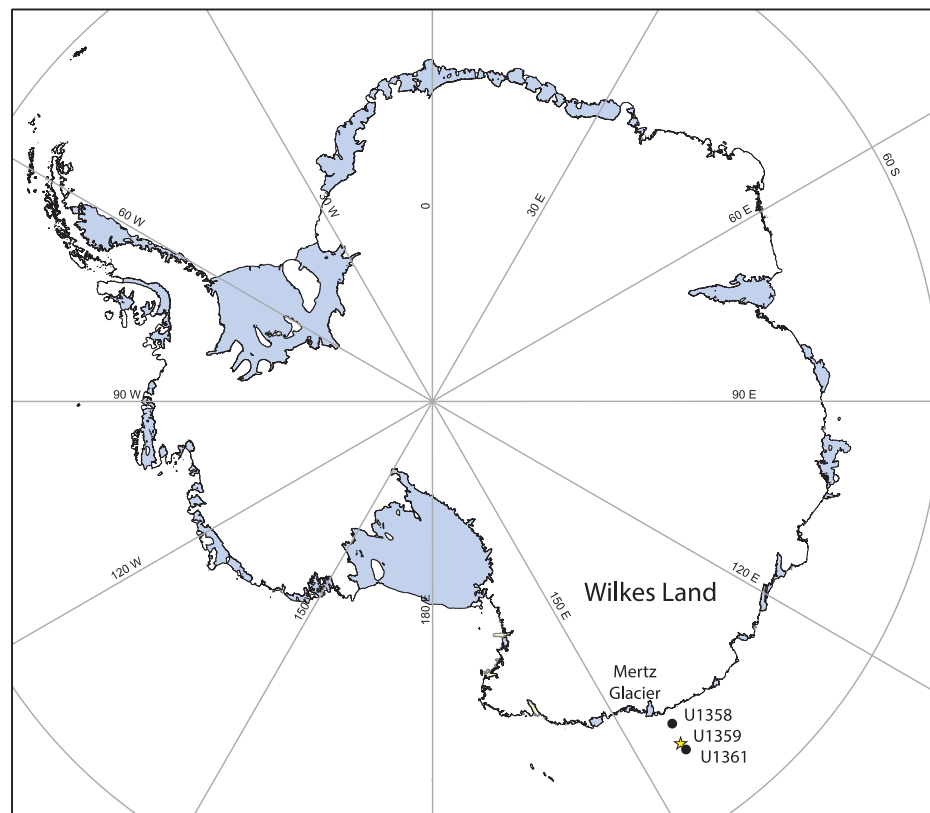


**Figure 1-1. Map of Antarctica showing the location of IODP Site U1359 (star) on the Wilkes Land continental rise in relation to shelf site U1358 and adjacent rise site U1361 (dots). Antarctica land cover shown in white and ice shelves shown in blue was acquired from the Antarctica Digital Database (ADD Consortium, 2000). The graticule was acquired from Natural Earth Data.**

The early Pliocene is a particularly interesting time period to understand the effects of climate in the polar regions because, in addition to being both tectonically and oceanographically comparable to today, CO<sub>2</sub> concentrations (~365 – 415 ppm) were similar to today's values and the lower limits projected by the IPCC for the end of the century (See Appendix A). For comparison, the modern world CO<sub>2</sub> concentrations are nearing 400 ppm—the highest observed value since 1958 when measurements began (NOAA/ESRL, 2013). Global temperatures in the early Pliocene were 3-3.5°C above preindustrial values (Raymo et al., 1996; Andersson et al., 2002; Fedorov et al., 2013) and sea surface temperatures (SSTs) in the Southern Ocean varied between 2° and 5.7°C (Fedorov et al., 2013; Whitehead & Bohaty, 2003; Escutia et al., 2009; McKay et al., 2012) making it a good analog in which to assess the response of the ice sheets in a warmer world.

The increase of atmospheric CO<sub>2</sub> is thought to be a driver for current and future anthropogenic climate change, however climate models for the early Pliocene suggest that CO<sub>2</sub> alone cannot explain the increased warming (Fedorov et al., 2013). In addition to CO<sub>2</sub>, dynamic mechanisms to explain early Pliocene warming include lower extratropical cloud albedo and ocean mixing. Not any of these mechanisms is solely responsible for Pliocene climate, but several may work in tandem.

The IPCC projects an average of 0.44 m of sea level rise by the end of the century (See Appendix A), which differs greatly from the estimates seen for the early Pliocene. Paleoclimate archives and climate models suggest no more than 20 m of global sea level rise above modern for the early Pliocene (Masson-Delmotte et al., 2013; Pollard &

DeConto, 2009; Winnick & Cave, 2015; Miller et al., 2012). During the early Pliocene, it is believed that Northern Hemisphere ice sheets were not yet fully developed and sea level changes must have been driven by fluctuations of the Antarctic ice sheet (Escutia et al., 2005). The WAIS was reduced (Pollard & DeConto, 2009) and is thought to have contributed to these changes in sea level, but there may have been a substantial contribution coming from the EAIS as well (Escutia et al., 2005). Much of East Antarctica is covered with ice above sea level and is considered stable with a slow response to climate changes. However, portions of the EAIS grounded below sea level, similar to the marine-based WAIS, are considered potentially unstable and more susceptible to changes in climate and may contribute to sea level rise during episodes of global warmth.

The behavior of the EAIS during the early Pliocene has led to a debate over the timing and establishment of a polar, stable ice sheet. The development for a ‘dynamic’ viewpoint stems from the Sirius Group within the Transantarctic Mountains, Dry Valleys, and Prince Charles Mountains in the Pliocene (Miller & Mabin, 1998). The Sirius Group is composed of thick layers of diamicts and glacially reworked diatom deposits that may have originated in marine seaways of the interior East Antarctica. Fielding et al. (2010) suggest that during the early Pliocene, the coastal realm of the East Antarctic was subjected to multiple glacial-interglacial cycles and coastal plains may have been vegetated at times. The dynamic scenario has been challenged by the ‘stabilists’ perspective which is based on 4 – 15 Ma unconsolidated and unweathered ash bed deposits at higher elevations within the Dry Valleys. Their deposition would preclude the

warmer climate assumed by a dynamic ice sheet and therefore cold, polar, desert conditions prevailed since the middle Miocene (Miller & Mabin, 1998) ruling out the possibility of a Pliocene dynamic ice sheet. The difference in behavior over such time scales may have something to do with how the EAIS responds to a climate forcing. Individual regions of the EAIS may display an independent dynamic to one another due to the different types of environments (terrestrial, coastal, marine, etc.) and their sensitivities to climate. To address this issue, polar paleoclimate archives or marine strata can be used to better understand the behavior of the EAIS in both a continental and regional context.

Within Antarctic marine strata are archives of past environmental changes. The process by which the sediments are deposited are controlled by climate and can be preserved for millions of years, allowing for climate reconstructions for key periods of time such as the early Pliocene. The use of paleoclimate data such as polar paleoclimate archives provides a means of developing a longer time series in which to understand the relationship between climate and ice dynamics and make up for the limitations of decadal-scale measurements. Polar paleoclimate archives, therefore, are key to evaluating whether climate models have the ability to simulate realistic climate change. While reconstructions have been assessed in several regions of the EAIS, these records are often of low-resolution or incomplete. Integrated Ocean Drilling Program (IODP) Expedition 318 Site U1359 is one of the most recently drilled archives targeting the early Pliocene and provides a complete, high-resolution record of ice sheet behavior in the Wilkes Land region. This Site provides a record of ice sheet behavior for a previously obscure area of

the EAIS and will contribute to the understanding of the overall behavior of the EAIS in response to warming.

The overarching goal for this study is to evaluate the sedimentological characteristics of IODP Site U1359 (Figure 1-1) in order to understand the behavior and response of a marine-based ice sheet in the Wilkes Land region during the early Pliocene and whether that response occurs on a continental or smaller, more local scale. For my dissertation, I illustrate the glacial history of the Wilkes Land continental margin by reconstructing the ice-rafting history and paleoceanographic conditions using IODP Site U1359. The ice sheet history was then compared to records from adjacent regions of the EAIS in order to relate how ice sheet behavior may have differed in a regional context to early Pliocene warming. With global temperatures expected to increase over the coming century and an uncertainty for their effect on the polar region, this study will lead to a more comprehensive understanding of this relationship on longer timescales. The loss of polar ice sheets due to the resultant warming will lead to an increase of sea level and severe consequences for coastlines and low-lying areas, making it all the more vital to understand their role in the climate system.

## **1.2 Site Location**

### **1.2.1 Wilkes Land**

The Wilkes Land margin is located near the Australian sector of the Southern Ocean (See Figure 1-1). The EAIS drains through the Adélie and George V coasts in a divergent flow pattern (Expedition 318 Scientists, 2011). Several ice cliffs and two prominent outlet glaciers, the Mertz and the Ninnis, make up the present coastline. The

segment of the EAIS that drains through the Wilkes subglacial basin is grounded mainly below sea level and is therefore, most susceptible to changes in the marine environment (Cook et al., 2013; Escutia et al., 2005; Orejola et al., 2014; Rignot et al., 2013). The Wilkes subglacial basin is the largest in the East Antarctica descending below -500 m in elevation (Fretwell et al., 2013). The presence of a landward overdeepening, a common feature around Antarctica, suggests the potential for unstable conditions and a sensitivity to ocean warming, which could cause accelerated glacial retreat. The topography on the shelf is irregular, with deep basins and troughs (>1000 m) carved out by ice streams that extended across the shelf during times of glacial maxima (Escutia et al., 2005). The presence of ice streams corresponds to areas of rapid ice-flow and drainage of the ice sheet. The ice sheet may have undergone deglaciation during the Neogene, making it a prime location in which to assess the ice sheets vulnerability to warming (Escutia et al., 2005).

Previous drilling on the Wilkes Land continental margin was completed by Deep Sea Drilling Program (DSDP) Leg 28 at Site 269 on the abyssal plain, just north of the Expedition 318 drill area (Expedition 318 Scientists, 2011). However, the core recovery was 42% for the Eocene-Holocene (Hayes et al., 1975; Expedition 318 Scientists, 2011) and there is little detail to describe the behavior of the Wilkes Land ice sheet during the early Pliocene. The presence of diatom oozes and diatom mud were found in the upper half of the core (Quaternary to late Miocene) and they suggest that water temperatures cooled in the Neogene coinciding with glaciation.

The Integrated Ocean Drilling Program (IODP) Expedition 318 drilled seven sites across the Wilkes Land Margin. Sites U1358, U1359, and U1361 (Figure 1-1) targeted the Neogene (23.03 to 2.58 Ma) in order to assess ice sheet variability during warm periods such as the early Pliocene (5.33 to 2.58 Ma). These sites were drilled in a shelf to rise transect and should give a complete history of the Wilkes Land margin. The Wilkes Land margin is the only known margin that can trace an unconformity from shelf to rise, which allows for sequences to be linked across the margin (Escutia et al., 2005). This thesis focuses on continental rise Site U1359 (64°S 143°E), which lies on the eastern levee of the Jussieu submarine channel within 100 km off the shelf edge (Expedition 318 Scientists, 2011).

At Site U1359, a total of four holes were drilled (U1359A-D), however the focus of this study will encompass U1359A-B. Both holes were drilled with a piston coring method and subsequent XCB for a total recovery of 80% (U1359A) and 79% (U1359B) (Expedition 318 Scientists, 2011). By combining the two cores together using a meters composite depth correlation, this core contributes a complete, high-resolution record of ice sheet behavior for the Wilkes Land region during the early Pliocene.

### **1.3 Thesis Aims & Objectives**

The first objective of this study was to evaluate sedimentation patterns in order to illustrate changes in ice sheet behavior. This objective strived to determine when within the early Pliocene were there periods of ice advance and retreat by assessing trends of ice-rafted debris mass accumulation rates (IRD MAR). Further, this objective sought to confirm the presence of glacially derived sediment and identify glacial transport

mechanisms by evaluating the degree of abrasion and crushing through microtextural analysis of sand grains extracted from intervals of high peaks of IRD MAR.

The second objective was to determine whether the driving factor behind ice sheet response was a global or local influence by evaluating the effect of ocean temperatures compiled from around east Antarctica (local forcing) and orbitally driven insolation patterns (global) as driving factors of ice sheet variability.

The third objective was to determine the effects of warming on the interaction between the ice sheet and Southern Ocean during the Pliocene climatic optimum (PCO) through geochemical assessment of sediment on the Wilkes Land continental rise.

The fourth objective was to assess variations in ice sheet extent during warm periods within the early Pliocene by compiling and correlating several stratigraphic records from various locations around Antarctica. Further, this objective sought to infer the potential impact the EAIS may have on sea level under similar climate conditions and determine whether the response is on a local/regional or continental scale.

#### **1.4 Organization of Thesis**

This thesis consists of four separate chapters that address the objectives mentioned above.

Chapter 2 entitled “Threshold behavior of a marine-based sector of the East Antarctic Ice Sheet in response to early Pliocene ocean warming,” addresses Objective 1 by identifying when there were periods of ice advance and retreat, and Objective 2 by determining how climate drivers affect the variability of ice sheet response. This work provides a high-resolution assessment of the behavior of the EAIS in the Wilkes



Subglacial Basin, during climate conditions similar to modern. The results highlighted three major ice-rafting episodes designated excursions I, II, and III from Integrated Ocean Drilling Program (IODP) Expedition 318 Site U1359, on the Wilkes Land continental rise and presents the affect of orbital variability and sea surface temperature on Early Pliocene ice-rafted debris mass accumulation rates (IRD MAR). The results suggest that the ice sheet exhibited threshold behavior as SSTs peaked above 3°C, resulting in a greater susceptibility to local insolation forcing. This work was published in the journal of *Paleoceanography* in the year of 2015 (Hansen et al., 2015).

Chapter 3 entitled “Ventilation of the Southern Ocean During the Pliocene Climatic Optimum,” addresses Objective 3 by determining the effects of warming on the interaction between the ice sheet and ocean circulation changes. The findings highlight the role of deepwater ventilation in the Southern Ocean carbon cycle during the PCO, a period of global warmth between ~4.5 and 4.0 Ma. This chapter presents a record of geochemical variations using Al/Ti (provenance), Mn/Al (paleoredox), and Ba-excess (primary productivity). While no significant provenance changes were found during this time, high peaks of Mn/Al indicate that oxic conditions may have been influenced by the enhanced production of AABW. A high primary productivity event, confirmed through a barite SEM investigation, was attributed to the increase of nutrients supplied by upwelling and terrigenous dust.

Chapter 4 entitled “The Behavior of the East Antarctic Ice Sheet During Periods of early Pliocene Warmth: Evidence from Polar Paleoclimate Archives,” addresses the fourth objective by compiling several sedimentological records to assess the behavior of

the EAIS during warm periods of the early Pliocene and whether their response was on a continental or local, smaller scale. Further, this chapter aids in identifying the warmest periods in which to understand EAIS behavior for future modeling and climate studies. Deglaciation of the EAIS began ~4.6 Ma, however, the retreat of the EAIS was not continuous in all regions as the Wilkes Land ice sheet displayed variable IRD MAR indicating episodes of advance and retreat despite warming during the PCO. Reduced ice conditions continued until the mid-Pliocene (~3.3 Ma) with the exception of the Wilkes Land ice sheet which remained in a more retreated position. Such implications highlight the need for greater focus on the behavior of the EAIS during the PCO.

Appendix A contains supplementary text containing background information concerning current climate and sea level projections. Appendix B contains the supplementary text and figures that were published with Chapter 2 in *Paleoceanography* (2015). Appendix C contains a more detailed method for the collection of SEM microtextural data, selected micrographs, and raw data referenced in Chapter 2. Additionally, Appendix C contains additional barite SEM micrographs and EDX spectra referenced in Chapter 3.

## 1.5 References

- ADD Consortium. (2000). Antarctic Digital Database, Version 3.0, database, manual and bibliography. *Scientific Committee on Antarctic Research, Cambridge, 93p.*
- Andersson, C., Warnke, D. A., Channell, J. E. T., Stoner, J., & Jansen, E. (2002). The mid-Pliocene (4.3–2.6 Ma) benthic stable isotope record of the Southern Ocean: ODP Sites 1092 and 704, Meteor Rise. *Palaeogeography, Palaeoclimatology, Palaeoecology, 182*(3), 165-181.
- Cook, C. P., van de Flierdt, T., Williams, T., Hemming, S. R., Iwai, M., Kobayashi, M., Jimenez-Espejo, F.J., Escutia, C., Gonzalez, J.J., Khim, B.K., McKay, R., Passchier, S., Bohaty, S.M., Riesselman, C.R., Tauxe, L., Sugisaki, S., Galindo, A.L., Patterson, M.O., Sangiorgi, F., Pierce, E.L., Brinkhuis, H., & Expedition 318 Scientists. (2013). Dynamic behaviour of the East Antarctic ice sheet during Pliocene warmth. *Nature Geoscience, 6*(9), 765-769.
- Escutia, C., De Santis, L., Donda, F., Dunbar, R. B., Cooper, A. K., Brancolini, G., & Eitrem, S. L. (2005). Cenozoic ice sheet history from East Antarctic Wilkes Land continental margin sediments. *Global and Planetary Change, 45*(1), 51-81.
- Escutia, C., Bárcena, M. A., Lucchi, R. G., Romero, O., Ballegeer, A. M., Gonzalez, J. J., & Harwood, D. M. (2009). Circum-Antarctic warming events between 4 and 3.5 Ma recorded in marine sediments from the Prydz Bay (ODP Leg 188) and the Antarctic Peninsula (ODP Leg 178) margins. *Global and Planetary Change, 69*(3), 170-184.

- Expedition 318 Scientists (2011). Wilkes land glacial history: Cenozoic East Antarctic Ice Sheet evolution from Wilkes Land margin sediments. *IODP Prel. Rept.*, 318.
- Fedorov, A. V., Brierley, C. M., Lawrence, K. T., Liu, Z., Dekens, P. S., & Ravelo, A. C. (2013). Patterns and mechanisms of early Pliocene warmth. *Nature*, 496(7443), 43-49.
- Fielding, C. R., Harwood, D. M., Winter, D. M., & Francis, J. E. (2012). Neogene stratigraphy of Taylor Valley, Transantarctic Mountains, Antarctica: evidence for climate dynamism and a vegetated early Pliocene coastline of McMurdo Sound. *Global and Planetary Change*, 96, 97-104.
- Fretwell, P., Pritchard, H. D., Vaughan, D. G., Bamber, J. L., Barrand, N. E., Bell, R., Bianchi, C., Bingham, R.G., Blankenship, D.D., Casassa, G., Catania, G., Callens, D., Conway, H., Cook, A.J., Corr, H.F.J., Damaske, D., Damm, V., Ferraccioli, F., Forsberg, R., Fujita, S., Gim, Y., Gogineni, P., Griggs, J.A., Hindmarsh, R.C.A., Holmlund, P., Holt, J.W., Jacobel, R.W., Jenkins, A., Jokat, W., Jordan, T., King, E.C., Kohler, J., Krabill, W., Riger-Kusk, M., Langlely, K.A., Leitchenkov, G., Leuschen, C., Luyendyk, B.P., Matsuoka, K., Mouginot, J., Nitsche, F.O., Nogi, Y., Nost, O.A., Popov, S.V., Rignot, E., Ripplin, D.M., Rivera, A., Roberts, J., Ross, N., Siegert, M.J., Smith, A.M., Steinhage, D., Studinger, M., Sun, B., Tino, B.K., Welch, B.C., Wilson, D., Young, D.A., Xiangbin, C., & Zirizzotti, A. (2013). Bedmap2: improved ice bed, surface and thickness datasets for Antarctica. *The Cryosphere*, 7(1).

- Golledge, N. R., Kowalewski, D. E., Naish, T. R., Levy, R. H., Fogwill, C. J., & Gasson, E. G. W. (2015). The multi-millennial Antarctic commitment to future sea-level rise. *Nature*, *526*(7573), 421-425.
- Hansen, M. A., Passchier, S., Khim, B. K., Song, B., & Williams, T. (2015). Threshold behavior of a marine-based sector of the East Antarctic Ice Sheet in response to early Pliocene ocean warming. *Paleoceanography*, *30*(6), 789-801.
- Hayes, D., & Frakes, L. (1975). Initial Reports of the Deep Sea Drilling Project, 28. *Initial Reports of the Deep Sea Drilling Project*.  
<http://dx.doi.org/10.2973/dsdp.proc.28.1975>
- Masson-Delmotte, V., Schulz, M., Abe-Ouchi, A., Beer, J., Ganopolski, A., Rouco, J., Jansen, E., Lambeck, K., Luterbacher, J., Naish, T., Osborn, T., Otto-Bliesner, B., Quinn, T., Ramesh, R., Rojas, M., Shao, X., & Timmermann, A. (2013). Information from Paleoclimate archives In *Climate Change 2013: the Physical Science Basis. Contribution of Working Group I to the Fifth Assessment Report of the Intergovernmental Panel on Climate Change*, Cambridge Univ. Press, Cambridge and New York.
- McKay, R., Naish, T., Carter, L., Riesselman, C., Dunbar, R., Sjunneskog, C., Winter, D., Sangiorgi, F., Warren, C., Pagani, M., Schouten, S., Willmott, V., Levy, R., DeConto, R., & Powell, R. D. (2012). Antarctic and Southern Ocean influences on Late Pliocene global cooling. *Proceedings of the National Academy of Sciences*, *109*(17), 6423-6428.

- Miller, M. F., & Mabin, M. C. G. (1998). Antarctic Neogene landscapes—in the refrigerator or in the deep freeze. *GSA Today*, 8(4), 1-3.
- Miller, K. G., Wright, J. D., Browning, J. V., Kulpecz, A., Kominz, M., Naish, T. R., Cramer, B.S., Rosenthal, Y., Peltier, W.R., & Sosdian, S. (2012). High tide of the warm Pliocene: Implications of global sea level for Antarctic deglaciation. *Geology*, 40(5), 407-410.
- Orejola, N., Passchier, S., & Expedition 318 Scientists (2014). Sedimentology of lower Pliocene to upper Pleistocene diamictites from IODP Site U1358, Wilkes Land margin, and implications for East Antarctic Ice Sheet dynamics, *Antarct. Sci.*, 26, 183–192, doi:10.1017/S0954102013000527.
- Pollard, D., & DeConto, R. M. (2009). Modelling West Antarctic ice sheet growth and collapse through the past five million years. *Nature*, 458(7236), 329-332.
- Raymo, M. E., Grant, B., Horowitz, M., & Rau, G. H. (1996). Mid-Pliocene warmth: stronger greenhouse and stronger conveyor. *Marine Micropaleontology*, 27(1), 313-326.
- Rignot, E., Jacobs, S., Mouginot, J., & Scheuchl, B. (2013). Ice-shelf melting around Antarctica. *Science*, 341(6143), 266-270.
- Whitehead, J. M., & Bohaty, S. M. (2003). Pliocene summer sea surface temperature reconstruction using silicoflagellates from Southern Ocean ODP Site 1165. *Paleoceanography*, 18(3).

Winnick, M. J., & Caves, J. K. (2015). Oxygen isotope mass-balance constraints on Pliocene sea level and East Antarctic Ice Sheet stability. *Geology*, 43(10), 879-882.

## CHAPTER 2

### **Threshold Behavior of a Marine-Based Sector of the East Antarctic Ice Sheet in Response to early Pliocene Ocean Warming**

[A portion of this chapter was published in *Paleoceanography*, (2015) DOI:  
10.1002/2014PA002704]

#### **Abstract**

We investigate the stability of the East Antarctic Ice Sheet (EAIS) on the Wilkes Land continental margin, Antarctica, utilizing a high-resolution record of ice-rafted debris (IRD) mass accumulation rates (MAR) from Integrated Ocean Drilling Program Site U1359. The relationship between orbital variations in the IRD record and climate drivers was evaluated to capture changes in the dynamics of a marine-based ice sheet in response to early Pliocene warming. Three IRD MAR excursions were observed and confirmed via scanning electron microscope microtextural analysis of sand grains. Time series analysis of the IRD MAR reveals obliquity-paced expansions of the ice sheet to the outer shelf prior to ~4.6 Ma. A decline in the obliquity and a transition into a dominant precession response of IRD MAR occur at ~4.6 Ma along with a decline in the amplitude of IRD MAR maxima to low background levels between ~4.0 and ~3.5 Ma. We speculate that as sea surface temperatures began to peak above 3°C during the early Pliocene climatic optimum, the ice shelves thinned, leading to a greater susceptibility to precession-forced summer insolation and the onset of persistent retreat of a marine-based portion of the EAIS.



**Keywords:** IRD MAR, Pliocene, Southern Ocean, Antarctica, Orbital Insolation, Climate Variability

## 2.1 Introduction

In evaluating the cryosphere and its response to changes in climate, the Pliocene epoch (5.33–2.58 Ma) is considered of great importance due to similar to present oceanographic settings [Haug et al., 2001; Jansen et al., 2007] and carbon dioxide concentrations ranging from ~300 to 415 ppm [Bartoli et al., 2011; Pagani et al., 2010; Seki et al., 2010]. Pliocene warmth can be attributed to the high CO<sub>2</sub> levels [Crowley, 1996]. Compared to today, the high-latitude Southern Hemisphere was warmer and global temperatures were 3–3.5°C above present [Andersson et al., 2002; Fedorov et al., 2013; Raymo et al., 1996].

A global compilation shows that sea surface temperatures (SSTs) were the highest during the early Pliocene climatic optimum, ~ 4.4 Ma [Fedorov et al., 2013]. Early Pliocene sea surface temperatures (SSTs) in the Southern Ocean varied between 2° and 5.7°C [Whitehead and Bohaty, 2003; Escutia et al., 2009; McKay et al., 2012] and may have influenced ice sheet dynamics [Passchier, 2011]. Early Pliocene ice-rafted detritus, however, has been found at lower latitudes, despite sea surface warming [Kennett and Hodell, 1993].

A strong obliquity cycle appears to be present in high-latitude Southern Hemisphere ice volume and climate records [Grützner et al., 2005; Naish et al., 2009; Paul et al., 2000; Zachos et al., 2001]. Summer insolation in the high latitudes is dominated by the precession period, whereas obliquity controls mechanisms of meridional heat and moisture transport [Raymo and Nisancioglu, 2003]. Astronomical

forcing of surface temperatures can vary in intensity throughout geologic time, and other features may distort, dampen, or reinforce the astronomical signal [de Boer and Smith, 1994]. For example, by the end of the Miocene, a reorganization of the oceanic gateways may have caused a major shift within the Earth's climate system and its response to orbital forcing [Paul et al., 2000].

The Integrated Ocean Drilling Program (IODP) drilled seven sites within the Wilkes Land continental margin in order to provide a long-term sedimentary archive encompassing Cenozoic glaciations and their relationship to global climate and oceanographic change [Expedition 318 Scientists, 2011]. The portion of the East Antarctic Ice Sheet (EAIS) that drains through the Wilkes subglacial basin is grounded mainly below sea level. This segment of the EAIS is considered less stable than other areas of the EAIS and more susceptible to climate change [Cook et al., 2013; Escutia et al., 2005; Orejola et al., 2014]. Currently, Antarctic ice shelves are thinning as a result of encroachment of circumpolar deep water (CDW) onto the continental shelves. This effect on ice shelves is amplified in glacial drainage systems that are grounded below sea level, where glacial ice is most susceptible to changes in the marine environment [Rignot et al., 2013].

IODP Site U1359 (Figure 2-1) is located on the Wilkes Land continental rise at 4003 meters below sea level (mbsl), within 100km off the shelf edge [Expedition 318 Scientists, 2011]. In order to assess the extent of the Earth's polar climate sensitivity and the stability of the EAIS during the Pliocene climatic optimum, we present a high-resolution record of ice-rafted debris mass accumulation rates (IRD MAR) at Site U1359.

Through microtextural analysis of the sand fraction ( $>63\text{--}2000\ \mu\text{m}$ ), we establish that IRD MAR is glacially derived material transported to the continental rise.

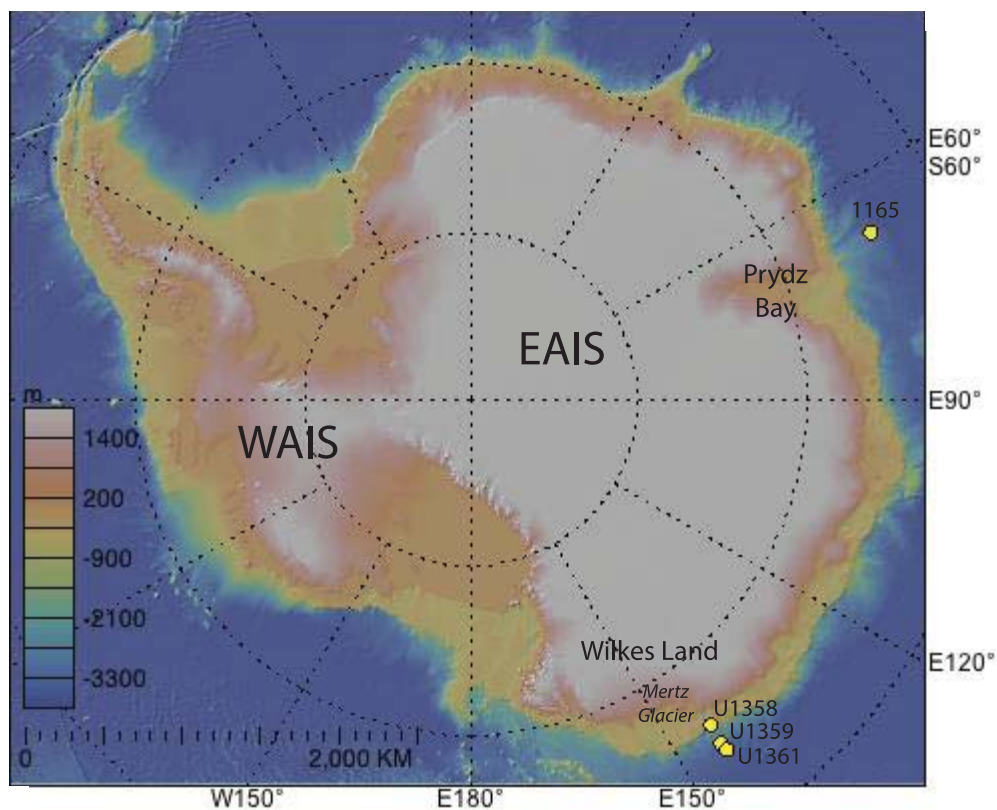


**Figure 2-1. Location of Antarctic Wilkes Land continental rise Sites U1359 and U1361, continental shelf Site U1358 near Mertz Glacier and Prydz Bay continental rise Site 1165.**

In order for icebergs to be generated, ice sheets must extend toward the continental margins, and surface waters must be cold enough that calving icebergs can survive transport and deposit detritus in the deep ocean [Hemming et al., 2002]. The ultimate volume of sediment deposited depends on the size and numbers of icebergs released and can vary with climatic and glacial regime [Powell and Domack, 1995]. Ice sheets behave like a dynamical system—as climate forcings change over time so do their

states of equilibrium [Abe-Ouchi et al., 2013]. Cores in ice-proximal continental margin settings typically capture the complete record of ice sheet dynamics on the adjacent continental shelf [Rashid et al., 2012], whereas distal cores are more strongly influenced by changes in currents and SSTs and thus capture a regional climate signal only partially influenced by ice dynamics [Murphy et al., 2002]. Using a high-resolution IRD MAR record from an ice-proximal site, the relationships between iceberg calving and climate drivers are assessed on orbital time scales. A record of ice rafting by Patterson et al. [2014] from a nearby drill hole extends from 2.2 to 4.3 Ma across a condensed interval at ~3.3–3.5 Ma. Relatively continuous sedimentation between ~5.1 and 3.6 Ma at Site U1359 allows us to capture the full extent of the Pliocene climatic optimum including the response of the East Antarctic Ice Sheet at the onset of peak warming ~4.4 Ma.

## **2.2 Materials and Methods**

### **2.2.1 Study Site**

Holes U1359A, U1359B, and U1359C were drilled to total depths of 193.5, 252.0, and 168.7 meters below seafloor (mbsf), respectively. The stratigraphy of the early Pliocene interval is characterized by cyclical variations of three sedimentary facies: (a) bioturbated or weakly laminated light greenish gray diatom-rich silty clays and oozes with dispersed clasts; (b) massive olive gray silty clay with dispersed clasts; and (c) laminated olive gray silty clay with millimeter-to-centimeter-scale silt and fine sand laminae and dispersed clasts [Expedition 318 Scientists, 2011]. This facies assemblage is consistent with the seismic interpretation of channel levee systems [Escutia et al., 2005], and the individual facies are indicative of variable degrees of surface productivity (higher in facies A) and

terrigenous supply (higher in facies B), and distal muddy turbidite deposition (facies C). Deposition of all three facies was associated with intermittent deposition of gravel-sized (>2 mm) ice-rafted debris, even within intervals of muddy turbidite laminae. Facies A and B also contained sediment silt and sand clots or clasts, similar to sediment pellets described from other ice-rafted sediments [Goldschmidt et al., 1992].

### **2.2.2 Age Model**

Age tie points were generated through magneto-biostratigraphic correlation [Tauxe et al., 2012]. All ages are based on Gradstein et al.'s [2004] age scale. Holes U1359A, U1359B, and U1359C were correlated shipboard using the natural gamma radiation and magnetic susceptibility measurements to generate a meter composite depth (mcd) scale [Expedition 318 Scientists, 2011]. The correlation is most accurate in sections with high recovery because natural gamma ray and magnetic susceptibility signatures of thicker stratigraphic units can be matched. Age data in core intervals with significant recovery gaps were omitted from the age model as a consequence of uncertainty in the stratigraphic correlation between the holes. Our sampling targeted the well-recovered early Pliocene interval at ~67–139 mcd in holes U1359A and U1359B. Fifteen age tie points across Holes U1359A, U1359B, and U1359C generate a constant linear sedimentation rate of approximately 45 m/Myr for the interval between ~69 and ~212 mcd (Table 2-1 and Figure B1 in the supporting information found in Appendix B). To account for a condensed interval in the uppermost part of the studied interval (between 68.84 and 69.94 mcd), a stepwise regression model was generated for that section using age tie points from Hole U1359A (Table 2-1 and Figure B1 in the

supporting information found in Appendix B).

**Table 2-1. Age tie points in Ma for Site U1359**

AVG Depth (mcd <sup>a</sup> )	Depth Error (m)	Age <sup>b</sup> (Ma)	Hole
41.41	0.02	2.5810	U1359C
59.29	0.05	3.0320	U1359C
61.52	0.03	3.1160	U1359C
64.61	n/a	3.2070	U1359A
68.94	n/a	3.3300	U1359A
69.84	0.02	3.5960	U1359A
96.60	0.18	4.1870	U1359B
98.78	0.03	4.3000	U1359B
113.61	0.08	4.4930	U1359B
117.93	0.03	4.6310	U1359B
123.49	1.69	4.7990	U1359B
125.40	0.02	4.7990	U1359C
139.03	0.03	4.9970	U1359C
143.82	0.00	4.9970	U1359B
149.59	n/a	5.2350	U1359C
150.55	2.76	5.2350	U1359B
190.12	0.00	6.0330	U1359B
194.66	1.34	6.2520	U1359B
201.53	0.02	6.4360	U1359B
212.36	0.02	6.7330	U1359B

<sup>a</sup>Meters composite depth.

<sup>b</sup>Ages are based on the magneto-biostratigraphy from Tauxe et al. (2012); Depth error listed in Expedition 318 Scientists (2011).

### 2.2.3 Biogenic Opal

The biogenic opal contents at Site U1359 were generated using 74 samples selected from cores 9H (68.92 mcd) to 15H (138.81 mcd) in Hole U1359A. The biogenic silica content was measured using a wet alkaline extraction method modified from

DeMaster [1981] and Müller and Schneide, [1993] at Pusan National University by B.K. Khim and Buhan Song. Approximately 10mg of sample was transferred into a 50mL polypropylene tube. About 30 mL of a 1N NaOH solution was added to the tubes, which were then closed and placed in a drying oven at 85°C for 5h. The tubes were vigorously shaken to resuspend the solids at every hour; then 0.10mL solution was taken into a 10mL vial containing 2mL 0.10N HCl. Dissolved silica was measured using a molybdate blue spectrophotometric method. The analytical precision of standard samples as a relative standard deviation ( $\pm 1\sigma$ ) is  $\pm 1\%$ . The biogenic opal content was calculated by multiplying biogenic silica content by 2.40 [Mortlock and Froelich, 1989].

#### **2.2.4 Ice-Rafted Debris**

A high-resolution record for the early Pliocene was generated using 348 samples from Hole U1359A and 143 samples from Hole U1359B, spanning a total depth of 67.17–139.15 mcd. Each sample was measured on a dual light source Malvern Mastersizer 2000 laser particle sizer at Montclair State University, which can determine grain size distributions ranging from 0.020 to 2000 $\mu\text{m}$ . Instrument settings followed the recommendations of Sperazza et al. [2004]. All samples were pretreated to remove the biogenic component, and to preserve the terrigenous silicate fraction, by using the methodology employed by Konert and Vandenberghe [1997]. Following Krissek [1995], IRD MAR values were determined using the bulk particle size distribution based on the equation:

$$\text{IRD MAR} = \text{IRD} \times \text{TERR} \times \text{DBD} \times \text{LSR}$$

where IRD is defined as the volume percent of the terrigenous coarse fraction ( $>125 \mu\text{m}$ )



derived from laser particle size measurements divided by 100, and the terrigenous (TERR) fraction is defined as  $1 - \text{biogenic silica fraction} - \text{carbonate fraction}$ . The biogenic silica fraction was interpolated from the opal data set of U1359A. The carbonate fraction was determined to be negligible ( $<0.9\%$ ) by Expedition 318 Scientists [2011], and no corrections were made. The dry bulk density (DBD) is derived from shipboard measurements [Expedition 318 Scientists, 2011], and the linear sedimentation rate (LSR) is calculated using the age model we developed for Site U1359.

A peak in IRD MAR is expected to coincide with poor sorting of the fine fraction indicative of a supply of poorly sorted glacial debris. Sorting of the fine fraction ( $<125\mu\text{m}$ ) was calculated using the program GRADISTAT [Blott and Pye, 2001] following the scheme of Folk and Ward [1957], where values are derived based on the lognormal distribution of phi size values. Poorly sorted values are those greater than 1.00, while moderate to well-sorted values are less than 1.00 [Blott and Pye, 2001]. The sorting parameter does not require a correction for biogenic material or sedimentation rates because it is based on the terrigenous particle size distribution [Passchier, 2011].

### **2.2.5 Microtextural Analysis**

Samples were prepared by sieving through a  $63\mu\text{m}$  screen, with grains selected at random through a microscope before being mounted onto an aluminum stub. Each sample contained 40 grains. All samples were gold coated and viewed on the Hitachi S-3400N scanning electron microscope (SEM) at Montclair State University using a 12 kV accelerating voltage. Each grain was assessed for its microtextural abundances (See Appendix C for more details). Additionally, each grain was assessed for its mineralogy

through the use of the Bruker energy dispersive X-ray spectrometer (EDX) to verify that all grains selected were quartz. Samples were then interpreted using a classification scheme derived from Antarctic sediments with six different grain types that are representative of different sedimentary and diagenetic regimes [Damiani et al., 2006]. Type 1 grains are characterized as having abundant mechanical breakage features such as conchoidal fractures, arc/straight steps, and fractured plates with absent to very moderate chemical alterations (i.e., solution pits and silica precipitation). Type 2 and Type 3 grains show varying degrees of chemical alteration mixed with mechanical features with Type 2 still preserving the majority of the visible mechanical features and mostly angular to subangular outline. In the case of Type 3 grains, the mechanical features are nearly or completely obliterated by a thick coat of silica precipitation but still retain a subangular to subrounded outline. Abundances of grain types within these higher peaks are used to evaluate the sediment transport histories, in particular the degree of abrasion by eolian and aquatic sediment transport processes, of these glacially sourced grains.

### **2.2.6 Time Series Analysis**

Time series analysis was performed on the stratigraphically continuous section dated between ~5.1 and 3.6 Ma (70–139 mcd) and excluded the condensed interval. The age model for this section is based on a linear regression with  $r^2 = 0.99$  through eleven age tie points in Hole U1359B (Table 2-1 and Figure B1 in the supporting information found in Appendix B), and the regression line also provides an excellent fit through age tie points in Holes U1359A and U1359C (Figure B1 in the supporting information found in Appendix B). Time series analysis was conducted using a continuous wavelet

transform, which allows a data series to be studied at both low and high frequencies simultaneously. Wavelet analysis identifies periodicities that are not stationary, i.e., they can change in amplitude or frequency over time [Torrence and Compo, 1998]. The analysis requires evenly spaced data. However, when the data were interpolated from ~5.1 to 3.6 Ma (generating an average sampling spacing of 3,180 years), there was little difference in the results compared to the same analysis with the original, slightly unevenly spaced record. Thus, the interpolated record was used for wavelet analysis. All analyses were performed within the PAleontological STatistics Software ver. 2.17 [Hammer et al., 2001]. Wavelet analysis was done using the Morlet basis function, and responses with Milankovitch periodicities were extracted using band pass filters, where precession was filtered at 19–23 kyr, obliquity at 37–43 kyr, and eccentricity at 98–125 kyr. The 95% confidence contours in the wavelet plots were derived using chi-square distribution [Torrence and Compo, 1998].

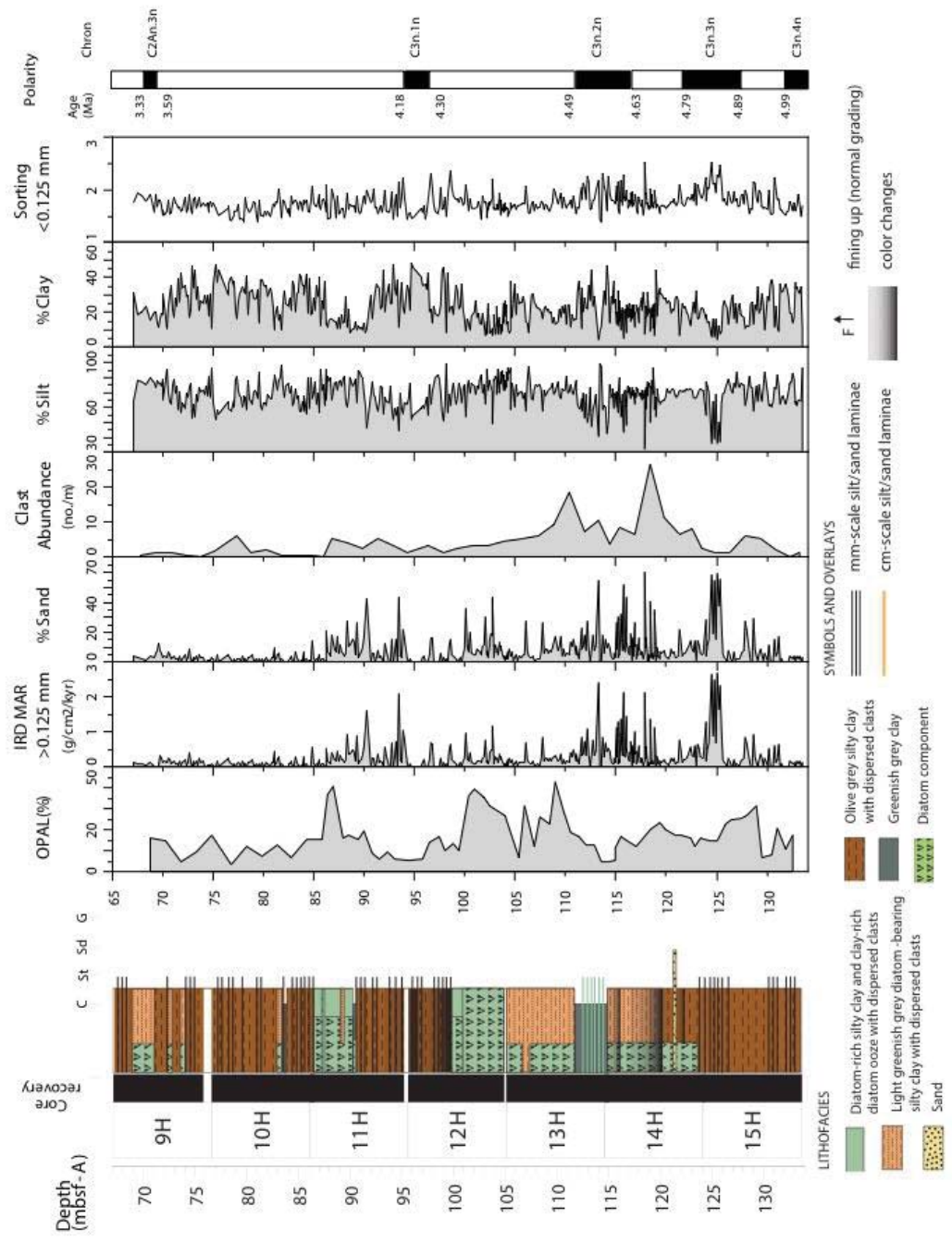


**Figure 2-2. Distribution of opal, ice-rafted debris (IRD) mass accumulation rates (MAR), sand percentage, gravel (clast abundance), terrigenous silt and clay percentage and sorting of fine fraction at Site U1359 (Encompasses both Hole A and B). Data for Site U1359 are shown on the depth scale for Hole U1359A (mbsf-A) to allow correlation to the lithological log of Hole U1359A. The lithology log for Hole U1359A is based on the data recorded on the shipboard Visual Core Description sheets and smear-slide observations [Expedition 318 Scientists, 2011] augmented with postcruise observations of high-resolution line-scan images. Magnetostratigraphy log after Tauxe et al. [2012].**

## **2.3 Results**

### **2.3.1 Biogenic Opal**

Biogenic opal contents of the sediment range from ~3 to 43 wt % (Figure 2-2). Prominent opal maxima occur between 86 and 87 mbsf-A, 101 and 104 mbsf-A, and 107 and 110 mbsf-A. The downcore distribution of opal is in reasonable agreement with the shipboard lithological and smear-slide observations as recorded on the Visual Core Description sheets [Expedition 318 Scientists, 2011]. Core intervals with numerous millimeter-scale silt and sand laminae coincide with lower opal percentages.

### **2.3.2 Particle Size Distributions and IRD MAR**

To allow comparison with the detailed lithology log of Hole U1359A (modified from Visual Core Description sheets [Expedition 318 Scientists, 2011]), IRD data from Holes U1359A and U1359B were plotted on the U1359A depth scale by converting from

med to meters below seafloor (mbsf-A). Within the U1359 record are three distinct intervals of high amplitude and highly variable IRD MAR, which we designate as IRD MAR excursions I, II, and III (Figures 2-2 and 2-3a). The most prominent IRD MAR maxima can be identified at depths 123–126 mbsf-A (excursion I), 111–119 mbsf-A (excursion II), and 86–94 mbsf-A (excursion III) and generally have values of  $\sim 2$  g/cm<sup>2</sup>/kyr or higher, while smaller, intermittent peaks tend to be  $\sim 1$  g/cm<sup>2</sup>/kyr or less. Stratigraphically below each IRD MAR maximum is an interval of very low, intermittent IRD MAR followed by an abrupt upward increase and then gradual decrease. These sharp-based IRD maxima are marked by very poor sorting of the fine fraction ( $<125\mu\text{m}$ ). A steady leveling off of IRD MAR occurs between 67 and 87 mbsf-A.

Overall, the shipboard lithological observations are in agreement with the general trends of silt and clay with lower amounts of clay in the diatomaceous facies than in silty clay with dispersed clasts facies. The diatom- rich silty clay facies coincides with sections of higher terrigenous silt and lower clay percentages. In contrast, the grey clay facies coincides with a relatively high clay percentage with the exception of one IRD MAR peak ( $\sim 113$  mbsf-A).

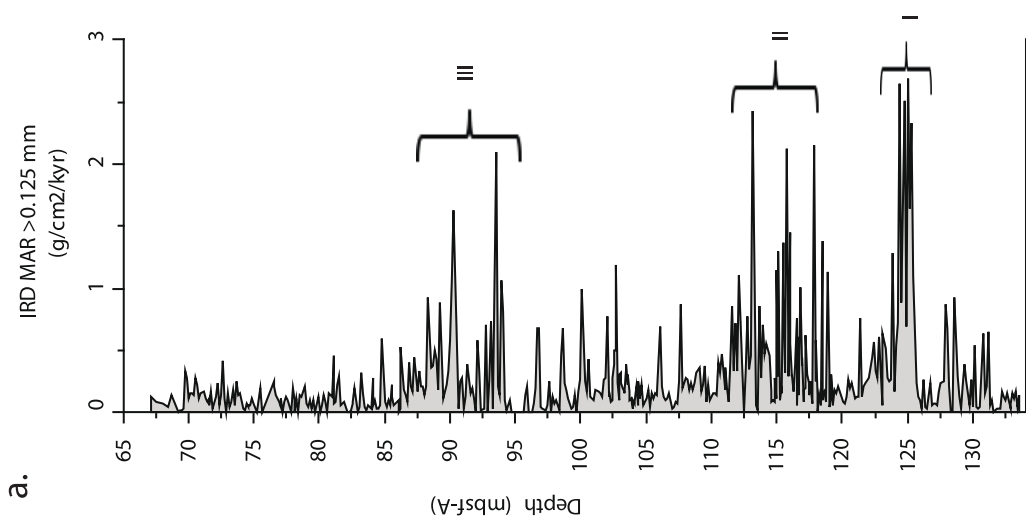
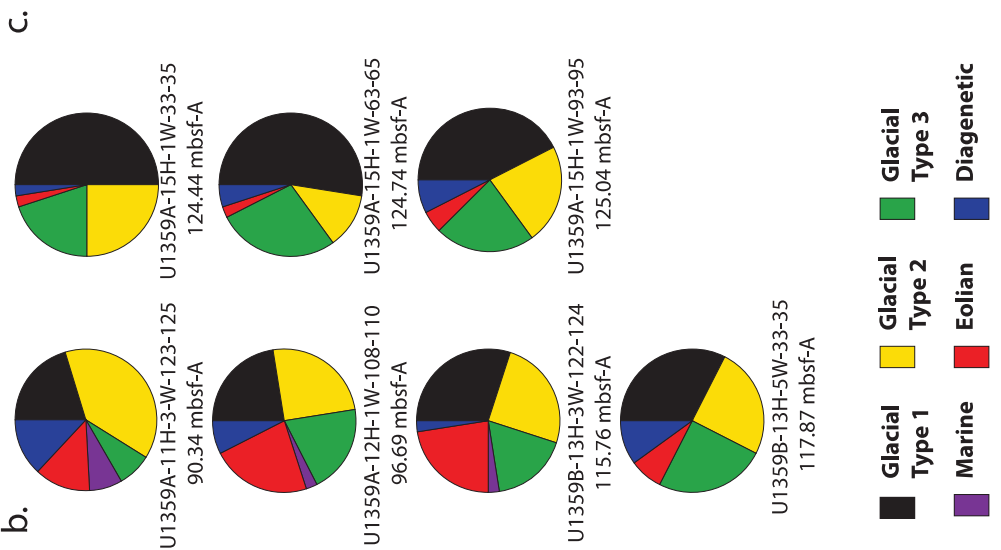
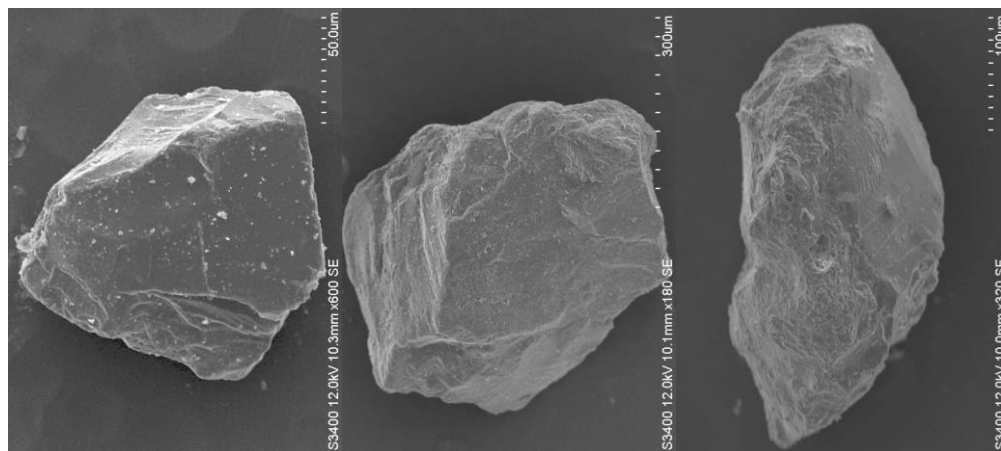
### **2.3.3 Quartz Grain Surface Textures**

Based on observations of the calculated IRD MAR, a total of seven samples were selected in order to assess sand grain shapes and surface microtextures (Figure 2-3a).

Large peaks in IRD ( $>1$  g/cm<sup>2</sup>/kyr) were the main focus in order to determine the amount of iceberg rafted (i.e., glacially derived) material. The grain outlines ranged from angular to subrounded and show numerous mechanical breakage features with absent to moderate

chemical alterations (See Appendix C Figure C1 and Table C1-7). As a whole, the samples show a similarity between them with dominance in glacial Types 1–3 grains (Figure 2-3b, See Appendix C Figure C2 and Table C8) [Damiani et al., 2006].

It should be noted that the samples within IRD MAR excursion I are from a section of less variable, persistently high IRD MAR, where the peaks are very closely spaced. Samples from this lower interval show a dominance in Type 1 grains (Figure 2-3c, top). The samples within the upper intervals are from a more variable part of the IRD MAR record and show higher proportions of grain Types 2 and 3 (Figure 2-3c, middle and bottom, respectively).



**b.**



**Figure 2-3. (A) IRD MAR distribution highlighting three main intervals of variability and sample selection (B) Abundances of each grain type for each sample identified on mbsf-A depth scale (C) Selected micrographs from the SEM Secondary Electron detector showing glacial texture types 1-3 [per Damiani et al., 2006] found on sample grains. Fresh mechanical textures indicating glacial type 1 present on micrograph (top) and varying degrees of silica precipitation indicative of glacial type 2 (middle) and type 3 (bottom).**

#### **2.3.4 Time Series Analysis**

Wavelet analysis found precession, obliquity, and eccentricity cycles at varying intensities throughout the record (Figure 2-4a). The presence of two lower wavelet frequencies that equate to ~467,000 and ~268,000 years decrease in intensity and span only a few complete cycles (Figure 2-4a). These lower frequencies could be the result of a convolution of the other cycles found within the record or nonorbital influences on ice dynamics. When the data were detrended using the log10 centered on 0, lower frequencies such as obliquity were enhanced (Figure 2-4b), particularly between 4.3 and 3.9Ma. When compared to summer insolation forcing (at 65°S) (Figure 4c) [Laskar et al., 2004], obliquity does not have a strong presence. The band-pass filtered record initially shows a dominant response in the obliquity band (Figure 2-5c), with a transition to a dominant response in the precession band at ~4.6 Ma (Figure 2-5b). IRD MAR maxima coincide with eccentricity minima at ~4.9 and 4.2–4.0 Ma (Figure 2-5e).

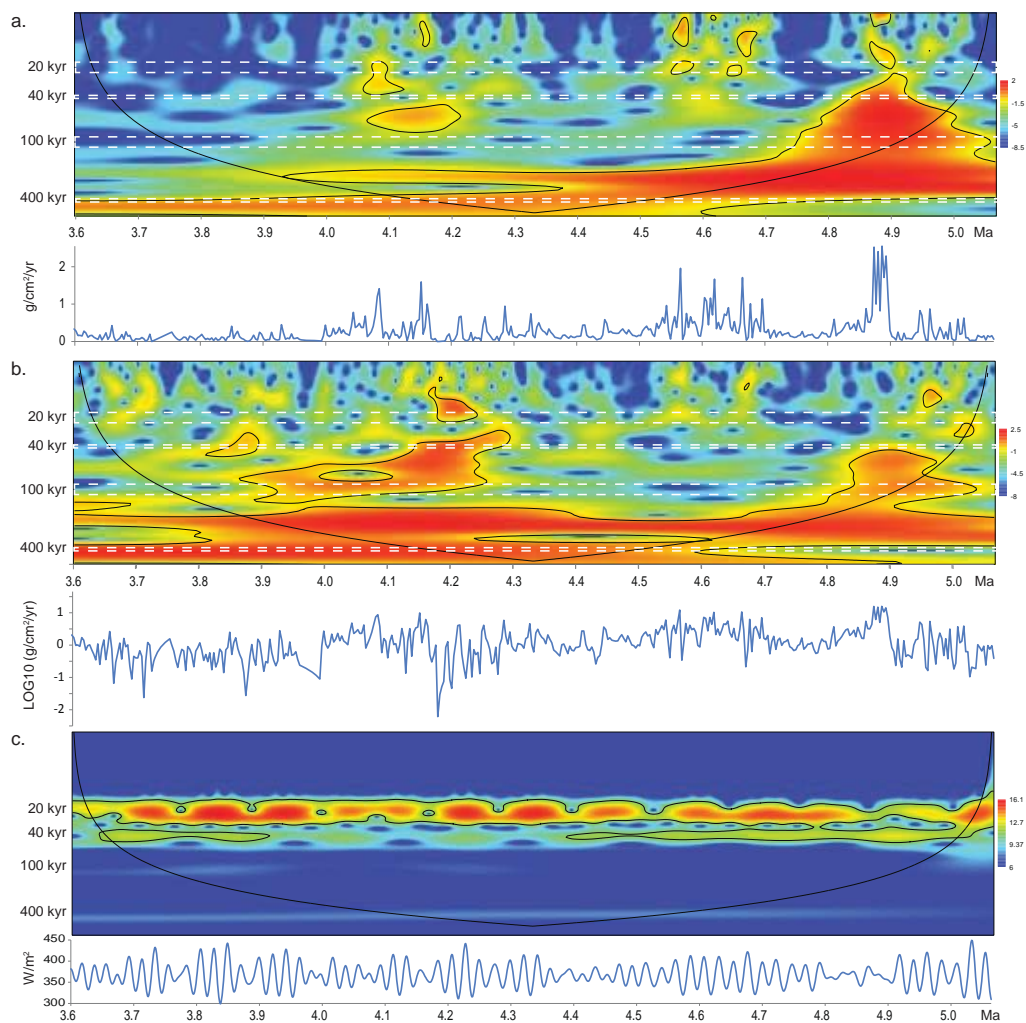


**Figure 2-4. Morlet powered wavelet spectrum of Site U1359 (A) evenly spaced IRD MAR (B) Detrended (Log10) IRD MAR and (C) Mean monthly summer insolation at 65°S [Laskar *et al.*, 2004], highlighting orbital signal intensities over time. The 95% confidence contour was derived using chi-square distribution [Torrence and Compo, 1998].**

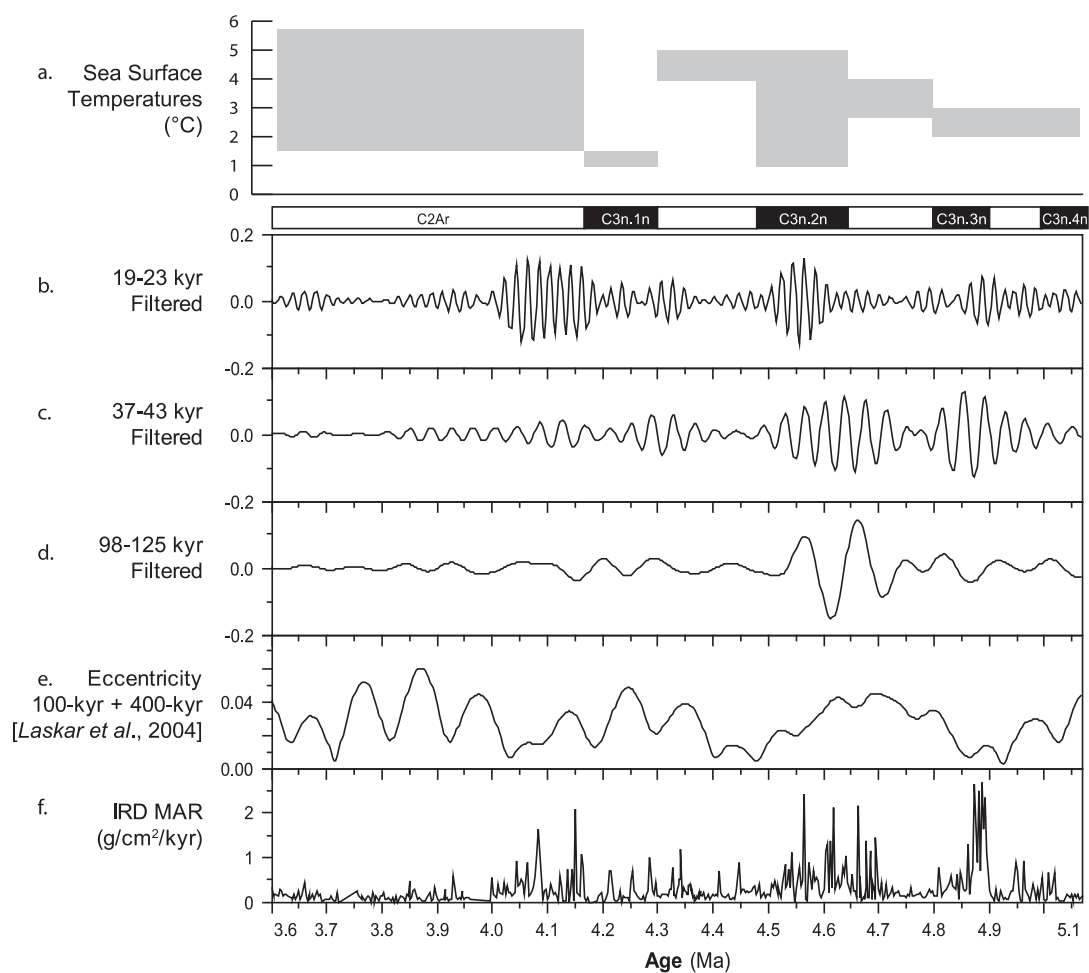


**Figure 2-5. (A) Early Pliocene sea surface temperatures based on values compiled in Table 2 [McKay et al. 2012; Whitehead and Bohaty, 2003; and Escutia et al. 2009]. Site U1359 IRD MAR band-pass filtered periodicities of (B) precession, (C) obliquity and (D) eccentricity with (E) Laskar et al. [2004] eccentricity cycle (400-kyr and 100-kyr) and (F) IRD MAR.**

## 2.4 Discussion

### 2.4.1 Sedimentation at Site U1359

The sedimentology of the intervals with IRD MAR maxima changes from excursion I (~4.9–4.8Ma) with respect to excursions II and III (4.7–4.5 and 4.2–4.0 Ma, respectively) in U1359 (Figure 2-2). The high peaks of IRD MAR within excursion I occur within sections of laminated millimeter-scale silty sand with dispersed clasts. In contrast, the intervals encompassing excursions II and III are not positioned in laminated sections and contain more abundant silt- to sand-sized sedimentary aggregates and higher opal contents [Expedition 318 Scientists, 2011]. Unmodified Type 1 glacial microtextures are also more abundant in excursion I (Figure 2-3) with respect to excursions II and III.

The sedimentary facies with very low opal contents and high mass accumulation rates of IRD ( $>2 \text{ g/cm}^2/\text{kyr}$ ) within excursion I (~4.9–4.8Ma) are consistent with ice sheet advance to the shelf edge. The greater abundance of Type 1 grains within excursion I indicates continuous deposition from a glacial source with little influence from current-controlled sedimentation. This IRD maximum occurs within graded laminated mud facies, which can be explained by a combination of iceberg rafting and sediment lofting from hyperpycnal flows under increased meltwater discharge of an ice sheet grounded on the outer shelf [Hesse and Khodabakhsh, 2006; Rashid et al., 2003]. This interpretation is corroborated by the presence of early Pliocene ice-proximal diamictons older than 3.99 Ma [5.12–4.40 Ma; Iwai, personal communication, 2013] at Site U1358 on the adjacent continental shelf [Orejola et al., 2014]. In the Southern Ocean, extensive Pliocene-Pleistocene ice rafting events occur during glacial/cold stages at the onset of

deglaciations when ice sheets are still large and grounded on the continental shelves [Murphy et al., 2002; Passchier, 2011; Weber et al., 2014]. In contrast to modern day, a high amount of far traveled ice-rafted debris with a Wilkes Land and Adélie Land source was deposited during this time at Site 1165 [Williams et al., 2010].

The onset of ice retreat from the shelf at ~ 4.7 Ma can be denoted by a spike in the gravel fraction and high IRD MAR followed by diminution (Figure 2-2). Under warming, but still relatively cold SSTs, gravelly muds are typically deposited during ice shelf breakup [Evans and Pudsey, 2002], followed by hemipelagic sedimentation [Caburlotto et al., 2010].

Poor sorting and paucity of laminations within IRD rich diatom-bearing sediments of the two upper intervals (excursions II and III; ~4.7–4.5 Ma and ~4.2–4.0 Ma, respectively) indicates deposition due to terrigenous fall out from sediment plumes and/or iceberg rafting [Caburlotto et al., 2010]. High opal contents are indicative of interglacial periods with reduced sea ice coverage and warm climatic conditions when ocean heat transport exerts a maximum influence in the Southern Ocean [Whitehead and Bohaty, 2003; Grützner et al., 2005; Escutia et al., 2009; McKay et al., 2012].

SEM analysis of grains out of excursions II and III shows higher proportions of grain Types 2 and 3 (Figure 2-3b), indicating some abrasion and chemical alteration of glacially derived grains. An increase in the chemical alteration of grain surfaces may suggest a sea ice-rafted debris origin for those grains as discussed in St. John et al. [2015]. SSTs at the time of excursions II and III were highly variable and ranged between 1 and 5°C (Table 2 and Figure 2-5a). Alternatively, the scarcity of “fresh” glacial grains

within the upper intervals II and III as well as the presence of common sand and silt aggregates dispersed within the mud fraction [Expedition 318 Scientists, 2011] may be explained by the overdeepening of the Wilkes basin. Glaciohydraulic supercooling, a process that occurs when a glacier flows through an overdeepening, is associated with periods of high water flux and ice accretion (frazil ice) in response to hydraulically regulated temperature and pressure changes [Lawson et al., 1998]. The presence of supercooled meltwater may have encouraged the accretion of chemically altered glacial grains. The formation and suspension of sand and silt as aggregates may also have resulted from the growth of frazil ice on sediment particles and subsequent rapid entrainment into the growing basal ice. After incorporation into sea ice or glacial ice, the consolidated aggregates can melt out after ice rafting and survive a drop of several kilometers through the water column retaining their integrity even after burial [Goldschmidt et al., 1992].

**Table 2-2. Early Pliocene sea surface temperatures**

Chron	Age Range [Ma]	SST Range [°C]
C2An.3n	3.330 - 3.596	1-5
C2Ar	3.596 - 4.187	1.5 - 5.7
C3n.1n	4.187 - 4.300	1 - 1.5
C3n.1r	4.300 - 4.493	4 - 5
C3n.2n	4.493 - 4.631	1 - 5
C3n.2r	4.631 - 4.799	2.5 - 4
C3n.3n	4.799 - 4.896	2 - 3
C3n.3r	4.896 - 4.997	2 - 3
C3n.4n	4.997 - 5.235	2 - 3

**Early Pliocene East Antarctic SSTs compiled from *McKay et al.* [2012], *Whitehead and Bohaty*, [2003], and *Escutia et al.* [2009].**

#### **2.4.2 Iceberg Calving Mechanisms and Climate Forcings**

IRD MAR excursion I coincides with a 400 kyr eccentricity minimum [Laskar et al., 2004] and shows a strong obliquity response in the IRD record of Site U1359 (Figures 2-4a and 2-5). This is in agreement with other records: (1) Miocene stable isotope data that predate the onset of significant Northern Hemisphere glaciation also show Antarctic ice sheet growth during 400 kyr eccentricity minima [Liebrand et al., 2011]; (2) Obliquity-paced Antarctic sedimentation records are known from Ocean Drilling Program (ODP) Site 1165 (Prydz Bay) and AND-1B (Ross Sea) for the same period of ~5.2–4.6 Ma [Grützner et al., 2005; Naish et al., 2009]. During ice advances to the shelf break in chron C3n.3n (4.99–4.79 Ma), which encompasses IRD MAR excursion I, SSTs were relatively consistent between 2 and 3°C (Table 2-2 and Figure 2-5a). To allow for ice sheet advances to the shelf break under these relatively warm SST

conditions, high snow accumulation is necessary to maintain a positive ice sheet mass balance, perhaps similar to the “snow-gun hypothesis” [Prentice and Matthews, 1991], which has also been put forward to explain Miocene Antarctic ice growth under warm SST conditions [Shevenell et al., 2008].

Obliquity controls the ice sheet surface mass balance through its effect on meridional moisture transport. During times of reduced summer insolation, snow and ice can persist and survive through the meltback season [Raymo and Nisancioglu, 2003]. The increased snow accumulation from year to year would eventually lead to full glacial conditions paced by obliquity cycles. Moreover, early in the Pliocene, the summer insolation at 65°S was paced by obliquity, with weaker precession due to low eccentricity [Laskar et al., 2004] (Figure 2-4c). These variables explain the obliquity-paced discharge of glacially derived material from the Wilkes Land margin between ~5.1 and 4.6 Ma.

The onset of ice retreat in chron C3n.2r (4.79–4.63 Ma), coincident with IRD MAR excursion II, shows a combined precession, obliquity, and 100kyr eccentricity response (Figures 2-4a and 2-5) and marks a transition from a dominant obliquity to precession response of iceberg discharge at ~ 4.6 Ma. Summer insolation at 65°S from ~4.6 Ma onward is controlled by precession [Laskar et al., 2004] (Figure 2-4c), and variability in ice shelf surface melt [Hulbe et al., 2004] could account for a change in iceberg discharge. In excursion II, IRD MAR are low ( $<2\text{g/cm}^2/\text{kyr}$ ) and variable during the latter half of this transition and suggest that the ice sheet was no longer building up in mass similar to the excursion I scenario. As a feedback, ice retreat may have periodically allowed incursion of relatively warm CDW onto the Wilkes Land continental shelf with



basal melt enhancing ice retreat. Higher IRD MAR peaks within excursions II and III signify the survival of the ice shelves under gradual warming. Weakening of an ice shelf through subsurface warming has also been a recent conjecture to explain iceberg discharge [Alvarez-Solas et al., 2010; Marcott et al., 2011].

Ocean temperature likely played an important role in controlling the long-term marginal fluctuations of ice sheets [Joughin et al., 2012]. A broader range of SSTs is reconstructed around East Antarctica between ~4.5 and 3.6 Ma (Table 2-2 and Figure 2-5a), including abrupt warming events to 5.7°C documented during C2Ar (4.18–3.59 Ma) [Whitehead and Bohaty, 2003; Escutia et al., 2009]. These rapid ocean warming events may have caused the marine-based ice to thin and retreat substantially as a result of subsurface melt. In agreement with our findings, a modeling study targeting the Wilkes subglacial basin indicates that although warming of any kind likely forces the ice sheet to retreat, the marine-based ice might be particularly susceptible to fast changes in ocean heat supply [Mengel and Levermann, 2014], as observed for the Southern Ocean between ~4.5 and 3.6 Ma. IRD MAR declines to low background levels between ~4.0 and 3.6 Ma, indicative of a greater role of basal melt rather than iceberg discharge. Modeling studies show that rapid ice retreat occurs through basal melt rather than calving under high SSTs so that IRD MAR is expected to be minimal under full interglacial conditions [Rignot et al., 2013; Joughin et al., 2014; Mengel and Levermann, 2014].

We speculate that a major regime change from a large, obliquity-paced marine-based ice sheet to a smaller, precession-paced ice sheet may have occurred around 4.6 Ma. A larger ice sheet persisted with SSTs of 2–3°C. When SSTs began to warm, ice

volume initially increased due to the snow gun effect. The ice sheet-ocean system, however, exhibited threshold behavior as SSTs peaked above 3°C and tipped the balance of accumulation and ablation in favor of the latter. Continued warming initiated a system change where the marine-based ice thinned and became more susceptible to high-latitude insolation forcing.

The timing of the transition from an obliquity-paced to a precession-paced ice sheet at ~4.6 Ma contrasts with a recent study by Patterson et al. [2014] at nearby Site U1361, who argued for a change in the periodicity of ice dynamics between 3.3 and 3.5 Ma. This change coincides with a condensed interval in that record [Patterson et al., 2014, Figure S5 in their supporting information]. At Site U1361, an obliquity signal is expressed when analyzing a short interval of low-amplitude IBRD MAR between 4.0 and 3.5 Ma [Patterson et al., 2014, Figure 3a] (Figure B-4b in the supporting information found in Appendix B). The main difference with our initial approach is that Patterson et al. [2014] (1) isolated short segments and detrended their record before time series analysis and (2) tuned their age model using the IBRD MAR data set and then interpreted this signal as ice dynamics. However, even without detrending and in the untuned record, the obliquity signal is expressed below the condensed interval dated between 4.0 and 3.5 Ma [Patterson et al., 2014, Figure 3a] (Figure B-3 in the supporting information found in Appendix B). The tuning of the age model further diminished the higher frequency signal and accentuated the response in the obliquity band [Patterson et al., 2014, Figure 4b] (Figure B-4 in the supporting information found in Appendix B). Our detrended record (Figure 2-4b) also shows an obliquity signal between 4.3 and 3.9 Ma.

For the interval of 4.0–3.5 Ma, however, our IRD MAR values at Site U1359 are very low (Figure 2-5f and Figure B-2 in the supporting information found in Appendix B), and the absolute values of IBRD MAR at Site U1361 do not exceed  $0.2 \text{ g/cm}^2/\text{kyr}$  [Patterson et al., 2014] (Figure B-2 in the supporting information, found in Appendix B). Values this low are more typical of distant ice rafting events involving far-traveled icebergs [e.g., Kennett and Hodell, 1993]. The interpretation of such low signals of long-distance ice rafting is complicated by the influence of SST and currents on iceberg survival rates and routing and may not accurately depict ice dynamics.

In contrast to Patterson et al. [2014], we do not interpret the low-amplitude obliquity cycles in the interval between 4.0 and 3.6 Ma as an expression of the dynamics of the East Antarctic Ice Sheet. We argue that only the larger amplitude variations in IRD MAR carry that signal (Figure 2-5). At Site U1359, we analyzed the periodicities of the complete IRD MAR record, through the early Pliocene (5.1–3.6 Ma), which provides evidence of larger ice rafting events that are likely more locally sourced from the Wilkes Subglacial Basin. Our ice rafting events broadly correlate to interpretations of ice dynamics by Cook et al. [2013] based on a low-resolution  $\epsilon\text{Nd}$  record for Site U1361 (Figure B-2 in the supporting information found in Appendix B). Based on our analysis of a record of IRD MAR events, we argue for a change from an obliquity to precession-paced marine-based East Antarctic Ice Sheet at  $\sim 4.6$  Ma.

The shift in early Pliocene ice dynamics around  $\sim 4.6$  Ma coincides with major changes in ocean circulation. The closing of the Central American Seaway between 4.7 and 4.2 Ma gradually altered the transport of heat [Haug et al., 2001; Haug and

Tiedemann, 1998; Steph et al., 2010], concurrent with warming in the Southern Ocean [Whitehead and Bohaty, 2003; Escutia et al., 2009]. The LR04 benthic stack also shows a shift toward coherency with precession starting ~4.5 Ma, which becomes significant at ~4.1–2.8 Ma, and is attributed to Northern Hemisphere glaciation or northern deepwater formation [Lisiecki and Raymo, 2005]. On the other hand, an Earth System modeling study with mid-Pliocene boundary conditions [Zhang et al., 2013] challenges a North Atlantic origin of deepwater formation. Under reduced Pliocene ice sheet boundary conditions, the model simulates a poleward migration of the westerlies, reduced ocean stratification, and no sea ice but deepwater formation in the Southern Ocean [Zhang et al., 2013]. In the context of this modeling study, the precession-paced ice discharges ~4.6–4.0 Ma provide an alternate interpretation for the increased coherency with precession in the deep-sea isotope data ~4.5 Ma [Lisiecki and Raymo, 2005]. A southern source of precession-driven deepwater formation is in line with other emerging evidence of feedbacks involving EAIS dynamics and ocean circulation [Goldner et al., 2014; Woodard et al., 2014].

## **2.5 Conclusions**

We acquired high-resolution ice-rafted debris mass accumulation rates (IRD MAR), SEM surface texture data, and opal weight percent to assess marine ice sheet dynamics in the Wilkes basin during the early Pliocene. Three major ice rafting episodes were recognized that show a significant evolution in ice dynamics from the early Pliocene into the mid-Pliocene:

1. Excursion I (4.9–4.8 Ma) is characterized by the laminated, graded mud facies

with high IRD MAR ( $>2 \text{ g/cm}^2/\text{kyr}$ ) indicative of ice sheet expansion to the outer shelf. Intense iceberg discharge episodes were accompanied by increased meltwater discharge during an insolation minimum and relatively warm SSTs ( $2\text{--}3^\circ\text{C}$ ).

2. Excursions II/III ( $\sim 4.7\text{--}4.5 \text{ Ma}$  and  $\sim 4.2\text{--}4.0 \text{ Ma}$ , respectively) have lower amounts of IRD MAR ( $<2 \text{ g/cm}^2/\text{kyr}$ ) and a paucity of laminations and fresh glacial textures of a more retreated ice margin. Along with a transition in sedimentological properties at  $\sim 4.6 \text{ Ma}$ , the filtered IRD MAR record shows a shift from an obliquity to a precession influence concurrent with an intermittent rise in SSTs in the Southern Ocean above  $3^\circ\text{C}$ .

Based on the sedimentological records, we speculate that during this transition at  $\sim 4.6 \text{ Ma}$ , basal melt led to thinning of the ice sheet margin and variability in ice shelf surface melt due to a larger influence of high-latitude insolation. The implication is that a larger marine-based ice sheet can be maintained in the Wilkes Basin with SSTs up to  $2\text{--}3^\circ\text{C}$ . However, once SSTs periodically rise above  $3^\circ\text{C}$ , continued warming may have caused the ice sheet to become more susceptible to high-latitude warming, in agreement with previous modeling studies [Mengel and Levermann, 2014].

## 2.6 References

- Abe-Ouchi, A., F. Saito, K. Kawamura, M. E. Raymo, J. I. Okuno, K. Takahashi, and H. Blatter (2013), Insolation-driven 100,000-year glacial cycles and hysteresis of ice sheet volume, *Nature*, 500(7461), 190–193.
- Alvarez-Solas, J., S. Charbit, C. Ritz, D. Paillard, G. Ramstein, and C. Dumas (2010), Links between ocean temperature and iceberg discharge during Heinrich events, *Nat. Geosci.*, 3(2), 122–126.
- Andersson, C., D. Warnke, J. Channell, J. Stoner, and E. Jansen (2002), The mid-Pliocene (4.3 – 2.6 Ma) benthic stable isotope record of the Southern Ocean: ODP Sites 1092 and 704, Meteor Rise, *Palaeogeogr. Palaeoclimatol. Palaeoecol.*, 182, 165–181.
- Bartoli, G., B. Hönisch, and R. E. Zeebe (2011), Atmospheric CO<sub>2</sub> decline during the Pliocene intensification of Northern Hemisphere glaciations, *Paleoceanography*, 26, PA4213, doi:10.1029/2010PA002055.
- Blott, S. J., and K. Pye (2001), GRADISTAT: A grain size distribution and statistics package for the analysis of unconsolidated sediments, *Earth Surf. Processes Landforms*, 26(11), 1237–1248.
- Caburlotto, A., R. G. Lucchi, L. De Santis, P. Macrì, and R. Tolotti (2010), Sedimentary processes on the Wilkes Land continental rise reflect changes in glacial dynamic and bottom water flow, *Int. J. Earth Sci.*, 99(4), 909–926.

- Cook, C. P., et al. (2013), Dynamic behaviour of the East Antarctic Ice Sheet during Pliocene warmth, *Nat. Geosci.*, 6(9), 765–769. Crowley, T. J. (1996), Pliocene climates: The nature of the problem, *Mar. Micropaleontol.*, 27(1), 3–12.
- Damiani, D., G. Giorgetti, and I. M. Turbanti (2006), Clay mineral fluctuations and surface textural analysis of quartz grains in Pliocene–Quaternary marine sediments from Wilkes Land continental rise (East-Antarctica): Paleoenvironmental significance, *Mar. Geol.*, 226(3), 281–295.
- de Boer, P. L., and D. G. Smith (1994), *Orbital Forcing and Cyclic Sequences*, IAS Spec. Publ., vol. 19, pp. 1–14, Blackwell Scientific Publ., Oxford. DeMaster, D. J. (1981), The supply and accumulation of silica in the marine environment, *Geochim. Cosmochim. Acta*, 5, 1715–1732. Escutia, C., L. De Santis, F. Donda, R. B. Dunbar, A. K. Cooper, G. Brancolini, and S. L. Eittreim (2005), Cenozoic ice sheet history from East Antarctic Wilkes Land continental margin sediments, *Global Planet. Change*, 45(1), 51–81.
- Escutia, C., M. A. Bárcena, R. G. Lucchi, O. Romero, A. M. Ballegeer, J. J. Gonzalez, and D. M. Harwood (2009), Circum-Antarctic warming events between 4 and 3.5 Ma recorded in marine sediments from the Prydz Bay (ODP Leg 188) and the Antarctic Peninsula (ODP Leg 178) margins, *Global Planet. Change*, 69(3), 170–184.

- Evans, J., and C. J. Pudsey (2002), Sedimentation associated with Antarctic Peninsula ice shelves: Implications for palaeoenvironmental reconstructions of glacial marine sediments, *J. Geol. Soc.*, 159(3), 233–237.
- Expedition 318 Scientists (2011), Wilkes land glacial history: Cenozoic East Antarctic Ice Sheet evolution from Wilkes Land margin sediments IODP Prel. Rept., 318.
- Fedorov, A. V., C. M. Brierley, K. T. Lawrence, Z. Liu, P. S. Dekens, and A. C. Ravelo (2013), Patterns and mechanisms of early Pliocene warmth, *Nature*, 496(7443), 43–49. Folk, R. L., and W. C. Ward (1957), Brazos River bar: A study in the significance of grain size parameters, *J. Sediment. Res.*, 27(1), 3–26, doi:10.1306/74D70646-2B21-11D7-8648000102C1865D.
- Goldner, A., N. Herold, and M. Huber (2014), Antarctic glaciation caused ocean circulation changes at the Eocene-Oligocene transition, *Nature*, 511(7511), 574–577.
- Goldschmidt, P. M., S. L. Pfirman, I. Wollenburg, and R. Henrich (1992), Origin of sediment pellets from the Arctic seafloor: Sea ice or icebergs?, *Deep-Sea Res., Part A*, 39(2), S539–S565.
- Gradstein, F. M., J. G. Ogg, and A. G. Smith (Eds.). (2004), *A Geologic Time Scale 2004*, vol. 86, Cambridge Univ. Press, Cambridge, U. K.
- Grützner, J., C. D. Hillenbrand, and M. Rebesco (2005), Terrigenous flux and biogenic silica deposition at the Antarctic continental rise during the late Miocene to early Pliocene: Implications for ice sheet stability and sea ice coverage, *Global Planet. Change*, 45(1), 131–149.



- Hammer, Ø., D. A. Harper, and P. D. Ryan (2001), PAST: Paleontological statistics software package for education and data analysis, *Palaeontol. Electron.*, 4(1), 1–9.
- Haug, G., R. Tiedemann, R. Zahn, and A. Ravelo (2001), Role of Panama uplift on oceanic freshwater balance, *Geology*, 29(3), 207–210. Haug, G. H., and R. Tiedemann (1998), Effect of the formation of the Isthmus of Panama on Atlantic Ocean thermohaline circulation, *Nature*, 393(6686), 673–676.
- Hemming, S. R., C. M. Hall, P. E. Biscaye, S. M. Higgins, G. C. Bond, J. F. McManus, D. C. Barber, J. T. Andrews, and W. S. Broecker (2002),  $^{40}\text{Ar}/^{39}\text{Ar}$  ages and  $^{40}\text{Ar}^*$  concentrations of fine-grained sediment fractions from North Atlantic Heinrich layers, *Chem. Geol.*, 182(2), 583–603.
- Hesse, R., and S. Khodabakhsh (2006), Significance of fine-grained sediment lofting from melt-water generated turbidity currents for the timing of glaciomarine sediment transport into the deep sea, *Sediment. Geol.*, 186(1), 1–11.
- Hulbe, C. L., D. R. MacAyeal, G. H. Denton, J. Kleman, and T. V. Lowell (2004), Catastrophic ice shelf breakup as the source of Heinrich event icebergs, *Paleoceanography*, 19, PA1004, doi:10.1029/2003PA000890.
- Jansen, E., et al. (2007), Palaeoclimate, in *Climate Change 2007: The Physical Science Basis. Contribution of Working Group I to the Fourth Assessment Report of the Intergovernmental Panel on Climate Change*, edited by S. Solomon et al., pp. 433–497, Cambridge Univ. Press, Cambridge, U. K., and New York.

- Joughin, I., R. B. Alley, and D. M. Holland (2012), Ice-sheet response to oceanic forcing, *Science*, 338(6111), 1172–1176.
- Joughin, I., B. E. Smith, and B. Medley (2014), Marine ice sheet collapse potentially under way for the Thwaites Glacier Basin, West Antarctica, *Science*, 344(6185), 735–738.
- Kennett, J. P., and D. A. Hodell (1993), Evidence for relative climatic stability of Antarctica during the early Pliocene: A marine perspective, *Geogr. Ann. Ser. A. Phys. Geogr.*, 75, 205–220.
- Konert, M., and J. E. F. Vandenberghe (1997), Comparison of laser grain size analysis with pipette and sieve analysis: A solution for the underestimation of the clay fraction, *Sedimentology*, 44(3), 523–535.
- Krissek, L. (1995), Late Cenozoic ice-rafting records from Leg 145 sites in the North Pacific: Late Miocene onset, late Pliocene intensification, and Pliocene-Pleistocene events, in *Proceedings of the Ocean Drilling Program, Sci. Results*, vol. 145, edited by D. K. Rea et al., pp. 179–194, Ocean Drilling Program, College Station, Tex.
- Laskar, J., P. Robutel, F. Joutel, M. Gastineau, A. C. M. Correia, and B. Levrard (2004), A long-term numerical solution for the insolation quantities of the Earth, *Astron. Astrophys.*, 428(1), 261–285.

- Lawson, D. E., J. C. Strasser, E. B. Evenson, R. B. Alley, G. J. Larson, and S. A. Arcone (1998), Glaciohydraulic supercooling: A freeze-on mechanism to create stratified, debris-rich basal ice: I. Field evidence, *J. Glaciol.*, 44(148), 547–562.
- Liebrand, D., L. J. Lourens, D. A. Hodell, B. De Boer, R. S. W. Van de Wal, H. Pälike, and L. Beaufort (2011), Antarctic ice sheet and oceanographic response to eccentricity forcing during the early Miocene, *Clim. Past*, 7(3), 869–880.
- Lisiecki, L. E., and M. E. Raymo (2005), A Pliocene-Pleistocene stack of 57 globally distributed benthic  $\delta^{18}\text{O}$  records, *Paleoceanography*, 20, PA1003, doi:10.1029/2004PA001071.
- Marcott, S. A., et al. (2011), Ice-shelf collapse from subsurface warming as a trigger for Heinrich events, *Proc. Natl. Acad. Sci. U.S.A.*, 108(33), 13,415–13,419.
- McKay, R., et al. (2012), Antarctic and Southern Ocean influences on Late Pliocene global cooling, *Proc. Natl. Acad. Sci. U.S.A.*, 109(17), 6423–6428.
- Mengel, M., and A. Levermann (2014), Ice plug prevents irreversible discharge from East Antarctica, *Nat. Clim. Change*, 4(6), 451–455.
- Mortlock, R. A., and P. N. Froelich (1989), A simple method for the rapid determination of biogenic opal in pelagic marine sediments, *Deep-Sea Res., Part A*, 36, 1415–1426.
- Müller, P. J., and R. Schneide (1993), An automated leaching method for the determination of opal in sediments and particulate matter, *Deep Sea Res., Part I*, 40, 425–444.

- Murphy, L., D. A. Warnke, C. Andersson, J. Channell, and J. Stoner (2002), History of ice rafting at South Atlantic ODP Site 177–1092 during the Gauss and late Gilbert Chrons, *Palaeogeogr. Palaeoclimatol. Palaeoecol.*, 182(3), 183–196.
- Naish, T., et al. (2009), Obliquity-paced Pliocene West Antarctic ice sheet oscillations, *Nature*, 458(7236), 322–328.
- Orejola, N., S. Passchier, Expedition 318 Scientists (2014), Sedimentology of lower Pliocene to upper Pleistocene diamictons from IODP Site U1358, Wilkes Land margin, and implications for East Antarctic Ice Sheet dynamics, *Antarct. Sci.*, 26, 183–192, doi:10.1017/S0954102013000527.
- Pagani, M., Z. Liu, J. LaRiviere, and A. Ravelo (2010), High Earth-system climate sensitivity determined from Pliocene carbon dioxide concentrations, *Nat. Geosci.*, 3, 27–30.
- Passchier, S. (2011), Linkages between East Antarctic Ice Sheet extent and Southern Ocean temperatures based on a Pliocene high-resolution record of ice-rafted debris off Prydz Bay, East Antarctica, *Paleoceanography*, 26, PA4204, doi:10.1029/2010PA002061.
- Patterson, M. O., et al. (2014), Orbital forcing of the East Antarctic ice sheet during the Pliocene and Early Pleistocene, *Nat. Geosci.*, 7(11), 841–847.
- Paul, H. A., J. C. Zachos, B. P. Flower, and A. Tripathi (2000), Orbitally induced climate and geochemical variability across the Oligocene/Miocene boundary, *Paleoceanography*, 15(5), 471–485, doi:10.1029/1999PA000443.

- Powell, R. D., and E. Domack (1995), Modern glaciomarine environments, *Glacial Environ.*, 1, 445–486.
- Prentice, M. L., and R. K. Matthews (1991), Tertiary ice sheet dynamics: The snow gun hypothesis, *J. Geophys. Res.*, 96(B4), 6811–6827, doi:10.1029/90JB01614.
- Rashid, H., R. Hesse, and D. J. Piper (2003), Origin of unusually thick Heinrich layers in ice-proximal regions of the northwest Labrador Sea, *Earth Planet. Sci. Lett.*, 208(3), 319–336.
- Rashid, H., F. Saint-Ange, D. C. Barber, M. E. Smith, and N. Devalia (2012), Fine scale sediment structure and geochemical signature between eastern and western North Atlantic during Heinrich events 1 and 2, *Quat. Sci. Rev.*, 46, 136–150.
- Raymo, M. E., and K. Nisancioglu (2003), The 41 kyr world: Milankovitch's other unsolved mystery, *Paleoceanography*, 18(1), 1011, doi:10.1029/2002PA000791.
- Raymo, M. E., B. Grant, M. Horowitz, and G. H. Rau (1996), Mid-Pliocene warmth: Stronger greenhouse and stronger conveyor, *Mar. Micropaleontol.*, 27(1), 313–326.
- Rignot, E., S. Jacobs, J. Mouginot, and B. Scheuchl (2013), Ice-shelf melting around Antarctica, *Science*, 341(6143), 266–270.
- Seki, O., G. L. Foster, D. N. Schmidt, A. Mackensen, K. Kawamura, and R. D. Pancost (2010), Alkenone and boron-based Pliocene pCO<sub>2</sub> records, *Earth Planet. Sci. Lett.*, 292(1), 201–211.

- Shevenell, A. E., J. P. Kennett, and D. W. Lea (2008), Middle Miocene ice sheet dynamics, deep-sea temperatures, and carbon cycling: A Southern Ocean perspective, *Geochem., Geophys., Geosyst.*, 9, Q02006, doi:10.1029/2007GC001736.
- Sperazza, M., J. N. Moore, and M. S. Hendrix (2004), High-Resolution particle size analysis of naturally occurring very fine-grained sediment through laser diffractometry: RESEARCH METHODS PAPERS, *J. Sediment. Res.*, 74(5), 736–743.
- St. John, K., S. Passchier, B. Tantillo, D. Darby, and L. Kearns (2015), Microfeatures of modern sea ice-rafted sediment and implications for paleo-sea ice reconstructions, *Ann. Glaciol.*, 56(69), 83–93.
- Steph, S., R. Tiedemann, M. Prange, J. Groeneveld, M. Schulz, A. Timmermann, D. Nürnberg, C. Rühlemann, C. Saukel, and G. H. Haug (2010), Early Pliocene increase in thermohaline overturning: A precondition for the development of the modern equatorial Pacific cold tongue, *Paleoceanography*, 25, PA2202, doi:10.1029/2008PA001645.
- Tauxe, L., et al. (2012), Chronostratigraphic framework for the IODP Expedition 318 cores from the Wilkes Land Margin: Constraints for paleoceanographic reconstruction, *Paleoceanography*, 27, PA2214, doi:10.1029/2012PA002308.
- Torrence, C., and G. P. Compo (1998), A practical guide to wavelet analysis, *Bull. Am. Meteorol. Soc.*, 79(1), 61–78. Weber, M. E., et al. (2014), Millennial-scale

variability in Antarctic ice sheet discharge during the last deglaciation, *Nature*, 510(7503), 134–138. Whitehead, J., and S. Bohaty (2003), Pliocene summer sea surface temperature reconstruction using silicoflagellates from Southern Ocean ODP Site 1165, *Paleoceanography*, 18(3), 1075, doi:10.1029/2002PA000829.

Williams, T., T. van de Flierdt, S. R. Hemming, E. Chung, M. Roy, and S. L. Goldstein (2010), Evidence for iceberg armadas from East Antarctica in the Southern Ocean during the late Miocene and early Pliocene, *Earth Planet. Sci. Lett.*, 290(3), 351–361.

Woodard, S. C., Y. Rosenthal, K. G. Miller, J. D. Wright, B. K. Chiu, and K. T. Lawrence (2014), Antarctic role in Northern Hemisphere glaciation, *Science*, 346(6211), 847–851.

Zachos, J., M. Pagani, L. Sloan, E. Thomas, and K. Billups (2001), Trends, rhythms, and aberrations in global climate 65 Ma to present, *Science*, 292(5517), 686–693. Zhang, Z., K. H. Nisancioglu, and U. S. Ninnemann (2013), Increased ventilation of Antarctic deep water during the warm mid-Pliocene, *Nat. Commun.*, 4, 1499.

## CHAPTER 3

### Ventilation of the Southern Ocean During the Pliocene Climatic Optimum

#### Abstract

We examine early Pliocene (~4.7-4.3 Ma) Southern Ocean circulation changes by reconstructing sedimentary redox and paleoproductivity at Integrated Ocean Drilling Program (IODP) Site U1359 on the Wilkes Land continental rise. The Southern Ocean plays a significant role in the formation of deep water and in the exchange of heat and dissolved gases with the atmosphere. At 4.6 Ma, Mn/Al maxima indicate a shift from suboxic to oxic conditions resulting from the enhanced production of Antarctic bottom water. The interval of high Mn/Al at 4.6 Ma is overlain by an interval of extremely high Ba-excess values exceeding 40,000 ppm, in the presence of sedimentary barite. Elevated levels of Ba-excess are the result of high productivity events in response to an increase in the availability of nutrients supplied by upwelling and terrigenous dust. Ventilation of deepwater during the Pliocene Climatic Optimum allows for a role for the Southern Ocean in carbon cycle feedbacks during previous warm periods.

**Keywords:** Southern Ocean, early Pliocene, deepwater formation, biogenic bloom



## 5.1 Introduction

The Pliocene Climatic Optimum (PCO) encompasses a period of time between ~4.5 and 4.0 Ma when the Southern Hemisphere was warmer and global temperatures were ~4°C higher than preindustrial (Fedorov et al., 2013). The mechanisms of early Pliocene warming are poorly understood and probably involve dynamical feedbacks related to changes in ocean mixing. Considerable climate variability and productivity changes have been observed in early Pliocene paleorecords of the Southern Ocean and the Ross Sea, where deposition of diatomaceous sediments was significantly increased and sea surface temperatures (SSTs) ranged between 1.5 and 5.7°C (Escutia et al., 2009; Naish et al., 2009; McKay et al., 2012; Whitehead & Bohaty, 2003).

Today, the Southern Ocean is a key component of the climate system with unconstrained westerlies allowing for intense mixing and exchange between deepwater and the atmosphere. Antarctic shelf waters are a major sink for CO<sub>2</sub> due to their high rates of primary productivity, intense winds, ventilation and sea ice cover (Arrigo et al., 2008). Ocean circulation changes, however, may impact the net rate of carbon uptake (Morrison et al., 2015). The PCO is a useful analog to assess the interactions of the Antarctic Ice Sheets with the ocean in a warmer world.

The purpose of this work is to determine the effects of warming on the interaction between the ice sheet and Southern Ocean circulation changes using major and trace elemental geochemistry. Major and trace elements exhibit differing redox behavior and can provide insight into paleoproductivity and ocean circulation changes. Seafloor redox evolution can be assessed using downcore Mn/Al ratios (Reinhard et al., 2013; Gallego-

Torres et al., 2014) while marine paleoproductivity can be evaluated using Ba-excess accumulation (Schenau et al., 2001). These paleoredox and paleoproductivity tracers are applied to marine sediments from Integrated Ocean Drilling Program (IODP) Site U1359 (Figure 1) located on the Wilkes Land continental rise (64°S 143°E) at 4003 meters below sea level (mbsl) (Expedition 318 Scientists, 2011). Site U1359 lies on the eastern levee of the Jussieu submarine channel, south of the current Polar Front (Figure 3-1), and the sedimentation may have been influenced by a change in the Southern Ocean currents and nutrient supply during the PCO. This study focuses specifically on Hole U1359B, which was drilled to a total depth of 252.0 meters below sea floor (mbsf) and contains a complete, high resolution record. Original core data was analyzed on a meters composite depth (mcd) scale and was converted to meters below seafloor in Hole U1359A (mbsf-A) to allow comparison to the detailed lithological log (Hansen et al., 2015). Age tie points were linearly correlated using magnetostratigraphic age datums from Tauxe et al. (2012) and the complete section of focus represents a time span between 4.3 and 4.7 Ma. This time period captures a major IRD MAR excursion identified by Hansen et al. (2015) that leads into the beginning of PCO (4.5 - 4.0 Ma). All major and trace element abundances were derived using 106 bulk sediment samples from IODP Hole U1359B on a Jobin-Yvon ULTIMA C inductively coupled plasma optical emission spectrometer (ICP-OES).

Paleoproductivity can be determined by analyzing downcore variations in Ba-excess. In deep-sea sediment, barium arrives mainly as barite particles ( $\text{BaSO}_4$ ) in association with decaying organic matter (Jaccard et al., 2009; Tribovillard et al., 2006;

Schenau et al., 2001; Dickens & Owen, 1996). The preservation of barium within marine sediment depends on certain environmental conditions such as barite saturation within the water column and the redox conditions of bottom water and surface sediment (Schenau et al., 2001). Ba-excess assumes that Ba concentrations above estimated detrital input represents marine barite and should be approached with caution when used as a paleoproductivity indicator as it may overestimate the amount of marine barite present (Eagle et al., 2003; Hendy, 2010). In order to confirm the presence of biogenic barite, bulk powdered sediment from Ba-excess maxima were prepared based on a method by Riedinger et al. (2006) and viewed on a Hitachi S-3400N Scanning Electron Microscope (SEM) with a Bruker-AXS Xflash Energy Dispersive X-ray spectrometer (EDX) (See Appendix C for more details).

## **5.2 Geochemical Variations in U1359B**

When sediments are comprised of a terrigenous fraction greater than 5-wt%, the Al/Ti ratio can be utilized as a way to assess changes in terrigenous provenance (Latimer et al., 2006). The lack of variation in the downcore trend of Al/Ti in Figure 3-2 suggests that there were no major provenance changes within the record. Any variations in elemental abundances and ratios discussed below can therefore be attributed to fluctuations in corresponding biogeochemical processes, including redox environment and paleoproductivity.

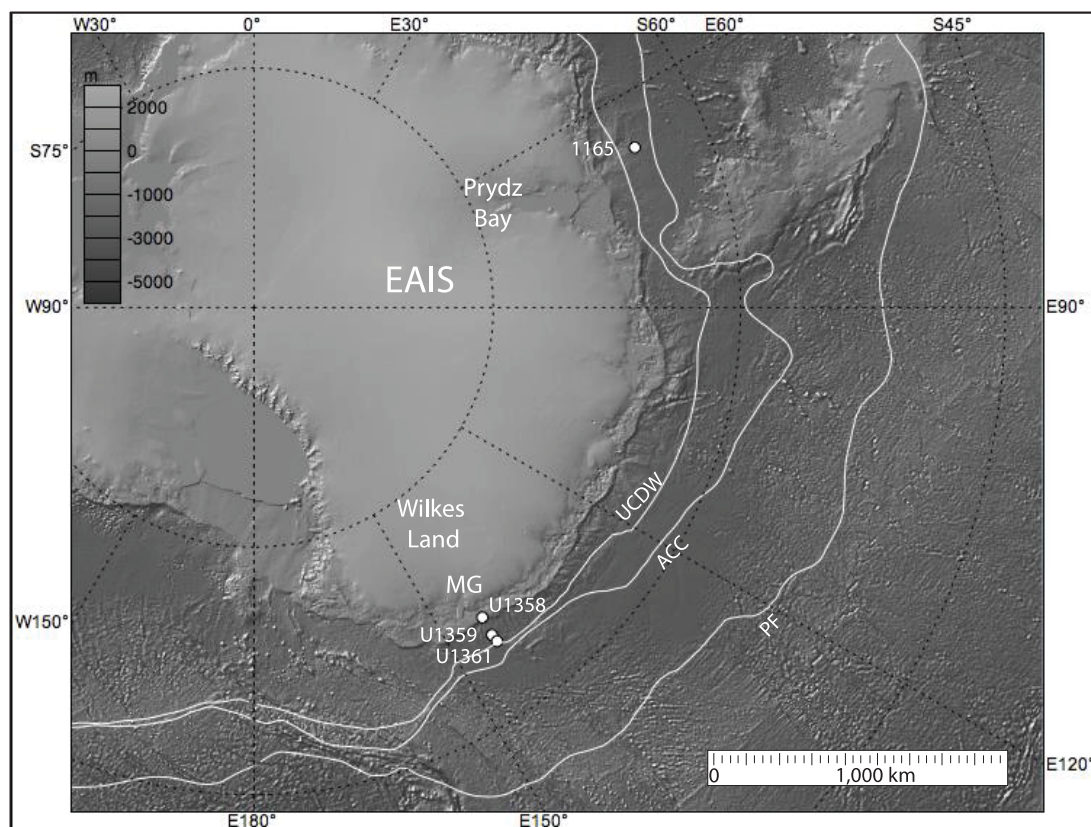


**Figure 3-1. The location of Mertz Glacier (MG) in Wilkes Land, Antarctica with continental rise Sites U1359 and U1361, shelf Site U1358, and Prydz Bay continental rise site 1165. The position of the Antarctic Polar Front (PF), southern boundary for the Antarctic Circumpolar Current (ACC) and southern limit of upwelling circumpolar deep water (UCDW) based on Orsi et al. (1995).**

### 3.2.1 Paleoredox Conditions

At Site U1359, prominent peaks of Mn/Al occur between 111 and 115 mbsf-A (Figure 3-2). Mn is present in microcrystalline form; manganese nodules or grains were not observed in these intervals. These peaks are concurrent with a section of alternating

clay with diatom laminae. Mn can be supplied to the ocean as oxide coatings on particulates delivered by wind, rivers or by diffusion from shelf sediments (Burdige, 1993; Calvert & Pedersen, 1993). The depth of the redox boundary for Mn within sediments is controlled by oxygen concentrations (Burdige, 1993). In reducing sediments, Mn is a very mobile element and can escape into the water column. In contrast, Mn can be trapped within authigenic Mn-carbonates or oxides under oxidizing conditions (Calvert & Pedersen, 1993, Mangini et al., 2001; Tribovillard et al., 2006).

The distribution of Mn/Al maxima in U1359 between 111 and 115 mbsf-A (Figure 3-2) could represent an intermittent period of enhanced downwelling of an oxygen rich water mass, such as AABW, which impacted the accumulation of Mn in the sediment. The deposition of clay-sized particles within this interval indicates a lack of strong current interaction with the seafloor. In a benthic marine environment, oxygen conditions can be determined by comparing Mn/Al ratios to those of upper continental crust (Pattan et al., 2013). During the decay of organic matter, microbes will utilize sequentially oxygen, nitrate, Fe (III), and Mn (IV, III) (Froelich, 1979; Pattan et al., 2013) resulting in suboxic conditions. Therefore, a high Mn/Al ratio will indicate a remobilization of Mn through pore waters and oxic conditions. The values (~0.01 to 0.08 wt%) between 111 and 115 mbsf-A are high compared to average upper continental crust (0.0075 for Mn/Al; Taylor & McLennan, 1985) and indicate oxic conditions. The relatively low values of Mn/Al (Figure 3-2) below and above the maxima, suggest that sediments are deposited under suboxic conditions.

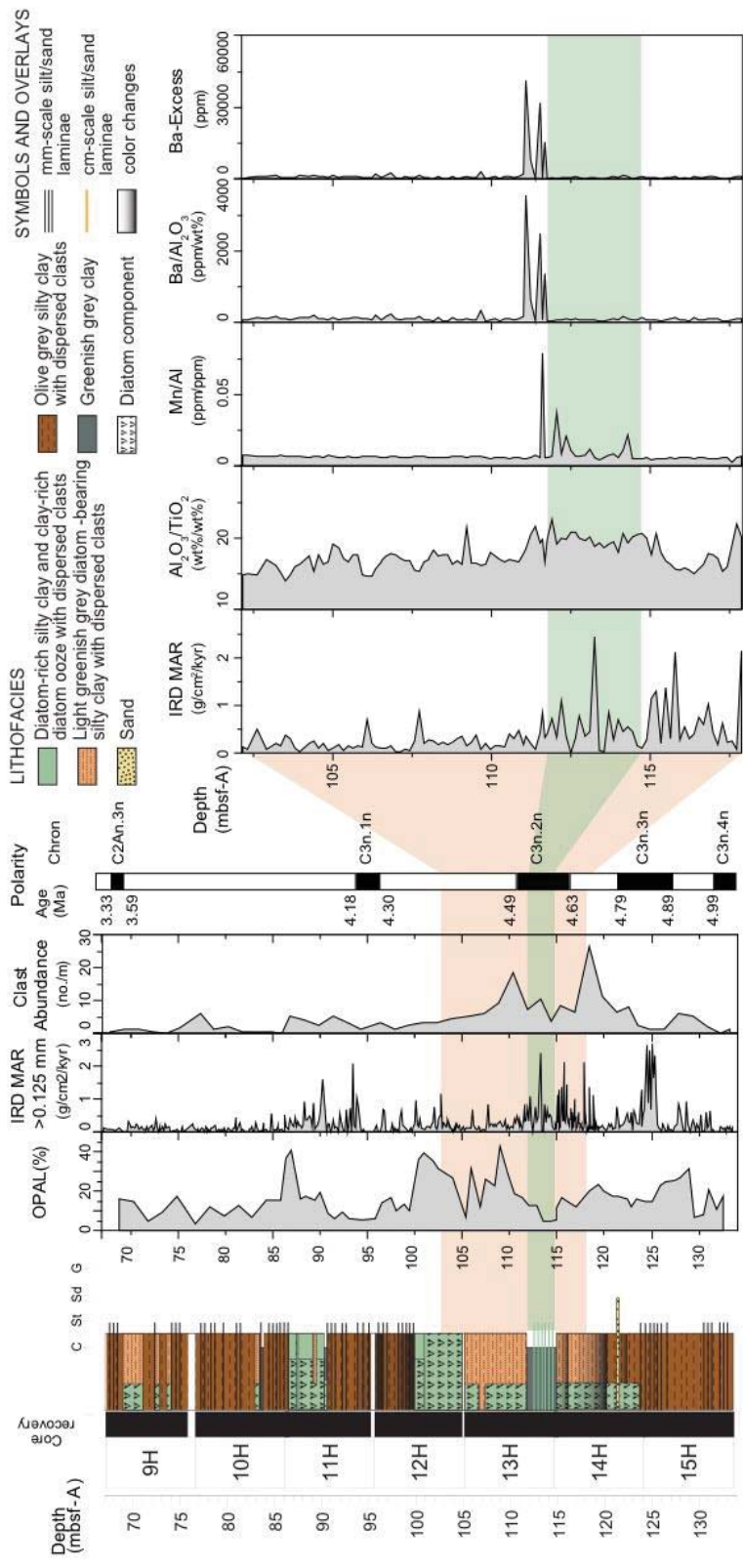


**Figure 3-2. Data for Hole U1359B are shown on mbsf-A scale to allow correlation to lithological log for Hole U1359A. Distribution of (A) Opal (B) ice-rafted debris (IRD) mass accumulation rates (MAR), and (C) Gravel (Clast Abundance) after Hansen et al. (2015). (D) Magnetostratigraphy log after Tauxe et al. (2012). (E – I) Detailed summary of IRD MAR and chemical ratios during the early Pliocene for section dated between ~4.7-4.3 Ma.**

### **3.2.1 Paleoproductivity Bloom**

In order to calculate Ba-excess (Schenau et al., 2001) we derived the lithogenic Ba-content from the average composition of clasts dredged from the seafloor near Mertz Glacier determined by Goodge & Fanning (2010). The clasts may be derived from the Mertz Glacier and are assumed to be representative of the local bedrock, which is inaccessible due to the current presence of ice. Ba-excess shows enrichment stratigraphically above the clay/diatom laminae interval with maxima reaching in excess of 40,000 ppm (Figure 3-2). Two samples, representing the highest peaks of Ba-excess (at a depth of 111.06 and 11.51 mbsf-A), were selected to view on the SEM to confirm the presence of marine barite ( $\text{BaSO}_4$ ). The presence of marine barite was confirmed through EDX (Figure 3-3, See Also Appendix C Figure C-3) by comparing the collected spectra (Figure 3-3D) to a known reference spectrum presented in Riedinger et al. (2006).



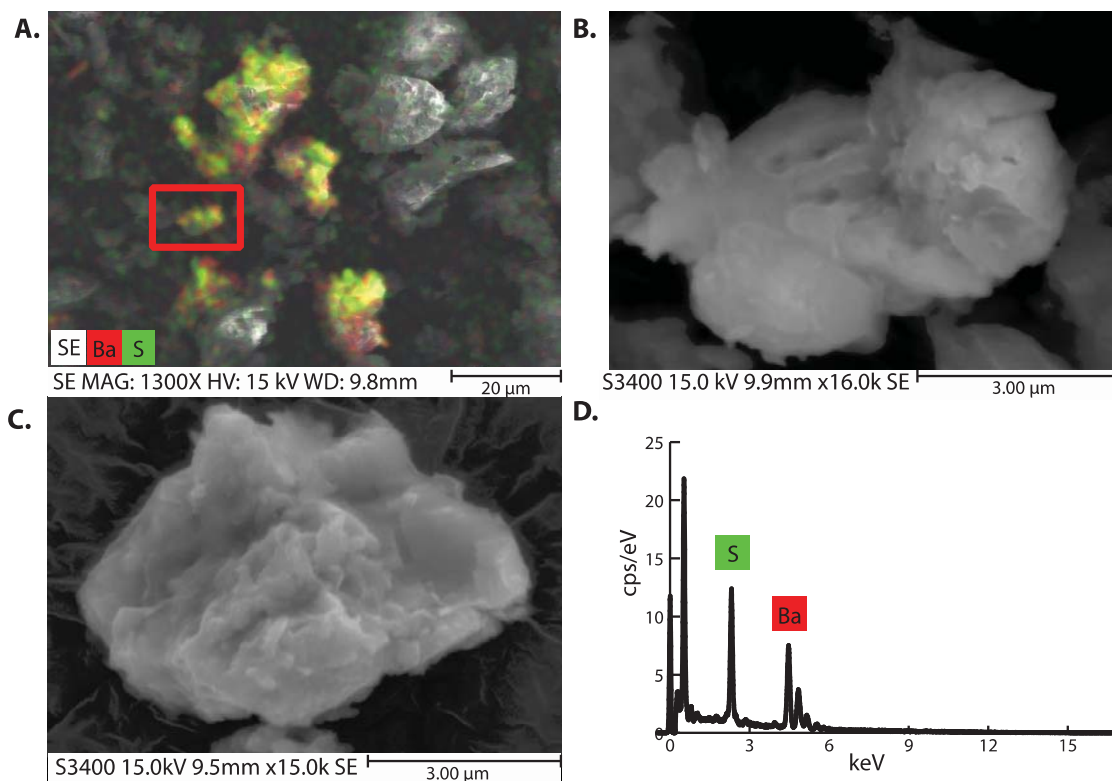


**Figure 3-3. Barite particles identified using EDS mapping tool highlighting elements Barium (red) and Sulfur (green) (A). Enlarged image of barite grain (highlighted in red box) (B). SEM micrograph of sedimentary barite (C) and EDS spectra (D).**

In the Southern Ocean, modern and Pleistocene Ba-excess concentrations in the bulk sediment are extremely high compared to the world ocean (Nürnberg et al., 1997, Bonn et al., 1998; Fagel et al., 2002). Ba-excess concentrations in the sediments vary on glacial-interglacial timescales and are highest during interglacials. At high latitudes, however, barite can also reach high concentrations in the sediment through the dissolution of  $\text{CaCO}_3$  (Anderson & Winckler, 2005). Maxima of 28 to >3000 ppm of excess Ba occur in cores from the Polar Front Zone and near the edge of the Seasonal Sea



Ice Zone, with a minimum within the Antarctic Divergence. There, upwelling of oxygen poor water masses diminishes the oxidation of suspended organic matter and prevents the release of sedimentary barite crystals from the water column (Dehairs et al., 1990).

Extremely high values of Ba-excess in U1359 occur in a core section that is well-dated to ~4.4-4.5 Ma (Figure 3-2). These high Ba-excess values are suggestive of increased primary productivity, barite preservation, and concentration in the Southern Ocean at the onset of the Pliocene Climatic Optimum. So-called “biogenic blooms” with global distribution have been documented during the Late Miocene-early Pliocene near upwelling zones (Dickens & Owen, 1999; Cortese et al., 2004). Primary productivity is limited by nutrient availability, ocean stratification and growing season duration, which, for the Southern Ocean, have been linked to sea ice, upwelling, wind strength, and glacier dynamics (Anderson et al., 2009; Denis et al., 2009).

### **5.3 Nutrient Pathways and Utilization in the Southern Ocean**

Iron is an essential and limiting nutrient for primary productivity in the Southern Ocean (Martin, 1990). However, iron can be delivered to the ocean through several different processes or a combination thereof: (1) enhanced upwelling of warm, nutrient rich deep water through a southward shift in the Southern Hemisphere Westerlies (Anderson et al., 2009); (2) southward migration of the polar front zone (an area rich in nutrients through upwelling) due to reduced winter sea-ice formation, a decrease in the salinity contrasts between the Antarctic and Subantarctic water masses, or weakening of the thermal gradient (Bohaty & Harwood, 1998); (3) release of dust loads from melting icebergs and sea ice that enhance the bioavailability of iron in surface waters (Abelmann

et al., 2006); (4) retreat of the ice sheet from the marine basin permitting aeolian transport of terrigenous iron dust to the open ocean. These processes are examined based on known climate and ice sheet conditions for the PCO.

Today, a polynya lies above the Adélie Depression west of the Mertz Glacier (Bindoff et al., 2000). Polynyas are active regions of sea ice formation, high salinity shelf water and AABW production (Arrigo & van Dijken, 2003; Bindoff et al., 2000). The Mertz coastal polynya is a region that contributes to the formation of oxygen-rich Antarctic Bottom Water (AABW), which occupies the abyssal layer of the ocean and provides oxygen and nutrients to deep marine environments through downwelling. Adélie Land Bottom Water is a cold, dense, and high-oxygen water mass that contributes up to 25% of the global volume of AABW, and forms locally near the Adélie Coast of Antarctica (Rintoul et al., 2001).

Changes in the delivery of a high oxygen bottom water mass have been indicated at U1359 by Mn/Al maxima (Figure 3-2) and suggest that the production of AABW was enhanced ~4.6-4.5 Ma. Sea surface temperatures (SSTs) in the early Pliocene (4.6 – 4.5 Ma) varied between 1 and 5°C (McKay et al., 2012; Whitehead & Bohaty, 2003; Escutia et al., 2009) and seasonal sea ice formation cannot be ruled out as a contributor to AABW formation.

Between 4.5 and 4.3 Ma, however, during the Pliocene Climatic Optimum, SSTs in the Southern Ocean were more stable and warm at 4-5°C (McKay et al., 2012; Whitehead & Bohaty, 2003; Escutia et al., 2009). During this time the Ba-excess at Site U1359 reach their maximum. Reduced sea ice coverage has been documented by high

opal contents at U1359 (Figure 3-2; Hansen et al., 2015). At Site U1358 (Figure 1) on the shelf, only ~100 km landward of Site U1359, elevated Ba-excess values were found (Orejola et al., 2014) between 4.45 and 4.38 Ma, using the new age model of Reinardy et al. (2015), indicating open marine and highly productive conditions. Furthermore, ice sheet retreat inland during Pliocene warmth was demonstrated by Cook et al. (2013) based on the provenance of marine sediment from nearby core Site U1361.

High gravel contents at 4.6-4.5 Ma in U1359 (Figure 2) are interpreted as ice shelf collapse in response to ocean warming, and are accompanied by a shift in orbital cyclicity of ice-rafted debris mass accumulation rates (IRD MAR) (Hansen et al., 2015). A greater number of aeolian quartz sand grains mixed with glacial grains were noted within this section and above, dated at ~4.5-4.0 Ma (Hansen et al., 2015 their Figure 3; see also Chapter 2 Figure 2-3) and may suggest an increase in the influx of dust-born sediment. Hence, wind-blown iron-bearing dust could have been a contributing factor to the increase in primary productivity at ~4.5 Ma as indicated by the high Ba-excess values.

Short term Pliocene diatom blooms have also been reported as the partial collapse of the Antarctic Peninsula Ice Sheet (APIS) generated pulses of freshwater, and allowed dust-bound iron fertilization (Hepp et al., 2009). Deglaciation and reduced sea ice combined with weak bottom currents may have enhanced the availability of light and nutrients through melt out (Abelmann et al., 2006; Hepp et al., 2009). Ice-free conditions can lead to a longer growing season and result in higher surface productivity and greater organic burial (Denis et al., 2009).

The iron-rich polar front has also been considered as a major contributor for primary production and greater magnitude of biogenic blooms in the Southern Ocean (de Baar et al., 1995). The current position of the Polar Front varies spatially and has a more southerly, poleward, position in the Pacific Ocean Sector (Dong et al., 2006; Orsi et al., 1995). The position of the Antarctic polar front may have been located further south from its present location in the Pliocene at ~4.5 Ma based on silicoflagellates recorded at Site 1165 (Figure 1) (Whitehead & Bohaty, 2003; Bohaty & Harwood, 1998). The polar front may have shifted landward near the Wilkes Land rise as well. These conditions concordant with warmer sea surface temperatures may have created a suitable environment for increased primary productivity.

Based on the climate conditions mentioned above, more than one process may have been in place and led to more oxic conditions and increased primary productivity. An earth system model by Zhang et al. (2013) using Pliocene boundary conditions shows that even in the absence of sea ice an intensified poleward shift of winds leads to greater downwelling and ventilation and reduced stratification. An increase in wind stress can lead to an increased Ekman convergence which causes enhanced downwelling. This shift in winds may have driven stronger downwelling of oxygenated, deep water towards Site U1359 at ~4.6-4.5 Ma. At ~4.5-4.3 Ma, however, circumpolar deepwater (CDW) brought heat and nutrients to the Wilkes Land continental rise (U1359) and shelf (U1358; Orejola et al., 2014; Reinardy et al., 2015), resulting in enhanced primary productivity. Barite concentrations in the sediment may be enhanced further due to  $\text{CaCO}_3$  dissolution by the corrosive water mass.

In the Southern Ocean, biogenic blooms are considered an important means of carbon export via CO<sub>2</sub> drawdown from the atmosphere (de Baar et al., 1995). The Southern Ocean's ability to take up CO<sub>2</sub>, however, may have weakened due to intense wind-driven upwelling and the associated ventilation of carbon rich subsurface waters (Le Quere et al., 2007). The importance of carbon cycle feedbacks in the warming during the Pliocene Climatic Optimum is corroborated by reconstructions of pCO<sub>2</sub> maxima for this time (Bartoli et al., 2011; Pagani et al., 2010; Seki et al., 2010). Thus, the results from this study emphasize the potential role of ice sheet – Southern Ocean-carbon cycle feedbacks in a warming world.

#### **5.4 Conclusion**

We provide a geochemical record to assess the impact of Southern Ocean circulation changes during the onset of the early Pliocene climatic optimum (~4.5-4.0 Ma). The data suggests that variations in ocean circulation affected the ventilation of water masses along the Antarctic continental rise. These conditions are transient, however, and encompassed a short period of time in the record. The Mn/Al ratios indicate a transition from suboxic to oxic conditions due to enhanced AABW production. The high Ba values indicate an increase in productivity due to greater nutrient availability in response to wind-driven upwelling or the supply of dust. The formation of deep water and supply of nutrients did not remain constant in the early Pliocene; and enhanced deepwater formation ceased following the productivity event. The implication is that with greater convection through ocean circulation during the early Pliocene, there may be an

indication for enhanced venting of CO<sub>2</sub> in the future or an enhanced carbon burial due to a biogenic bloom.

#### ACKNOWLEDGEMENTS

The preceding research was supported by the National Science Foundation (award OCE 1060080 to S.P.). Samples were provided by the Integrated Ocean Drilling Program. All data presented within this paper is available upon request.

## 5.5 References Cited

- Abelmann, A., Gersonde, R., Cortese, G., Kuhn, G., & Smetacek, V. (2006). Extensive phytoplankton blooms in the Atlantic sector of the glacial Southern Ocean. *Paleoceanography*, *21*(1).
- Anderson, R. F., Ali, S., Bradtmiller, L. I., Nielsen, S. H. H., Fleisher, M. Q., Anderson, B. E., & Burckle, L. H. (2009). Wind-driven upwelling in the Southern Ocean and the deglacial rise in atmospheric CO<sub>2</sub>. *Science*, *323*(5920), 1443-1448.
- Anderson, R. F., & Winckler, G. (2005). Problems with paleoproductivity proxies. *Paleoceanography*, *20*(3).
- Arrigo, K. R., van Dijken, G., & Long, M. (2008). Coastal Southern Ocean: A strong anthropogenic CO<sub>2</sub> sink. *Geophysical Research Letters*, *35*(21).
- Arrigo, K. R., & van Dijken, G. L. (2003). Phytoplankton dynamics within 37 Antarctic coastal polynya systems. *Journal of Geophysical Research: Oceans (1978–2012)*, *108*(C8).
- Bartoli, G., Hönisch, B., & Zeebe, R. E. (2011). Atmospheric CO<sub>2</sub> decline during the Pliocene intensification of Northern Hemisphere glaciations. *Paleoceanography*, *26*(4).
- Bindoff, N. L., Rintoul, S. R., & Massom, R. A. (2000). Bottom water formation and polynyas in Adélie Land, Antarctica. *Papers and Proceedings of the Royal Society of Tasmania*, *133*(3), 51-56.

- Bohaty, S. M., & Harwood, D. M. (1998). Southern Ocean Pliocene paleotemperature variation from high-resolution silicoflagellate biostratigraphy. *Marine Micropaleontology*, 33(3), 241-272.
- Bonn, W. J., Gingele, F. X., Grobe, H., Mackensen, A., & Fütterer, D. K. (1998). Palaeoproductivity at the Antarctic continental margin: opal and barium records for the last 400 ka. *Palaeogeography, Palaeoclimatology, Palaeoecology*, 139(3), 195-211.
- Burdige, D. J. (1993). The biogeochemistry of manganese and iron reduction in marine sediments. *Earth-Science Reviews*, 35(3), 249-284.
- Calvert, S. E., & Pedersen, T. F. (1993). Geochemistry of recent oxic and anoxic marine sediments: implications for the geological record. *Marine geology*, 113(1), 67-88.
- Cook, C. P., van de Flierdt, T., Williams, T., Hemming, S.R., Iwai, M., Kobayashi, M., Jimenez-Espejo, F.J., Escutia, C., González, J.J., Khim, B.K., McKay, R.M., Passchier, S., Bohaty, S.M., Riesselman, C.R., Tauxe, L., Sugisaki, S., Galindo, A.L., Patterson, M.O., Sangiorgi, F., Pierce, E., Brinkhuis, H., & Expedition 318 Scientists (2013). Dynamic behaviour of the East Antarctic ice sheet during Pliocene warmth. *Nature Geoscience*, 6(9), 765-769.
- Cortese, G., Gersonde, R., Hillenbrand, C. D., & Kuhn, G. (2004). Opal sedimentation shifts in the World Ocean over the last 15 Myr. *Earth and Planetary Science Letters*, 224(3), 509-527.



- De Baar, H. J., De Jong, J. T., Bakker, D. C., Löscher, B. M., Veth, C., Bathmann, U., & Smetacek, V. (1995). Importance of iron for plankton blooms and carbon dioxide drawdown in the Southern Ocean. *Nature*, *373*, 412-415.
- Dehairs, F., Goeyens, L., Stroobants, N., Bernard, P., Goyet, C., Poisson, A., & Chesselet, R. (1990). On suspended barite and the oxygen minimum in the Southern Ocean. *Global Biogeochemical Cycles*, *4*(1), 85-102.
- Denis, D., Crosta, X., Schmidt, S., Carson, D. S., Ganeshram, R. S., Renssen, H., Crespin, J., Ther, O., Billy, I., & Giraudeau, J. (2009). Holocene productivity changes off Adélie Land (East Antarctica). *Paleoceanography*, *24*(3), 1-12.
- Dickens, G. R., & Owen, R. M. (1996). Sediment geochemical evidence for an early-middle Gilbert (early Pliocene) productivity peak in the North Pacific Red Clay Province. *Marine Micropaleontology*, *27*(1), 107-120.
- Dickens, G. R., & Owen, R. M. (1999). The latest Miocene–early Pliocene biogenic bloom: a revised Indian Ocean perspective. *Marine Geology*, *161*(1), 75-91.
- Dong, S., Sprintall, J., & Gille, S. T. (2006). Location of the Antarctic polar front from AMSR-E satellite sea surface temperature measurements. *Journal of Physical Oceanography*, *36*(11), 2075-2089.
- Eagle, M., Paytan, A., Arrigo, K. R., van Dijken, G., & Murray, R. W. (2003). A comparison between excess barium and barite as indicators of carbon export. *Paleoceanography*, *18*(1), 1-13.
- Escutia, C., Bárcena, M. A., Lucchi, R. G., Romero, O., Ballegeer, A. M., Gonzalez, J. J., & Harwood, D. M. (2009). Circum-Antarctic warming events between 4 and 3.5

- Ma recorded in marine sediments from the Prydz Bay (ODP Leg 188) and the Antarctic Peninsula (ODP Leg 178) margins. *Global and Planetary Change*, 69(3), 170-184.
- Expedition 318 Scientists (2011). Wilkes Land Glacial History: Cenozoic East Antarctic Ice Sheet evolution from Wilkes Land margin sediments. *IODP Prel. Rept.*, 318.
- Fagel, N., Dehairs, F., André, L., Bareille, G., & Monnin, C. (2002). Ba distribution in surface Southern Ocean sediments and export production estimates. *Paleoceanography*, 17(2), 1-20.
- Fedorov, A. V., Brierley, C. M., Lawrence, K. T., Liu, Z., Dekens, P. S., & Ravelo, A. C. (2013). Patterns and mechanisms of early Pliocene warmth. *Nature*, 496(7443), 43-49.
- Froelich P.N., Klinkhammer., G.P, Bender., M.L., Luedtke, N.A., Heath, G.R., Cullen, D., Dauphin, P., Hammond, D., Hartman, B., & Maynard, V. (1979). Early oxidation of organic-matter in pelagic sediments of the eastern equatorial atlantic – suboxic diagenesis. *Geochimica et Cosmochimica Acta*, 43, 1075–1090.
- Gallego-Torres, D., Romero, O. E., Martínez-Ruiz, F., Kim, J. H., Donner, B., & Ortega-Huertas, M. (2014). Rapid bottom-water circulation changes during the last glacial cycle in the coastal low-latitude NE Atlantic. *Quaternary Research*, 81(2), 330-338.
- Goode, J. W., & Fanning, C. M. (2010). Composition and age of the East Antarctic Shield in eastern Wilkes Land determined by proxy from Oligocene-Pleistocene

- glaciomarine sediment and Beacon Supergroup sandstones, Antarctica. *Geological Society of America Bulletin*, 122(7-8), 1135-1159.
- Hansen, M. A., Passchier, S., Khim, B. K., Song, B., & Williams, T. (2015). Threshold Behavior of a Marine-Based Sector of the East Antarctic Ice Sheet in Response to Early Pliocene Ocean Warming. *Paleoceanography*, 30(6), 789-801.
- Hendy, I. L. (2010). Diagenetic behavior of barite in a coastal upwelling setting. *Paleoceanography*, 25(4), 1-9.
- Hepp, D. A., Mörz, T., Hensen, C., Frederichs, T., Kasten, S., Riedinger, N., & Hay, W. W. (2009). A late Miocene–early Pliocene Antarctic deepwater record of repeated iron reduction events. *Marine Geology*, 266(1), 198-211.
- Jaccard, S. L., Galbraith, E. D., Sigman, D. M., Haug, G. H., Francois, R., Pedersen, T. F., Dulski, P., & Thierstein, H. R. (2009). Subarctic Pacific evidence for a glacial deepening of the oceanic respired carbon pool. *Earth and Planetary Science Letters*, 277(1), 156-165.
- Latimer, J. C., Filippelli, G. M., Hendy, I. L., Gleason, J. D., & Blum, J. D. (2006). Glacial-interglacial terrigenous provenance in the southeastern Atlantic Ocean: The importance of deep-water sources and surface currents. *Geology*, 34(7), 545-548.
- Le Quéré, C., Rödenbeck, C., Buitenhuis, E. T., Conway, T. J., Langenfelds, R., Gomez, A., Labuschagne, C., Ramonet, M., Nakazawa, T., Metzl, N., Gillett, N., & Heimann, M. (2007). Saturation of the Southern Ocean CO<sub>2</sub> Sink due to recent climate change. *Science*, 316, 1735-1738.

- Mangini, A., Jung, M., & Laukenmann, S. (2001). What do we learn from peaks of uranium and of manganese in deep sea sediments? *Marine Geology*, 177(1), 63-78.
- Martin, J. H. (1990). Glacial-interglacial CO<sub>2</sub> change. *Paleoceanography*, 5(1), 1-13.
- McKay, R., Naish, T., Carter, L., Riesselman, C., Dunbar, R., Sjunneskog, C., Winter, D., Sangiorgi, F., Warren, C., Pagani, M., Schouten, S., Willmott, V., Levy, R., DeConto, R., & Powell, R. D. (2012). Antarctic and Southern Ocean influences on Late Pliocene global cooling. *Proceedings of the National Academy of Sciences*, 109(17), 6423-6428.
- Morrison, A. K., Frölicher, T. L., & Sarmiento, J. L. (2015). Upwelling in the Southern Ocean. *Physics today*, 68(1), 27.
- Naish, T., Powell, R., Levy, R., Wilson, G., Scherer, R., Talarico, F., Krissek, L., Niessen, F., Pompilio, M., Wilson, T., Carter, L., DeConto, R., Huybers, P., McKay, R., Pollard, D., Ross, J., Winter, D., Barrett, P., Browne, G., Cody, R., Cowan, E., Crampton, J., Dunbar, G., Dunbar, N., Florindo, F., Gebhardt, C., Graham, I., Hannah, M., Hansaraj, D., Harwood, D., Helling, D., Henrys, S., Hinnov, L., Kuhn, G., Kyle, P., Läufer, A., Maffioli, P., Magens, D., Mandernack, K., McIntosh, W., Milan, C., Morin, R., Ohnneiser, C., Paulsen, T., Persico, D., Raine, I., Reed, J., Riesselman, C., Sagnotti, L., Schmitt, D., Sjunneskog, C., Strong, P., Taviani M., Vogel, S., Wilch, T., & Williams, T. (2009). Obliquity-paced Pliocene West Antarctic ice sheet oscillations. *Nature*, 458(7236), 322-328.

- Nürnberg, C. C., Bohrmann, G., Schlüter, M., & Frank, M. (1997). Barium accumulation in the Atlantic sector of the Southern Ocean: Results from 190,000-year records. *Paleoceanography*, *12*(4), 594-603.
- Orsi, A. H., Whitworth, T., & Nowlin, W. D. (1995). On the meridional extent and fronts of the Antarctic Circumpolar Current. *Deep Sea Research Part I: Oceanographic Research Papers*, *42*(5), 641-673.
- Pagani, M., Liu, Z., LaRiviere, J., & Ravelo, A. C. (2010). High Earth-system climate sensitivity determined from Pliocene carbon dioxide concentrations. *Nature Geoscience*, *3*(1), 27-30.
- Pattan, J. N., Mir, I. A., Parthiban, G., Karapurkar, S. G., Matta, V. M., Naidu, P. D., & Naqvi, S. W. A. (2013). Coupling between suboxic condition in sediments of the western Bay of Bengal and southwest monsoon intensification: A geochemical study. *Chemical Geology*, *343*, 55-66.
- Reinardy, B. T. I., Escutia, C., Iwai, M., Jimenez-Espejo, F. J., Cook, C., van de Flierdt, T., & Brinkhuis, H. (2015). Repeated advance and retreat of the East Antarctic Ice Sheet on the continental shelf during the early Pliocene warm period. *Palaeogeography, Palaeoclimatology, Palaeoecology* *422*, 65-84.
- Reinhard, C. T., Planavsky, N. J., Robbins, L. J., Partin, C. A., Gill, B. C., Lalonde, S. V., Bekker, A., Konhauser, K., & Lyons, T. W. (2013). Proterozoic ocean redox and biogeochemical stasis. *Proceedings of the National Academy of Sciences*, *110*(14), 5357-5362.

- Riedinger, N., Kasten, S., Gröger, J., Franke, C., & Pfeifer, K. (2006). Active and buried authigenic barite fronts in sediments from the Eastern Cape Basin. *Earth and Planetary Science Letters*, 241(3), 876-887.
- Rintoul, S., Hughes, C., & Olbers, D. (2001). The Antarctic circumpolar current system. In: *Ocean Circulation and Climate/G. Siedler, J. Church and J. Gould, eds. New York: Academic Press.* 271-302.
- Schenau, S. J., Prins, M. A., De Lange, G. J., & Monnin, C. (2001). Barium accumulation in the Arabian Sea: Controls on barite preservation in marine sediments. *Geochimica et Cosmochimica Acta*, 65(10), 1545-1556.
- Seki, O., Foster, G. L., Schmidt, D. N., Mackensen, A., Kawamura, K., & Pancost, R. D. (2010). Alkenone and boron-based Pliocene pCO<sub>2</sub> records. *Earth and Planetary Science Letters*, 292(1), 201-211.
- Tauxe, L., Stickley, C.E., Sugisaki, S., Bijl, P.K., Bohaty, S.M., Brinkhuis, H., Escutia, C., Flores, J.A., Houben, A.J.P., Iwai, M., Jiménez-Espejo, F., McKay, R., Passchier, S., Pross, J., Riesselman, C.R., Röhl, U., Sangiorgi, F., Welsh, K., Klaus, A., Fehr, A., Bendle, J.A.P., Dunbar, R., González, J., Hayden, T., Katsuki, K., Olney, M.P., Pekar, S.F., Shrivastava, P.K., van de Flierdt, T., Williams, T., & Yamane, M. (2012). Chronostratigraphic framework for the IODP Expedition 318 cores from the Wilkes Land Margin: Constraints for paleoceanographic reconstruction. *Paleoceanography*, 27(2), 1-19.

- Taylor, S. R. & McLennan, S. M. (1985). The Continental Crust: Its Composition and Evolution: An Examination of the Geochemical Record Preserved in Sedimentary Rocks.
- Tribovillard, N., Algeo, T. J., Lyons, T., & Riboulleau, A. (2006). Trace metals as paleoredox and paleoproductivity proxies: an update. *Chemical Geology*, 232(1), 12-32.
- Whitehead, J. M., & Bohaty, S. M. (2003). Pliocene summer sea surface temperature reconstruction using silicoflagellates from Southern Ocean ODP Site 1165. *Paleoceanography*, 18(3), 1-11.
- Zhang, Z., Nisancioglu, K. H., & Ninnemann, U. S. (2013). Increased ventilation of Antarctic deep water during the warm mid-Pliocene. *Nature communications*, 4, 1499, 1-6.

## CHAPTER 4

### **The Behavior of the East Antarctic Ice Sheet During Periods of Early Pliocene Warmth: Evidence from Polar Paleoclimate Archives**

#### **Abstract**

The Pliocene (5.33 – 2.58 Ma) is characterized as having a warmer Southern Hemisphere with dynamic ice sheets and is often used as an analog to assess future climate trends. However, identifying the warmest time period in which to understand ice dynamics has long been debated. The Mid-Pliocene Warm Period (MPWP) is the most common time period used to assess a warmer climate (Stocker et al., 2013). The Pliocene climatic optimum (PCO), however, has been identified as a prolonged period of warmth that affected the Southern Hemisphere (Fedorov et al., 2013). The sensitivity of the East Antarctic Ice Sheet (EAIS) in response to early Pliocene warmth was identified through a regional correlation of sedimentological archives from three marine-based ice sheets: Prydz Bay, Wilkes Land, and the Ross Sea regions. The compilation of these records provides a stratigraphic approach as opposed to modeling methods to assess ice sheet behavior during warm periods of the early to mid-Pliocene. The onset of deglaciation for the EAIS was uniform between all regions beginning ~4.6 Ma near the onset of the Pliocene Climatic Optimum (~4.5-4.0 Ma). The Wilkes Land ice sheet had a discontinuous retreat possibly due to the influence of the regions subglacial topography. Reduced ice sheet conditions continued until ~3.3 Ma for all regions. Glacial advance of the EAIS was coincident with the MIS M2 glacial event (~3.3 Ma) near the onset of the mid-Pliocene Warm Period in both the Ross Sea and Prydz Bay regions but did not occur



in the Wilkes Land region. I speculate that the Wilkes Land ice sheet was sensitive to warming during the Pliocene Climatic Optimum and remained in a retreated position through the mid-Pliocene. The implications are that future ice dynamic studies should focus on the Pliocene Climatic Optimum in order to better understand the effects of warming rather than the mid-Pliocene which marks the onset of a cooling period.

**Keywords:** mid-Pliocene Warm Period, Pliocene Climatic Optimum, marine ice sheet, deglaciation, Wilkes Land

## 4.1 Introduction

The Antarctic Ice Sheet (AIS) plays a vital role in the Earth's climate system due to its influence on ocean circulation, marine productivity, planetary albedo, and sea level. Over the next century, climate change impacts within the polar regions are projected to produce feedbacks that can have major consequences worldwide. Observations of increased air and ocean temperatures, melting of snow and ice, as well as globally rising sea level provide evidence for a globally warming climate. There is also evidence of thinning and retreat of marine-based ice sheets, particularly the West Antarctic Ice Sheet (WAIS) and portions of the East Antarctic Ice Sheet (EAIS) (Shepherd et al., 2012; Vaughan et al., 2013). These regions of the EAIS are grounded below sea level and are therefore more susceptible to increased ocean warmth. However, the response of these regions of the EAIS to climate trends projected for the end of the century remains uncertain.

Since preindustrial times, CO<sub>2</sub> concentrations have risen from 280 ppm to over 400 ppm. Based on the Intergovernmental Panel on Climate Change (IPCC) new climate scenarios, even with strong mitigation practices, CO<sub>2</sub> concentrations could peak at 490 ppm and reduce to 400 ppm by the end of 2100 (Moss et al., 2010, see also Appendix A). Current ice sheet and sea level models used to project the future trends under these climate scenarios are based on satellite measurements that date back several decades. However, study of the present climate does not present sufficient temporal resolution to project ice sheet sensitivity to warming trends over multi-century timescales, limiting our understanding of ice sheet dynamics over longer periods of time. Specifically, current

physical climate models have restrictive assumptions, which imply a need for alternative methods to understand ice sheet behavior and its effect on sea level (Rahmstorf, 2010).

The use of semi-empirical models has also been criticized because they consider all ice as fixed, continuous bodies and may not differentiate or capture the full variability of individual ice sheet drainage basins.

The dynamic nature of the EAIS can be assessed using polar paleoclimate archives or geologic records that were deposited under climate conditions similar to the present day. These archives provide a means of developing a longer time series in which to understand ice sheet dynamics and make up for the limitations of decadal measurements. Using polar paleoclimate archives we can reconstruct the glacial history along the East Antarctic continental margin. Early Pliocene (5.33-2.58 Ma) climate conditions had a CO<sub>2</sub> range between ~365-415 ppm (Bartoli et al., 2011; Pagani et al., 2010; Seki et al., 2010), which are similar to the CO<sub>2</sub> concentrations predicted by the end of 2100 under strong mitigation practices (See also Appendix A). In addition, Pliocene sea level rise estimates average no more than ~20 m above modern (Masson-Delmotte et al., 2013; Pollard and DeConto, 2009; Winnick and Cave, 2015; Miller et al., 2012; Dolan et al., 2011; Hill et al., 2007) which differ greatly from the estimates for the end of the century based on MPWP climate conditions (See Appendix A). This time interval can be used to assess ice sheet behavior because it also represents a period of time in which the Earth was tectonically, oceanographically, and climatically similar to today.

Using the Pliocene epoch as an analog for understanding EAIS response to future climate warming requires identifying the warmest time periods in which to focus and test

climate models. The mid-Pliocene warm period (MPWP, ~3.3-3.0 Ma) has been the focus of numerous modeling studies (including the latest IPCC Report) that seek to understand ice dynamics. During the MPWP global mean temperatures were ~2-3°C higher than preindustrial (Fedorov et al., 2013). On the other hand, the Pliocene Climatic Optimum (PCO) between ~4.5 – 4.0 Ma has also been recognized as one of the warmest intervals in the Pliocene by Fedorov et al. (2013) with temperatures ~4°C higher than preindustrial. The dynamics of the EAIS and its response during warm periods are largely debated. By evaluating the extent of the ice sheet at various locations of the EAIS from a stratigraphic viewpoint, it may inspire the need for models to refocus their efforts on the Pliocene Climatic Optimum time slice.

The behavior of the EAIS during the Pliocene is not well understood due to the paucity of on-shore records, multiple hiatuses, core recovery and poor age control, which presents the need for higher resolution records. The Wilkes land continental rise site U1359 (Figure 4-1) ice-rafted debris mass accumulation rate (IRD MAR) record has provided a high-resolution, detailed account of ice sheet dynamics during the Pliocene. A threshold sensitivity to ocean warming was noted by Hansen et al. (2015) near the onset of the PCO, which may have implications for EAIS dynamics during periods of warming. Integrating multiple sediment records from a wide distribution of locations across the EAIS through regional correlations will provide a more comprehensive look at the response of marine-based ice sheets during the early Pliocene. The aim of this study is to assess the behavior of the EAIS during the PCO. Specifically, the Wilkes Land record will address the gap in knowledge of ice dynamics for a previously unstudied area of the

EAIS. For this chapter, I will first focus on describing the evolution of the EAIS during the early Pliocene by compiling previous works on terrestrial and marine records for marine-based portions of the EAIS (i.e. Prydz Bay, Wilkes Land, and Ross Sea shown in Figure 4-1). Then, I will speculate on the behavior of the EAIS and its implications for future climate trends.

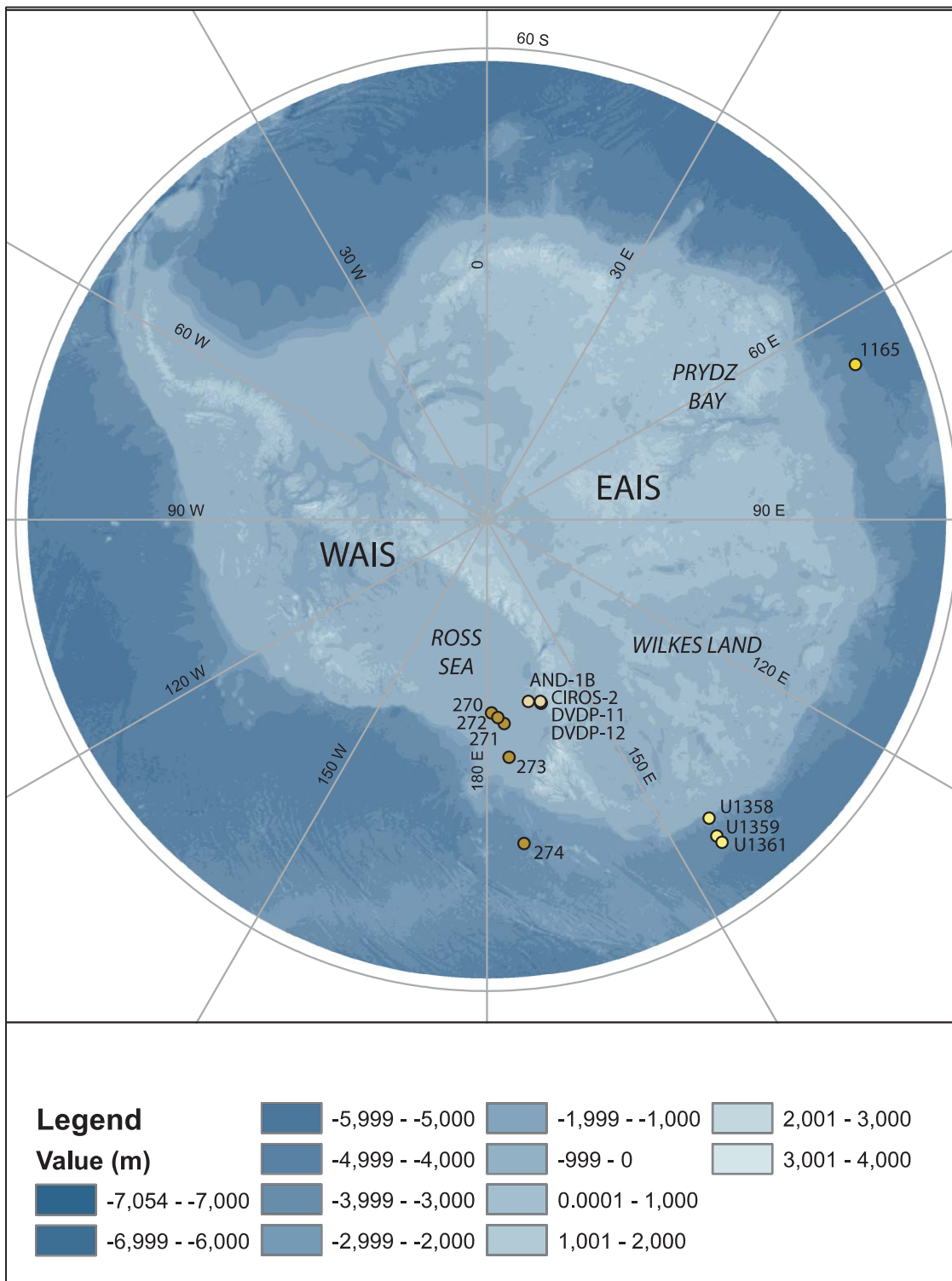


**Figure 4-1. Location of Antarctic drill core sites discussed within text. DVDP (tan) = Dry Valley Drilling Project, DSDP (brown) = Deep Sea Drilling Project, ODP (gold) = Ocean Drilling Program, and IODP (yellow) = Integrated Ocean Drilling Program. BEDMAP V2 showing bed topography from Fretwell et al. (2013).**

## **4.2 Ice sheet behavior during the early Pliocene**

There are several lines of evidence to suggest that the East Antarctic Ice sheet was dynamic throughout the early to mid-Pliocene. Records of glacial advance and retreat are preserved in stratigraphy taken along the Antarctic continental margin and were cored during various expeditions such as the ODP Leg 188 to the Prydz Bay region, IODP Expedition 318 to the Wilkes Land region, and DVDP, ANDRILL, and DSDP Expeditions to the Ross Sea Region. The preservation of older sequences is sometimes complicated by subsequent glaciations on the continent making terrestrial glacial sequences more convoluted in contrast to deposits in the oceans, which can remain unmodified for long periods of time (De Schepper et al., 2014). Marine records are often more advantageous because they are more continuous and easily datable as compared to ice-proximal glaciogenic sediments (Williams et al., 2010). Despite the fragmentary nature of terrestrial evidence for ice sheet behavior, when supplemented with marine records, a more complete account of glacial history can be depicted. The following sections will summarize the available data and literature that describe the behavior of marine-based portions of the EAIS during the early Pliocene in a regional context. All ages have been converted to the Gradstein et al. (2012) time scale using linear

interpolation (See Table 4-1 for original age models). Figure 4-1 shows the locations of all EAIS core sites reviewed below.



**Table 4-1.** Location of sites used for this study, age model used, and the references to the original works.

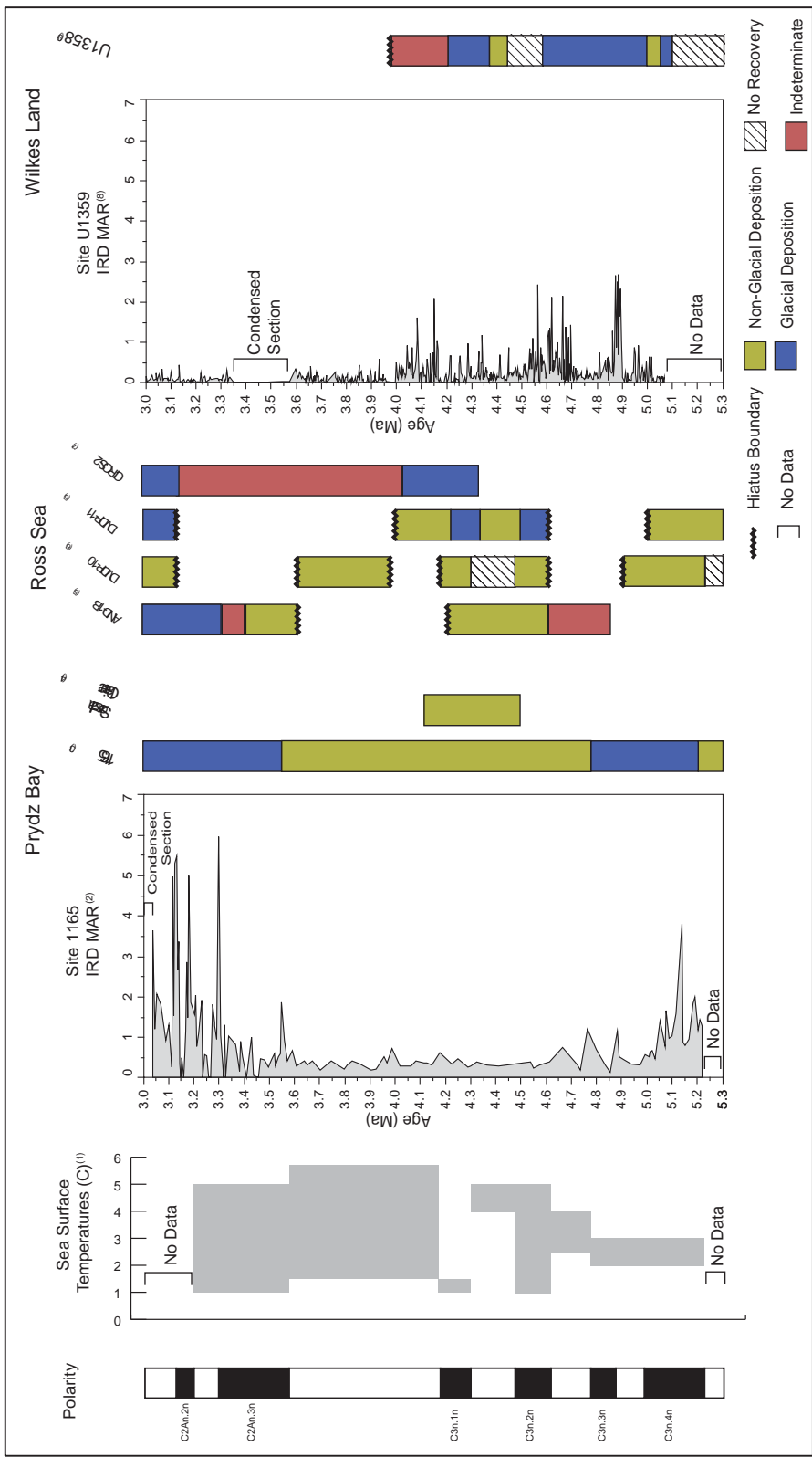
<b>Project</b>	<b>Site</b>	<b>Location</b>	<b>Age Model</b>	<b>Reference</b>
<i>Ross Sea</i>				
DSDP 28	270	Shelf	Hayes and Frakes, 1975	Hayes and Frakes, 1975
	271	Shelf		
	272	Shelf		
	273	Shelf		
	274	Rise		
ANDRILL				
	AND-1B	Shelf	Naish et al., 2009	Naish et al., 2009 McKay et al., 2012
DVDP				
	10	Terrestrial	Ishman and Rieck, 1992	McKelvey, 1981
	11	Terrestrial		Ishman and Rieck, 1992
CIROS				
	2	Terrestrial	Winter et al., 2012	Pyne et al., 1985 Barrett and Hambrey, 1992
<i>Prydz Bay</i>				
ODP 188	1165	Rise	Florindo et al. 2003	Passchier, 2011 Williams et al., 2010 Grützner et al. (2005)
<i>Wilkes Land</i>				
IODP 318	U1358	Shelf	Reinardy et al., 2015	Orejola et al., 2014
	U1359	Rise	Tauxe et al., 2012	Hansen et al., 2015
	U1361	Rise	Tauxe et al., 2012	Cook et al., 2013

Figure 4-2 provides a compilation of all records discussed within this paper. For the purpose of this paper, I will use the following to distinguish between glacial and non-glacial deposition. For terrestrial or shallow-water glaciomarine (i.e. continental shelf) records, the evidence of glacial deposition can be inferred by the presence of glacial diamicts. Diamicts are poorly sorted, and in the context of the high-latitude continental shelf environment, I interpret these as unconsolidated glacial material deposited directly from ice sheets through basal melt out. Non-glacial deposition can be inferred by the deposition of diatomite, which is deposited during open marine conditions. For deep-water glaciomarine records (i.e. continental rise), glacial deposition can be inferred by peaks of IRD MAR. Records of ice-rafted debris in high-latitude sediment cores near the Antarctic coast reflect the glacial activity on the continental shelves and thereby provide a record of glacial fluctuations over time. Deposition of IRD is the result of icebergs laden with sediment that have broken off and carried by ocean currents, depositing sediment as they melt. The peaks in IRD MAR are indicative of an ice sheet that has extended towards the coast to produce icebergs that reach the drill site. The extent of the ice sheet may be further corroborated by the relationship between ice advance phases based on  $\epsilon\text{Nd}$  that coincide with high IRD MAR peaks (See Appendix Figure B2). The absence of IRD MAR peaks would then suggest a retreat or absence of the ice sheet.

#### **4.2.1 Pliocene Climatic Optimum (~4.5 – 4.0 Ma)**

The behavior of the EAIS during prolonged warm periods such as the PCO is often assessed in the context of individual regions, and similar behavior across the EAIS is assumed when using semi-empirical modeling (Rahmstorf, 2010). This assumption

does not take into account an individual region's response to climate drivers and can lead to uncertainty for understanding cryospheric change. Based on a synthesis of sedimentological records (Figure 4-2), there are several lines of evidence to suggest that not only was the EAIS dynamic throughout the early Pliocene, but that individual regions may have behaved independently of each other in response to climate drivers.



**Figure 4-2. Regional comparison of Pliocene polar paleoclimate archives. Age boundaries are based on the Gradstein et al. (2012) time scale. Sea surface temperatures are compiled from (1) McKay et al. (2012); Whitehead and Bohaty (2003); and Escutia et al. (2009). References: (2) Passchier, (2011); (3) Grützner et al. (2005), Passchier. (2011); (4) Whitehead et al. (2001); (5) Naish et al. (2009), McKay et al. (2012); (6) Ishman and Rieck (1992), McKelvey (1981); (7) Pyne et al. (1985), Barrett and Hambrey (1992); (8) Hansen et al. (2015), Rosenberg, (2014); (9) Expedition 318 Scientists (2011)**

The first noticeable impact of PCO warmth on EAIS dynamics can be seen at ~4.6 Ma concordant with a rise in SSTs (Figure 4-2). Ocean temperatures likely played a crucial role in controlling fluctuations of ice sheets as can be seen in Figure 4-2. SSTs peak near the onset of the PCO at 4-5°C and then become more variable near the latter (~3.6 Ma) between 1° and 5°C (Whitehead and Bohaty, 2003; Escutia et al., 2009; McKay et al., 2012). A compilation of terrestrial and onshore records from the Prydz Bay and Ross Sea regions (Figure 4-2) indicate that between ~4.6-4.0 Ma, there was mostly non-glacial deposition, and the ice margins in these regions may have been further inland (Whitehead et al., 2001; Passchier, 2011). Reduced ice sheet conditions in Prydz Bay were inferred from the terrestrial record in Vestfold Hills where a ~7 m thick layer of sandy diatomite and diatomaceous sand was deposited (Whitehead et al., 2001). This was accompanied by low amplitude IRD MAR at ODP Site 1165 on the continental rise (Passchier, 2011; Whitehead et al., 2001). The low IRD MAR along with the lithology

and clay mineralogy interpretations were suggested to be a deepwater contourite setting by Passchier (2011).

As opposed to the relatively complete early Pliocene section of ODP 1165, the ice dynamic for the Ross Sea region during this time interval is not as straightforward. Multiple interpretations have been put forth for DVDP and CIROS cores for this time interval due to age model discrepancies and placement of hiatuses. Ishman and Rieck (1992) posited three hiatuses within the early Pliocene section that do not align with the later findings of Ohneiser and Wilson (2012). The ages of Ishman and Rieck (1992) and the original interpretations for glacial and non-glacial deposition described in McKelvey (1981) nearly align with the high and low amplitude IRD MAR of U1359. Despite age model discrepancies and periodic deposition of non-glacial sediment in DVDP cores, the dominant lithology is described as a deep marine fjord deposit between the time period of 4.6 and 4.0 for the Ross Sea region. Further, the deposition of a thick layer of diatomite in AND-1B at ~4.6-4.2 Ma, also implies retreat of the Ross Ice Shelf (Naish et al., 2009) and helps to define when the ice sheet began to retreat during the PCO. Prior to this there were multiple grounding line oscillations as determined by the deposition of diamicts and diatomite from <5 Ma to 4.6 Ma (Naish et al., 2009). Retreat of the Ross Ice Shelf has also been inferred from DSDP Leg 28 drill sites at ~4.15 Ma with cooling and minor fluctuations of ice extent taking place ~3.97 Ma (Hayes and Frakes, 1975).

The CIROS-2 core lacks paleomagnetic markers and relies solely on biostratigraphy to constrain the ages of glacial and non-glacial deposition as well as sections of no recovery. The base of the CIROS-2 core was estimated at 4.2 - <4.5 Ma

based on updated biomarkers from Winter et al. (2012). The period between 4.34 and 4.06 Ma (Winter et al., 2012) is comprised of diamicts and is interpreted as grounded glacial ice due to the presence of horizontal shear planes (Pyne et al., 1985; Barrett and Hambrey, 1992).

In contrast to the Prydz Bay and Ross ice margins, however, a more dynamic setting can be inferred for Wilkes Land. The lower Pliocene strata within core U1358 confirms this dynamic intermittent glaciomarine sedimentation with open marine conditions and extensive glacial advances to the outer shelf prior to ~4.4 Ma (Orejola et al., 2014; Reinardy et al., 2015). Ice sheet advances, concordant with the presence of locally sourced ice-proximal diamictos described at U1358 (Figure 4-2) and  $\epsilon\text{Nd}$  trends at U1361 (See Appendix B Figure B2), were identified at Site U1359 between ~4.9-4.8 and 4.7-4.5 Ma (Hansen et al., 2015). In addition, IRD MAR minima (Figure 4-2) and a productivity event found at U1359 ~4.5 Ma indicate reduced ice sheet conditions (Chapter 3, this thesis) near the onset of the PCO.

The compiled records illustrate the dynamic nature of the Wilkes Land ice sheet not found in the Prydz Bay and Ross Sea regions. A shift from a larger ice sheet to a smaller one can be seen near the onset of the PCO ~4.6 Ma (Figure 4-2) as also evidenced from a shift in obliquity to precession forced influence in the IRD MAR record of U1359 (See Chapter 2, Figure 2-5). However, this retreat of the EAIS was not continuous and suggests an oscillatory transition for retreat, particularly in the Wilkes Land region.

#### 4.2.2 Mid-Pliocene Warm Period (~3.3 – 3.0 Ma)

Behavior for the EAIS during the mid-Pliocene warm period greatly differs from its response during the PCO. This time period, most often associated as the warmest interval in the Pliocene, begins with the globally recognized glacial event (MIS M2) (Lisiecki and Raymo, 2005). The M2 glacial was described as an Antarctic wide event, however, the signal does not appear in all regions. The termination of warm conditions and glacial expansion in the Prydz Bay region is based on the return of high amplitude IRD MAR at 1165 (Passchier, 2011). Glacial advance and a decrease in bottom current in the Prydz Bay region occurred between ~3.55 to 3.0 Ma (Passchier, 2011). Despite hiatuses, and some uncertainties in age boundaries due to biostratigraphy, deposition of diamictite at DVDP and sedimentation at AND-1B and CIROS-2 implies multiple ice sheet grounding line oscillations between 3.4 and 3.0 Ma (McKay et al., 2012; Ishman and Rieck, 1992; McKelvey, 1981; Pyne et al., 1985; Barrett and Hambrey, 1992).

In spite of the cooling conditions found at other locations, the low amplitude IRD MAR in U1359 suggests reduced ice conditions in the Wilkes Land region began ~4.0 Ma and continued through the MPWP. The lack of a glacial signal at this location suggests that the ice sheet may have been particularly sensitive to warming during the PCO and did not return to its former extent. Based on the provenance of the material deposited at Site U1361 (See Appendix Figure B2), Cook et al. (2013) suggest that during longer warm intervals, active erosion occurred from within the Wilkes subglacial basin and the ice sheet may have retreated up to several kilometers inland. However, their provenance record does not extend into the MPWP. The MPWP was represented by



a hiatus ( $>3.99$  to  $<0.61/0.51$  Ma) in continental shelf Site U1358, however, Orejola et al. (2014) inferred cooler conditions in the Pleistocene, where sand provenance of shelf sediment indicate far-traveled icebergs sourced from Victoria Land (Orejola et al., 2014). These observations argue for a reduced state of the Wilkes Land ice sheet during the MPWP albeit under cooler conditions.

The reduced state of the Wilkes Land ice sheet may infer that the advance of the EAIS arrived first at Prydz Bay and some regions of the Ross Sea. Due to a lack of SST data at this time, it is difficult to speculate whether ocean temperatures played a role. The offset between regions may suggest that there was some variation of the EAIS growth and extent even under cooler climate conditions.

#### **4.3 Retreat of Wilkes Land ice sheet**

The regional correlation reveals a significant evolution in ice dynamics for the Wilkes Land portion of the EAIS not seen in Prydz Bay and Ross Sea regions during the PCO. The variability of the IRD MAR flux in U1359 indicates that while there is an overall decreasing trend, the actual retreat of the ice sheet was discontinuous throughout the PCO. The fluctuations of the Wilkes Land ice sheet, as opposed to other regions of the EAIS during the early Pliocene, suggest several factors may be at play.

Dowdeswell et al. (1999) found that individual ice sheet drainage basins in the Arctic responded asynchronously to a single external forcing, presumably due to variability in bathymetry and other boundary conditions. The asynchronous response of the EAIS to the warmer climate of the PCO may differ greatly due to the differences in the topography of the regions. The Wilkes subglacial basin is the largest subglacial basin

in East Antarctica (Figure 4-1), descending below -500 m in elevation (Fretwell et al., 2013). The encroachment of warm water into the basin, such as those warmer SSTs in the PCO (Figure 4-2), may have caused the discontinuous retreat of the ice. The stability and extent of the Wilkes Land ice sheet during the PCO may be linked to its subglacial topography. The subglacial topography is connected by a network of several subglacial troughs and its configuration may strongly influence the rate of growth and retreat for the Wilkes Land ice sheet. The Prydz Bay and Ross Sea regions lack this extensive network and may explain why the records differ in their retreat. For the ice to retreat in the Wilkes Land area, it must overcome several topographic barriers (See Figure 4-1) that may hinder its retreat whereas the Prydz Bay and Ross Sea regional topography would have a smoother and quicker retreat over a consistently landward sloping bed.

In Wilkes Land, the presence of an overdeepening is another topographic feature that may play a role in the fluctuation and retreat of the ice sheet through this region in the early Pliocene. The Prydz Bay regional topography also contains a landward overdeepening within the Lambert Graben, however, it is more narrow as opposed to the bigger and broader overdeepening of the Wilkes region. According to Schoof (2007), the shape of the bed controls the outflow of ice. Moreover, marine ice sheets with overdeepenings may be subject to a hysteresis effect when exposed to changes in external forcings. During deglaciation periods, the ice sheet undergoes a hysteretic transition from a larger to smaller configuration and the reverse for glaciation. In the case of the Wilkes Land region, the higher IRD MAR peaks between 4.6 and 4.0 Ma may signify small

glacial episodes coinciding with eccentricity cycles (See Chapter 2) and periodic return of the ice sheet after a retreat.

When melting is initiated, a deepening of the grounding line occurs and the ice sheet becomes more susceptible to further retreat. The marine ice sheet instability hypothesis posits that a retreat in the grounding line position will lead to an increase in ice discharge in a positive feedback loop on a landward sloping bed (Schoof, 2007). Areas where grounding lines are close to overdeepenings are particularly susceptible to this process. This feedback would continue until the ice disintegrates completely or stabilizes in a region with a downsloping bed. This type of behavior may explain the variable trend in IRD MAR during the PCO and low IRD MAR in the MPWP for the Wilkes Land region. Increased ocean temperatures would lead to increased basal melting and ice shelf thinning, which can be seen as SSTs increased during the PCO. Further warming would remove the buttressing effect of ice shelves and lead to glacier acceleration. Eventually, the ice may have retreated until it stabilized on a downward slope.

#### **4.4 Discussion and Implications**

Many of today's current ice sheet models are based on MPWP climate boundaries and do not predict the EAIS losing as much mass compared to the early Pliocene estimates. The differences in the behavior of the EAIS between the PCO and the MPWP highlight an important issue for modeling future ice sheet behavior in a warmer world. Based on the compilation of available sediment records, the effect of warming on the behavior of the EAIS was most prominent during the PCO. Therefore, in order to gain a

better comprehension of ice sheet dynamics and its potential sea level input, a greater focus on the PCO should be considered. The fluctuations of the Wilkes Land ice sheet to warming ocean temperatures may have important implications for modeling the EAIS response to future climate warming and its potential impact on sea level rise. The influence of increased warming from previous decades has already begun to have an effect on the EAIS.

Recent observations have revealed that the EAIS has both gained and lost mass in response to climatic warming (Shepherd et al., 2012; Vaughan et al., 2013). Satellite radar altimetry measurements have indicated that between 1992 and 2003, the EAIS interior north of 81.6°S experienced a gain in mass associated with an increase in precipitation (Davis et al., 2005). In particular, Prydz Bay, east of the Amery ice shelf basin, experienced moderate to strong thickening, while slight to moderate thinning occurred within the King George V Land basin. For the Pliocene, newly calculated exposure ages by Yamane et al. (2015) suggest that the ice sheet was thicker prior to ~4 Ma near Queen Maud Land and the Wilkes Land ice sheet was thinner and retreated. This type of behavior was observed for Wilkes Land by Cook et al. (2013) in the  $\epsilon\text{Nd}$  of U1361 and in the IRD MAR record of Site U1359 by Hansen et al. (2015) when SSTs peaked above 3°C near the onset of the PCO. Initial warming may increase ice thickness initially through the snow-gun effect, but eventually basal melt will outweigh any growth and cause retreat. The current response of the EAIS to warming trends may signify the initial precursor to early Pliocene conditions and ice retreat. Should global temperatures

continue to rise, one could assume that the EAIS may behave similar to the way it did during the PCO as global temperatures continue to rise.

Current modeling studies have been unable to produce the sea level rise (SLR) estimates of Pliocene (~20 m) reconstructions (DeConto & Pollard, 2016). A recent modeling study by DeConto & Pollard (2016) increased the Pliocene estimates from +7 m to +17 m by considering additional parameters such as marine ice sheet instability (MISI) and marine ice cliff instability (MICI). This new coupled ice sheet and climate dynamics model highlights the importance of paleoclimate data such as presented in this chapter. The regional assessment of EAIS behavior from a sedimentological perspective furthers our understanding of how the EAIS response to climate and may help to better constrain sea level estimates of the past and future.

An important question that remains is to what extent will the Wilkes Land ice sheet retreat when it does reach its threshold. Cook et al. (2013) inferred that the Wilkes Land ice sheet may have retreated several hundred kilometers inland during the early Pliocene. The Wilkes Land basin holds the largest volume of marine ice (~19 m of sea level equivalent; Mengel and Levermann, 2014). Depending on the extent of warming, there could be a potentially substantial sea level rise input from the Wilkes Land ice sheet, particularly if retreat reaches the overdeepening and rapid ice loss occurs. The eventual loss of ice sheets can incur meters of sea level rise resulting in changes of coastlines and severe flooding of low-lying areas (Church et al., 2013).

The timescales in which the ice sheet retreat will occur also remains uncertain. The rate at which ice sheets respond to climate changes are longer as compared to the

atmosphere and oceans (Golledge et al., 2015) and are not captured by the decadal scale modeling. Simulations of the present day Antarctic ice sheet to climate and oceanic forcings by Golledge et al. (2015) found that prolonged warming lead to loss of ice in East Antarctica, particularly the Wilkes and Aurora subglacial basins. Additionally, the influence of oceanic warming produced more rapid ice sheet response than atmospheric warming over centennial time scales.

Further research is needed focusing on the PCO and the effects of warming on the marine ice sheet contribution to sea level rise. Efforts should be concentrated on the rate of retreat in order to resolve how much sea level rise can be expected over the coming centuries, taking into account the topographic constraint and discontinuous pattern of retreat in the marine ice sheet of the Wilkes Land region. In particular, the observed patterns in ice sheet behavior may be related to the region's subglacial topography and should be taken into consideration.

#### **4.5 Conclusions**

A compilation of terrestrial and marine records were used to assess early Pliocene EAIS behavior by comparing how individual marine-based sectors responded during warm periods. A synthesis of these records has revealed continent wide retreat of marine-based portions of the EAIS during the PCO. Further, the Wilkes Land ice sheet retreated in a discontinuous pattern as compared to other regions of the EAIS, presumably due to the differences in its subglacial topography. Additionally, a temporal offset for the advance of the ice sheets marking the onset of a cooling period (McKay et al., 2012) was found within the Prydz Bay and Ross Sea regions in the mid-Pliocene warm period. This

glacial advance signal was absent for the Wilkes Land region and suggests that the area was not responding in tandem with other locations.

Current climate and sea level model projections treat the EAIS as a continuum instead of individual regions, which may lead to an underestimation of sea level rise and uncertainty of cryospheric climate response. Over the next century, global temperatures are expected to increase anywhere from  $<1.5^{\circ}\text{C}$  to  $>2.0^{\circ}\text{C}$  above preindustrial (IPCC, 2013). Should the current warming trend continue, the changes observed in the climate system during the PCO may be expected to occur. With this understanding, a consideration for not only the individual basin response of the EAIS should be taken into account when modeling ice dynamics for the EAIS, but a particular focus of ice dynamics under the PCO climate boundaries should be considered. Additionally, future studies should focus on obtaining higher resolution marine and terrestrial records that may help further constrain individual sector behavior.

#### 4.6 References

- Barrett, P. J., & Hambrey, M. J. (1992). Plio-Pleistocene sedimentation in Ferrar Fiord, Antarctica. *Sedimentology*, 39(1), 109-123.
- Bartoli, G., Hönisch, B. & Zeebe, R.E., (2011). Atmospheric CO<sub>2</sub> decline during the Pliocene intensification of Northern Hemisphere glaciations. *Paleoceanography*, 26(4).
- Church, J. A., Clark, P. U., Cazenave, A., Gregory, J. M., Jevrejeva, S., Levermann, A., Merrifield, M.A., Milne, G.A., Nerem, R.S., Nunn, P.D., Payne, A. J., Pfeffer, W.T., Stammer, D., & Unnikrishnan, A.S. (2013). Sea level change. *Climate Change 2013: The Physical Science Basis. Working Group I Contribution to the Fifth Assessment Report of the Intergovernmental Panel on Climate Change*.
- Cook, C.P., van de Flierdt, T., Williams, T., Hemming, S.R., Iwai, M., Kobayashi, M., Jimenez-Espejo, F.J., Escutia, C., González, J.J., Khim, B.K. & McKay, R.M. (2013). Dynamic behaviour of the East Antarctic ice sheet during Pliocene warmth. *Nature Geoscience*, 6(9), pp.765-769.
- Davis, C.H., Li, Y., McConnell, J.R., Frey, M.M. & Hanna, E. (2005). Snowfall-driven growth in East Antarctic ice sheet mitigates recent sea-level rise. *Science*, 308(5730), pp.1898-1901.
- De Schepper, S., Gibbard, P.L., Salzmann, U. & Ehlers, J. (2014). A global synthesis of the marine and terrestrial evidence for glaciation during the Pliocene Epoch. *Earth-Science Reviews*, 135, pp.83-102.



- Dolan, A. M., Haywood, A. M., Hill, D. J., Dowsett, H. J., Hunter, S. J., Lunt, D. J., & Pickering, S. J. (2011). Sensitivity of Pliocene ice sheets to orbital forcing. *Palaeogeography, Palaeoclimatology, Palaeoecology*, 309(1), 98-110.
- Dowdeswell, J.A., Elverhøi, A., Andrews, J.T. & Hebbeln, D. (1999). Asynchronous deposition of ice-rafted layers in the Nordic seas and North Atlantic Ocean. *Nature*, 400(6742), pp.348-351.
- Escutia, C., Bárcena, M. A., Lucchi, R. G., Romero, O., Ballegeer, A. M., Gonzalez, J. J., & Harwood, D. M. (2009). Circum-Antarctic warming events between 4 and 3.5 Ma recorded in marine sediments from the Prydz Bay (ODP Leg 188) and the Antarctic Peninsula (ODP Leg 178) margins. *Global and Planetary Change*, 69(3), 170-184.
- Fedorov, A.V., Brierley, C.M., Lawrence, K.T., Liu, Z., Dekens, P.S. & Ravelo, A.C. (2013). Patterns and mechanisms of early Pliocene warmth. *Nature*, 496(7443), 43-49.
- Florindo, F., Bohaty, S. M., Erwin, P. S., Richter, C., Roberts, A. P., Whalen, P. A., & Whitehead, J. M. (2003). Magnetobiostratigraphic chronology and palaeoenvironmental history of Cenozoic sequences from ODP sites 1165 and 1166, Prydz Bay, Antarctica. *Palaeogeography, Palaeoclimatology, Palaeoecology*, 198(1), 69-100.
- Fretwell, P., Pritchard, H. D., Vaughan, D. G., Bamber, J. L., Barrand, N. E., Bell, R., Bianchi, C., Bingham, R. G., Blankenship, D. D., Casassa, G., Catania, G., Callens, D., Conway, H., Cook, A. J., Corr, H. F. J., Damaske, D., Damm, V.,

Ferraccioli, F., Forsberg, R., Fujita, S., Gim, Y., Gogineni, P., Griggs, J. A., Hindmarsh, R. C. A., Holmlund, P., Holt, J. W., Jacobel, R. W., Jenkins, A., Jokat, W., Jordan, T., King, E. C., Kohler, J., Krabill, W., Riger-Kusk, M., Langley, K. A., Leitchenkov, G., Leuschen, C., Luyendyk, B. P., Matsuoka, K., Mouginot, J., Nitsche, F. O., Nogi, Y., Nost, O. A., Popov, S. V., Rignot, E., Rippin, D. M., Rivera, A., Roberts, J., Ross, N., Siegert, M. J., Smith, A. M., Steinhage, D., Studinger, M., Sun, B., Tinto, B. K., Welch, B. C., Wilson, D., Young, D. A., Xiangbin, C., & Zirizzotti, A. (2013). Bedmap2: improved ice bed, surface and thickness datasets for Antarctica, *The Cryosphere*, 7, 375-393, doi:10.5194/tc-7-375-2013.

Golledge, N. R., Kowalewski, D. E., Naish, T. R., Levy, R. H., Fogwill, C. J., & Gasson, E. G. W. (2015). The multi-millennial Antarctic commitment to future sea-level rise. *Nature*, 526(7573), 421-425.

Gradstein, F.M., Ogg, J.G., Schmitz, M. & Ogg, G. eds. (2012). *The Geologic Time Scale 2012 2-Volume Set* (Vol. 2). Elsevier.

Grützner, J., Hillenbrand, C. D., & Rebesco, M. (2005). Terrigenous flux and biogenic silica deposition at the Antarctic continental rise during the late Miocene to early Pliocene: implications for ice sheet stability and sea ice coverage. *Global and Planetary Change*, 45(1), 131-149.

Hansen, M.A., Passchier, S., Khim, B.K., Song, B. & Williams, T. (2015). Threshold Behavior of a Marine-Based Sector of the East Antarctic Ice Sheet in Response to

- Early Pliocene Ocean Warming. *Paleoceanography*, 30, 789-801,  
doi:10.1002/2014PA002704.
- Hayes, D.E. & Frakes, L.A. (1975). General synthesis, deep sea drilling project leg  
28. *Initial Reports of the Deep Sea Drilling Project*, 28, 919-942.
- Hill, D. J., Haywood, A. M., Hindmarsh, R. C. A., & Valdes, P. J. (2007). Characterizing  
ice sheets during the Pliocene: evidence from data and models. Geological  
Society of London.
- Stocker, T. F., Qin, D., Plattner, G. K., Tignor, M., Allen, S. K., Boschung, J., Nauels, A.,  
Xia, Y., Bex, V., and Midgley, B. M. (2013). IPCC, 2013: Climate Change 2013:  
The Physical Science Basis. Contribution of Working Group I to the Fifth  
Assessment Report of the Intergovernmental Panel on Climate Change.
- Ishman, S. E., & Rieck, H. J. (1992). A Late Neocene Antarctic Glacio-Eustatic Record,  
Victoria Land Basin Margin, Antarctica. *The Antarctic Paleoenvironment: A  
Perspective on Global Change: Part One*, 327-348.
- Lisiecki, L. E., & Raymo, M. E. (2005). A Pliocene-Pleistocene stack of 57 globally  
distributed benthic  $\delta^{18}\text{O}$  records. *Paleoceanography*, 20(1).
- Masson-Delmotte, V., Schulz, M., Abe-Ouchi, A., Beer, J., Ganopolski, A., Rouco, J.,  
Jansen, E., Lambeck, K., Luterbacher, J., Naish, T., Osborn, T., Otto-Bliesner, B.,  
Quinn, T., Ramesh, R., Rojas, M., Shao, X., & Timmermann, A. (2013).  
Information from Paleoclimate archives In Climate Change 2013: the Physical  
Science Basis. *Contribution of Working Group I to the Fifth Assessment Report of*

*the Intergovernmental Panel on Climate Change, Cambridge Univ. Press, Cambridge and New York.*

- McKay, R., Naish, T., Carter, L., Riesselman, C., Dunbar, R., Sjunneskog, C., Winter, D., Sangiorgi, F., Warren, C., Pagani, M., Schouten, S., Willmott, V., Levy, R., DeConto, R., & Powell, R.D. (2012). Antarctic and Southern Ocean influences on Late Pliocene global cooling. *Proceedings of the National Academy of Sciences*, 109(17), 6423-6428.
- McKelvey, B. C. (1981). The lithologic logs of DVDP cores 10 and 11, eastern Taylor Valley. *Dry valley drilling project*, 63-94.
- Mengel, M. & Levermann, A. (2014). Ice plug prevents irreversible discharge from East Antarctica. *Nature Climate Change*, 4(6), 451-455.
- Miller, K. G., Wright, J. D., Browning, J. V., Kulpecz, A., Kominz, M., Naish, T. R., Cramer, B.S., Rosenthal, Y., Peltier W.R., & Sostdian, S. (2012). High tide of the warm Pliocene: Implications of global sea level for Antarctic deglaciation. *Geology*, 40(5), 407-410.
- Moss, R.H., Edmonds, J.A., Hibbard, K.A., Manning, M.R., Rose, S.K., Van Vuuren, D.P., Carter, T.R., Emori, S., Kainuma, M., Kram, T. & Meehl, G.A. (2010). The next generation of scenarios for climate change research and assessment. *Nature*, 463(7282), pp.747-756.
- Ohneiser, C. & Wilson, G. (2012). Revised magnetostratigraphic chronologies for New Harbour drill cores, southern Victoria Land, Antarctica. *Global and Planetary Change*, 82, pp.12-24.

- Orejola, N., Passchier, S. & Expedition 318 Scientists (2014). Sedimentology of lower Pliocene to Upper Pleistocene diamictites from IODP Site U1358, Wilkes Land margin, and implications for East Antarctic Ice Sheet dynamics. *Antarctic Science*, 26(2), 183-192.
- Naish, T., Powell, R., Levy, R., Wilson, G., Scherer, R., Talarico, F., Krissek, L., Niessen, F., Pompilio, M., Wilson, T., Carter, L., DeConto, R., Huybers, P., McKay, R., Pollard, D., Ross, J., Winter, D., Barrett, P., Browne, G., Cody, R., Cowan, E., Crampton, J., Dunbar, G., Dunbar, N., Florindo, F., Gebhardt, C., Graham, I., Hannah, M., Hansaraj, D., Harwood, D., Helling, D., Henrys, S., Hinnov, L., Kuhn, G., Kyle, P., Laufer, A., Maffioli, P., Magens, D., Mandernack, K., McIntosh, W., Millan, C., Morin, R., Ohneiser, C., Paulsen, T., Persico, D., Rain, I., Reed, J., Riesselman, C., Sagnotti, L., Schmitt, D., Sjunneskog, C., Strong, P., Taviani, M., Vogel, S., Wilch, T., & Williams, T. (2009). Obliquity-paced Pliocene West Antarctic ice sheet oscillations. *Nature*, 458(7236), 322-328.
- Pagani, M., Liu, Z., LaRiviere, J. & Ravelo, A.C. (2010). High Earth-system climate sensitivity determined from Pliocene carbon dioxide concentrations. *Nature Geoscience*, 3(1), 27-30.
- Passchier, S. (2011). Linkages between East Antarctic Ice Sheet extent and Southern Ocean temperatures based on a Pliocene high-resolution record of ice-rafted debris off Prydz Bay, East Antarctica. *Paleoceanography*, 26(4).
- Pollard, D., & DeConto, R. M. (2009). Modelling West Antarctic ice sheet growth and collapse through the past five million years. *Nature*, 458(7236), 329-332.

- Pyne, A., Robinson, P. H., & Barrett, P. J. (1985). *CIROS 2 Core Log, Description, Photographs and Grain Size Analysis, Ferrar Fjord, Antarctica*. Antarctic Research Centre, Research School of Earth Sciences, Victoria University.
- Rahmstorf, S. (2010). A new view on sea level rise. *Nature reports climate change*, 44-45.
- Reinardy, B. T. I., Escutia, C., Iwai, M., Jimenez-Espejo, F. J., Cook, C., van de Flierdt, T., & Brinkhuis, H. (2015). Repeated advance and retreat of the East Antarctic Ice Sheet on the continental shelf during the early Pliocene warm period. *Palaeogeography, Palaeoclimatology, Palaeoecology*, 422, 65-84.
- Rosenberg, J. (2014) *Late-Pliocene ice-rafting, IODP Site U1359, Antarctica* (Master's Thesis). Montclair State University, NJ.
- Schoof, C. (2007), Ice sheet grounding line dynamics: Steady states, stability, and hysteresis, *J. Geophys. Res.*, 112.
- Seki, O., Foster, G.L., Schmidt, D.N., Mackensen, A., Kawamura, K. & Pancost, R.D., 2010. Alkenone and boron-based Pliocene pCO<sub>2</sub> records. *Earth and Planetary Science Letters*, 292(1), 201-211.
- Shepherd, A., Ivins, E.R., Geruo, A., Barletta, V.R., Bentley, M.J., Bettadpur, S., Briggs, K.H., Bromwich, D.H., Forsberg, R., Galin, N. & Horwath, M. (2012). A reconciled estimate of ice-sheet mass balance. *Science*, 338(6111), 1183-1189.
- Tauxe, L., Stickley, C. E., Sugisaki, S., Bijl, P. K., Bohaty, S. M., Brinkhuis, H., Escutia, C., Flores, J.A., Houben, A.J.P., Iwai, M., Jimenez-Espejo, F., McKay, R., Passchier, S., Pross, J., Riesselman, C.R., Rohl, U., Sangiorgi, F., Welsh, K.,

- Klaus, A., Fehr, A., Bendle, J.A.P., Dunbar, R., Gonzalez, J., Hayden, T., Katsuki, K., Olney, M.P., Pekar, S.F., Shrivastava, P.K., van de Flierdt, T., Williams, T., & Yamane, M. (2012). Chronostratigraphic framework for the IODP Expedition 318 cores from the Wilkes Land Margin: Constraints for paleoceanographic reconstruction. *Paleoceanography*, 27(2).
- Vaughan, D.G., Comiso, J.C., Allison, I., Carrasco, J., Kaser, G., Kwok, R., Mote, P., Murray, T., Paul, F., Ren, J., Rignot, E., Solomina, O., Steffen, K. & Zhange, T. (2013). Observations: Cryosphere. In *Climate Change 2013: the Physical Science Basis. Contribution of Working Group I to the Fifth Assessment Report of the Intergovernmental Panel on Climate Change*, Cambridge Univ. Press, Cambridge and New York.
- Whitehead, J. M., & Bohaty, S. M. (2003). Pliocene summer sea surface temperature reconstruction using silicoflagellates from Southern Ocean ODP Site 1165. *Paleoceanography*, 18(3).
- Whitehead, J.M., Quilty, P.G., Harwood, D.M. & McMinn, A., (2001). Early Pliocene paleoenvironment of the Sørødal Formation, Vestfold Hills, based on diatom data. *Marine Micropaleontology*, 41(3), pp.125-152.
- Williams, T., van de Flierdt, T., Hemming, S.R., Chung, E., Roy, M. & Goldstein, S.L. (2010). Evidence for iceberg armadas from East Antarctica in the Southern Ocean during the late Miocene and early Pliocene. *Earth and Planetary Science Letters*, 290(3), pp.351-361.

- Winnick, M. J., & Caves, J. K. (2015). Oxygen isotope mass-balance constraints on Pliocene sea level and East Antarctic Ice Sheet stability. *Geology*, *43*(10), 879-882.
- Winter, D., Sjunneskog, C., Scherer, R., Maffioli, P., & Harwood, D. (2012). Diatom-based correlation of early to mid-Pliocene drillcores from the southwestern Ross Sea, Antarctica. *Global and Planetary Change*, *96*, 131-142.
- Yamane, M., Yokoyama, Y., Abe-Ouchi, A., Obrochta, S., Saito, F., Moriwaki, K., & Matsuzaki, H. (2015). Exposure age and ice-sheet model constraints on Pliocene East Antarctic ice sheet dynamics. *Nature communications*, *6*, 1-8.



## CHAPTER 5

### Summary and Future Outlook

#### 5.1 Summary

The principal aim of this dissertation was to assess the behavior of the East Antarctic Ice Sheet on the Wilkes Land continental margin using a sediment core from the early Pliocene. This chapter seeks to summarize how that aim was achieved by discussing the major findings of each objective and their significance, potential future research directions, and broader environmental implications.

#### **Objective 1: Evaluate sedimentation patterns to illustrate changes in ice sheet behavior.**

As discussed in Chapter 2, through assessment of a high resolution ice-rafted debris (IRD) mass accumulation rates (MAR) record from ice proximal IODP Site U1359, I identified three major ice-rafting excursions in the early Pliocene. By confirming that the high peaks were of glacial origin through SEM assisted microtextural analysis, these IRD MAR peaks help to establish the presence of an ice sheet that periodically advanced and calved icebergs that deposited detritus on the continental rise.

The findings in U1359 are significant because it not only captures a complete, high-resolution record of the variability of the EAIS on the Wilkes margin but it also stresses the sensitivity of the largest marine-based region of the EAIS to Pliocene climatic conditions. It is also important to note that the ice sheet history for the Wilkes Land margin was incomplete for the early Pliocene, with portions inferred from shelf site

U1358 (Orejola et al., 2014) and distal rise site U1361 (Cook et al., 2013). Because this time period is a major focus of study for future ice sheet behavior, this research contributes to this topic by providing a complete glacial history for a previously obscure area of the EAIS.

**Objective 2: Determine whether the driving factor behind ice sheet response was a global or local influence.**

Chapter 2 addresses the relationship between orbital variations in the IRD MAR of U1359 and revealed the influence of orbital rhythms and SSTs on ice sheet behavior. The transition of an obliquity forced to precession forced signal concordant with an increase in SSTs pinpoints the onset of persistent retreat of the EAIS on the Wilkes Margin. These results are significant because it identifies a conditional climate threshold where the EAIS can maintain its stability before being pushed towards a new state of equilibrium and may provide an important target for ice sheet modeling. This is important for climate models that are assessing the ice-sheet response to future climate change.

**Objective 3: Determine the effects of warming on the interaction between the ice sheet and Southern Ocean during the Pliocene Climatic Optimum (PCO).**

The results from Chapter 3 were based on a bulk geochemical analysis of U1359. The data spanned the early portion of the warm PCO, capturing the transition in orbital rhythms found in Chapter 2 and suggests that variations in ocean circulation affected the ventilation of water masses and carbon near the Wilkes Land coast. This is considered

important because in the future we may see this enhanced ventilation of CO<sub>2</sub> or carbon burial due to the biogenic bloom.

**Objective 4: Assess variations in ice sheet extent during warm periods within the early Pliocene.**

Chapter 4 presented a compilation of EAIS sediment records from early Pliocene warm intervals such as the Pliocene climatic Optimum (4.5 – 4.0 Ma) and the mid-Pliocene Warm Period (3.3 – 3.0 Ma). The analysis shows that under MPWP climate conditions, the EAIS underwent a glacial expansion in the Prydz Bay and Ross Sea regions. The effects of warming and onset of retreat of the EAIS were found to be most prominent during PCO. These findings are significant due to the fact that most models used for future estimates are largely based on MPWP boundary conditions—which have been unable to hindcast Pliocene sea level estimates and ice sheet behavior as observed through sedimentological records. The behavior of the EAIS is vastly different between these two time periods of focus. Moreover, the regional correlation revealed a continent wide response to warming during the PCO at ~4.6 Ma, the same time that the EAIS on the Wilkes Land margin exhibited threshold behavior (See Objective 2).

The findings support the idea that to better understand the regional variability between basins a greater spatial and temporal resolution in the geologic record is needed in order to more accurately model the EAIS in the future.

## 5.2 Environmental Implications

The IPCC projects that with strong mitigation practices the level of CO<sub>2</sub> will be in a range similar to Pliocene. Under these conditions global temperatures are expected to increase to 1.5°C above preindustrial and sea level would rise <1 m (See Appendix A). What is important to note is that global temperatures have already increased 1°C since preindustrial. During the Pliocene, global temperatures were 4°C above preindustrial. Throughout the Pliocene, the EAIS shows a very dynamic response. It underwent a significant change at ~4.6 Ma where a continent wide response to warming was identified (See Chapter 4). Climate models that use MPWP (2-3°C) boundary conditions have been unable to capture this dynamic response of the EAIS and according to the models sea level rose no more than 20 m. The fact that the entire EAIS shows a response at this time may indicate a point of no return—the switch or threshold to be avoided—and expresses the need for a greater focus on this particular time period.

It is also important to note that areas that were most susceptible to this change were marine-terminating regions of the EAIS (i.e. Wilkes Land and Prydz Bay). This is important because the Wilkes Land sector holds ~19 m of sea level equivalent. The response of the EAIS seen during the PCO highlights the potential for a much larger sea level contribution than is currently projected. Everything considered, the PCO time interval as evident from the sediment record may hold the answers to the future EAIS response and what we're seeing now may be a precursor.

### **5.3 Concluding Remarks**

The results presented in this dissertation shed new light on the behavior of the EAIS during a period of similar climatic warmth to today. The findings show that low-lying areas of the EAIS, such as the Wilkes land margin, are particularly susceptible to changes in climate and the potential for greater sea level rise contribution.

IRD MAR studies using deep marine ice proximal cores such as Prydz Bay Site 1165 and Wilkes Land Site U1359 have shown a strong potential for understanding ice dynamics as they provide a complete and higher-resolution record of ice sheet variability as opposed to discontinuous shelf sites. Taken together, they can provide a much clearer picture of ice dynamics. A future strategy to further address EAIS stability in the early Pliocene may be to sample similar cores on continental rise sites off other ice-sheet drainage basins.

## LIST OF APPENDICES

APPENDIX A – Supplementary text for Chapter 1

APPENDIX B – Supporting Information for Chapter 2

APPENDIX C – Microtexture Raw Data and Methods

## APPENDIX A

### A.1: State of the Climate and Sea Level Rise Projections

Over the past few decades, global mean surface temperatures have steadily increased, with the first decade of the 21<sup>st</sup> century documented as the warmest on record (Hartmann et al., 2013). Human activities, such as the burning of fossil fuels (coal, oil, and gas), are contributing to the increase in greenhouse gases. Greenhouse gases, such as CO<sub>2</sub>, are thought to be the dominant cause of the observed warming (IPCC, 2013). Satellite and instrumental observation systems show increases in land and ocean temperature as well as a reduction in glaciers and ice sheets (Cubasch et al., 2013). The observed rate of sea level has not been globally uniform due to regional factors, however, there is no doubt that it is an increasing trend (Overpeck & Weiss, 2009). Tide gauge measurements and satellite data (post 1993) have indicated that between 1901 and 2010, global mean sea level rose ~0.19 m (Rhein et al., 2013). The AIS, which represents the largest potential source of future sea level rise (Church et al., 2013), contributed an estimated 3.8 mm of sea level equivalent between 1993 and 2010 (Vaughan et al., 2013).

Global sea level rise is primarily based on two processes: thermal expansion of the ocean and the addition of water to the ocean from melting land ice (Rahmstorf, 2010). When it comes to sea level projections, climate models focus on thermal expansion and input from glaciers, they do not consider the dynamical response of individual regions of continental ice sheets. The IPCC (AR4) did not provide a strong constraint on estimates of sea level rise due to rapid dynamical changes in the flow of Greenland and Antarctica because there is an incomplete understanding of the dynamics (Overpeck & Weiss,

2009). Currently, there is no literature that investigates the amount of sea level rise generated by dynamic change under different emission scenarios (IPCC Sea level change). However, the latest IPCC (2013) suggests that dynamical change within the Antarctic ice sheet will likely contribute to sea level rise during the next century and possibly associated with marine ice sheet instability (Church et al., 2013).

The upper bound limits of Antarctica's sea level rise contributions are derived from regions where current mass loss is concentrated (Pine Island, Thwaites and Smith Glacier) despite the uncertainties that exist how other drainage basins will contribute to future discharge (Little et al, 2013). Using a probabilistic framework approach, they assessed sea level changes due to ice sheet contributions by explicitly accounting for mass balance uncertainty and calculated the sum of regional contributions. They demonstrated that by excluding the dynamic changes, particularly outside the current areas of focus, a gross underestimation of sea level rise by 2100 would result—such results that are essential to decision-making processes. The biggest argument against the current method is that the models do not treat mountain glaciers separate from ice sheets—instead it treats all ice as a continuum (Rahmstorf, 2010).

Representative Concentration Pathways (RCP) are the newly developed climate scenarios discussed in the latest IPCC report used by climate modelers. The scenarios differ from the previous IPCC SRES scenarios in that they are not based on socio-economic storylines. Each scenario is named according to a radiative forcing target level by the end of the century (van Vuuren et al., 2011). These estimates are based on the forcing of greenhouse gases and include a mitigation scenario (RCP2.6), two medium



stabilization scenarios (RCP4.5 and RCP6) and a high baseline emission scenario (RCP8.5) summarized in further detail in Table 1. The RCP2.6, also known as the peak and decline scenario, assumes a strong mitigation action and yields a smaller temperature increase compared to the previous SRES scenarios (Collins et al., 2013). Under this scenario, CO<sub>2</sub> concentrations would peak at ~490 ppm by mid-century and then reduce towards 400 ppm by 2100, and further to 360 by 2300 [extended scenario] (Collins et al., 2013; Moss et al., 2010; van Vuuren et al., 2011).

<b>Scenario</b>	<b>Mean SL (m)</b>	<b>SL Range (m)</b>	<b>CO<sub>2</sub> (ppm) upper limit</b>	<b>Global Temp. Increase</b>
RCP2.6	0.44	0.28-0.61	490 - 400	<1.5°C
RCP4.5	0.53	0.36-0.71	~650	<2.0°C
RCP6.0	0.55	0.38-0.73	~850	>2.0°C
RCP8.5	0.74	0.52-0.98	>1,370	>2.0°C

**Table A1.** A comparison of the projected trends by the end of 2100 for each RCP

scenario. Mean sea level and sea level range in meters from Church et al. (2013); the CO<sub>2</sub> upper limit from Moss et al. (2010) and Van Vuuren et al. (2010); and estimates of global temperature increase relative to average from 1850-1900 from IPCC (2013).

**References:**

- Church, J. A., Clark, P. U., Cazenave, A., Gregory, J. M., Jevrejeva, S., Levermann, A., Merrifield, M.A., Milne, G.A., Nerem, R.S., Nunn, P.D., Payne, A.J., Pfeffer, W.T., Stammer, D., & Unnikrishnan, A.S. (2013). Sea level change. *Climate Change 2013: The Physical Science Basis. Working Group I Contribution to the Fifth Assessment Report of the Intergovernmental Panel on Climate Change.*
- Collins, M., Knutti, R., Arblaster, J., Dufresne, J.L., Fichefet, T., Friedlingstein, P., Gao, X., Gutowski, W.J., Johns, T., Krinner, G., Shongwe, M., Tebaldi, C., Weaver, A.J. & Wehner, M. (2013). Long-term Climate Change: Projections, Commitments and Irreversibility. *Climate Change 2013: The Physical Science Basis. Working Group I Contribution to the Fifth Assessment Report of the Intergovernmental Panel on Climate Change.*
- Cubasch, U., Wuebbles, D., Chen, D., Facchini, M.C., Frame, D., Mahowald, N., & Winther, J.G. (2013). Introduction. *Climate Change 2013: The Physical Science Basis. Working Group I Contribution to the Fifth Assessment Report of the Intergovernmental Panel on Climate Change.*
- Hartmann, D.L., Klein Tank, A.M.G., Rusticucci, M., Alexander, L.V., Brönnimann, S., Charabi, Y., Dentener, F.J., Dlugokencky, E.J., Easterling, D.R., Kaplan, A., Soden, B.J., Thorne, P.W., Wild, M. & Zhai, P.M. (2013). Observations: Atmosphere and Surface. *Climate Change 2013: The Physical Science Basis. Working Group I Contribution to the Fifth Assessment Report of the Intergovernmental Panel on Climate Change.*

- Moss, R. H., Edmonds, J. A., Hibbard, K. A., Manning, M. R., Rose, S. K., Van Vuuren, D. P., Carter, T.R., Emori, S., Kainuma, M., Kram, T., Meehl, G.A., Mitchell, J.F.B., Nakicenovic, N., Riahi, K., Smith, S.J., Stouffer, R.J., Thomson, A.M., Weyant, J.P., & Wilbanks, T.J. (2010). The next generation of scenarios for climate change research and assessment. *Nature*, *463*(7282), 747-756.
- Overpeck, J. T., & Weiss, J. L. (2009). Projections of future sea level becoming more dire. *Proceedings of the National Academy of Sciences*, *106*(51), 21461-21462.
- Rahmstorf, S. (2010). A new view on sea level rise. *Nature reports climate change*, 44-45.
- Rhein, M., Rintoul, S.R., Aoki, S., Campos, E., Chambers, D., Feely, R.A., Gulev, S., Johnson, G.C., Josey, S.A., Kostianoy, A., Mauritzen, C., Roemmich, D., Talley, L.D. & Wang, F. (2013). Observations: Ocean. *Climate Change 2013: The Physical Science Basis. Working Group I Contribution to the Fifth Assessment Report of the Intergovernmental Panel on Climate Change*.
- Van Vuuren, D. P., Edmonds, J., Kainuma, M., Riahi, K., Thomson, A., Hibbard, K., Hurtt, G.C., Kram, T., Krey, V., Lamarque, J.F., Masui, T., Meinshausen, M., Nakicenovic, N., Smith, S.J. & Rose, S.K. (2011). The representative concentration pathways: an overview. *Climatic change*, *109*, 5-31.
- Vaughan, D.G., Comiso, J.C., Allison, I., Carrasco, J., Kaser, G., Kwok, R., Mote, P., Murray, T., Paul, F., Ren, J., Rignot, E., Solomina, O., Steffen, K. & Zhange, T. (2013). Observations: Cryosphere. In *Climate Change 2013: the Physical Science Basis. Contribution of Working Group I to the Fifth Assessment Report of the*

*Intergovernmental Panel on Climate Change, Cambridge Univ. Press, Cambridge and New York.*

## APPENDIX B

### B.1: Supporting Information for Chapter 2

#### **Introduction**

The supporting information includes: (1) Supporting Figure S1 for the age model; (2) Supporting Figure S2, which shows our variations of IRD MAR from Site U1359,  $\epsilon\text{Nd}$  values, and IBRD MAR for adjacent continental rise Site U1361 [Cook *et al.*, 2013; Patterson *et al.*, 2014]; (3) Supporting Figures S3 and S4, which shows wavelet plots for the IBRD MAR at Site U1361 [Patterson *et al.*, 2014], and (4) a summary of the raw data that was generated to calculate IRD MAR and used to produce Figure 2 found within the manuscript.

#### **Supporting Figure B1 - Age Model**

Age tie points were generated through paleomagnetostratigraphic age correlation [Tauxe *et al.*, 2012] and based on the Gradstein *et al.* [2004] age-scale. A total of fifteen age tie points across Holes U1359A, U1359B and U1359C, generate a constant linear sedimentation rate of ca. 45 m/Myr for the interval between ~69 and ~212 mcd. To account for a condensed interval in the uppermost part of the studied interval (between 68.84 and 69.94 mcd) a stepwise regression model was generated using age tie points from Hole U1359A.

#### **Supporting Figure B2**

Figure S2 includes the IRD MAR from Site U1359 (top), which is based on the coarse fraction  $>125\ \mu\text{m}$  [this study],  $\epsilon\text{Nd}$  values for samples from the fine fraction ( $<63\ \mu\text{m}$ ) of U1361 [Cook *et al.*, 2013] (middle), and the IBRD MAR from Patterson *et al.* [2014],

which is calculated based on the sieve fraction between 250  $\mu\text{m}$  and 2 mm (bottom). IRD MAR from U1359 shows high variability between 5.1 and 4.0 Ma with maxima greater than 2  $\text{g}/\text{cm}^2/\text{kyr}$ . High amplitude variability in  $\epsilon\text{Nd}$ , coincides with the IRD MAR excursions of U1359. The IBRD record of *Patterson et al.* [2014] does not extend beyond 4.4 Ma.

### **Dataset ds01**

Dataset ds01 contains the parameters used to calculate IRD MAR and are listed by increasing depth (mbsf-A). All grain size diameters are based on the Wentworth size classes.

Sample ID: Sample ID is based on Site, Hole, Core, Section and Section Depth in cm.

Depth (mcd): Meters composite depth was used to join samples from both U1359A and U1359B onto a common depth scale.

Depth (mbsf-A): All samples were converted to the depth scale in meters below seafloor for Hole-A in order for comparisons to be made to the lithology log [*Expedition 318 Scientists*, 2011].

Age (Ma): Age was calculated in millions of years based on paleomagnetostratigraphic age correlation from U1359A, U1359B, and U1359C (See Table 2-1 and Supporting Figure B-1) and according to the *Gradstein et al.* [2004] timescale.

IRD ( $\text{cm}^3/\text{cm}^3$ ): The IRD fraction is defined as the volume percent of the terrigenous coarse fraction  $>125$  micrometers derived from laser particle size measurements, divided by 100.

LSR (cm/ky): The linear sedimentation rates were calculated from the age model. The LSR differs near the top of the core due to a condensed section (See Supporting Figure B-1).

Opal (g/g): The opal % represents the weight percent biogenic silica fraction.

TERR: The terrigenous fraction defined as (1-biogenic silica fraction-carbonate fraction).

DBD (g/cm<sup>3</sup>): The dry bulk density derived from shipboard measurements [*Expedition 318 Scientists*, 2011].

IRD MAR (g/cm<sup>2</sup>/kyr): Ice-rafted debris (IRD) mass accumulation rates (MAR) is calculated based on the equation  $IRD\ MAR = IRD \times TERR \times DBD \times LSR$ .

%Silt: The %Silt is the volume percent of the particle size measurements between 3.9 and 62.5 micrometers.

%Clay: The %Clay is the volume percent of the particle size measurements between 0.02 and 3.9 micrometers (0.02 is the lower limit of the Malvern Mastersizer 2000).

Sorting: Sorting of the fine fraction (<125 micron) was calculated using the program GRADISTAT [*Blott and Pye*, 2001] following the scheme of *Folk and Ward* [1957] where values are derived based on the lognormal distribution of phi size values.

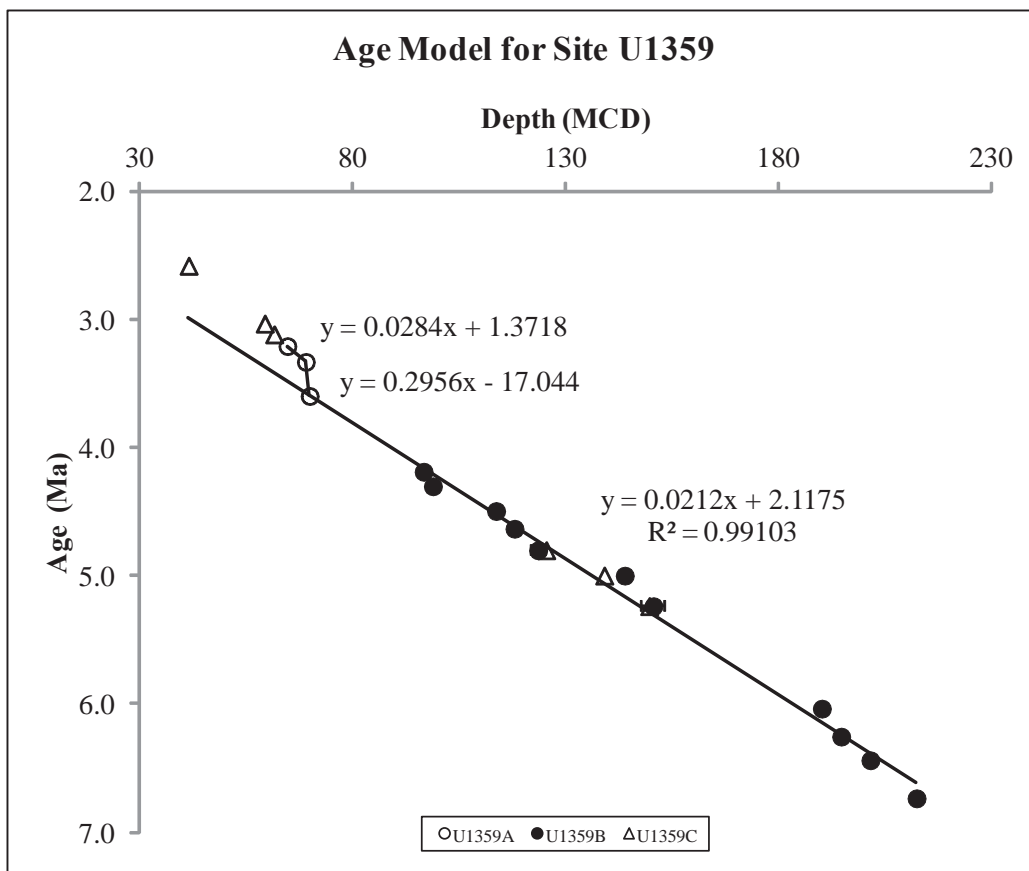


**Figure B1.** Age-tie points for Site U1359 using linear correlation between magnetostratigraphic age tie points from *Tauxe et al.* [2012] referred to in Table 2-1. Age datums encompass Holes U1359A, U1359B, and U1359C.



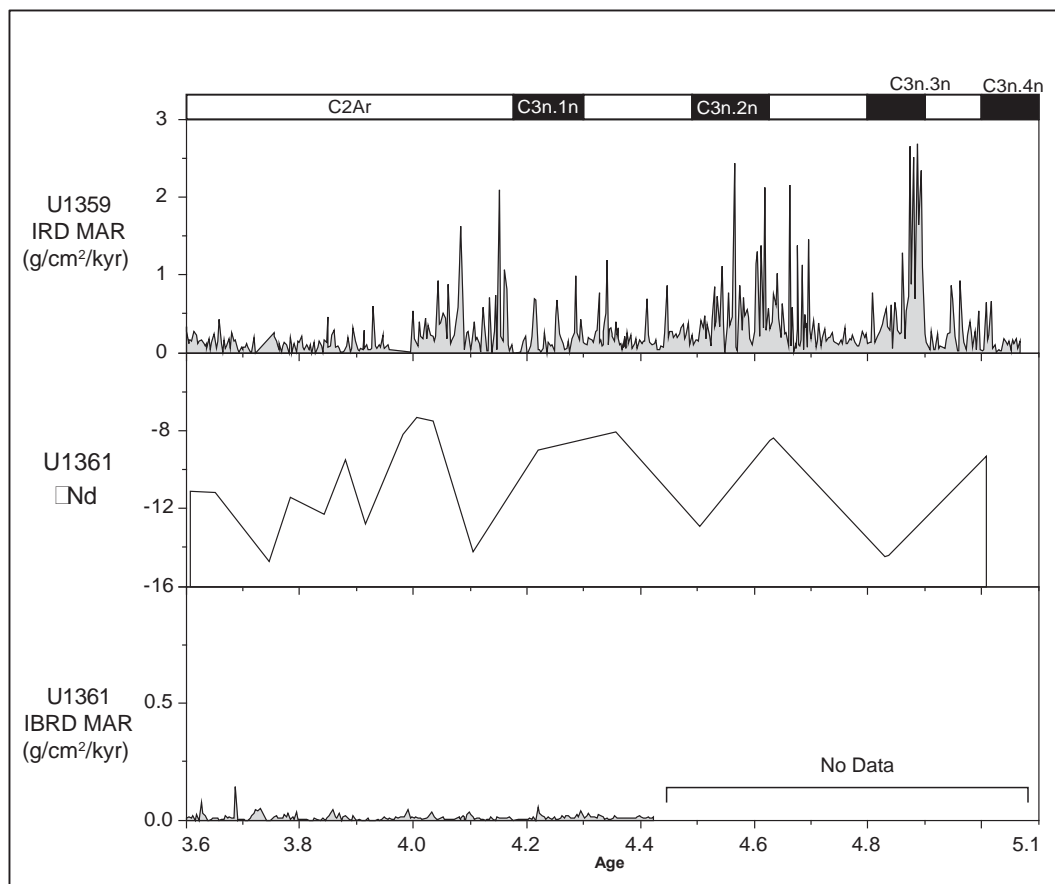


**Figure B2.** Time series of IRD MAR from Site U1359 (Top), and  $\epsilon$ Nd [Cook *et al.*, 2013] (Middle) and IBRD MAR (Bottom) from Site U1361 [Patterson *et al.*, 2014, Robert McKay, pers. comm., 2015]. The IRD MAR from Site U1359 was based on the sand fraction  $>125$   $\mu$ m and the IBRD MAR from U1361 was calculated based on the sieve fraction between 250  $\mu$ m and 2 mm.

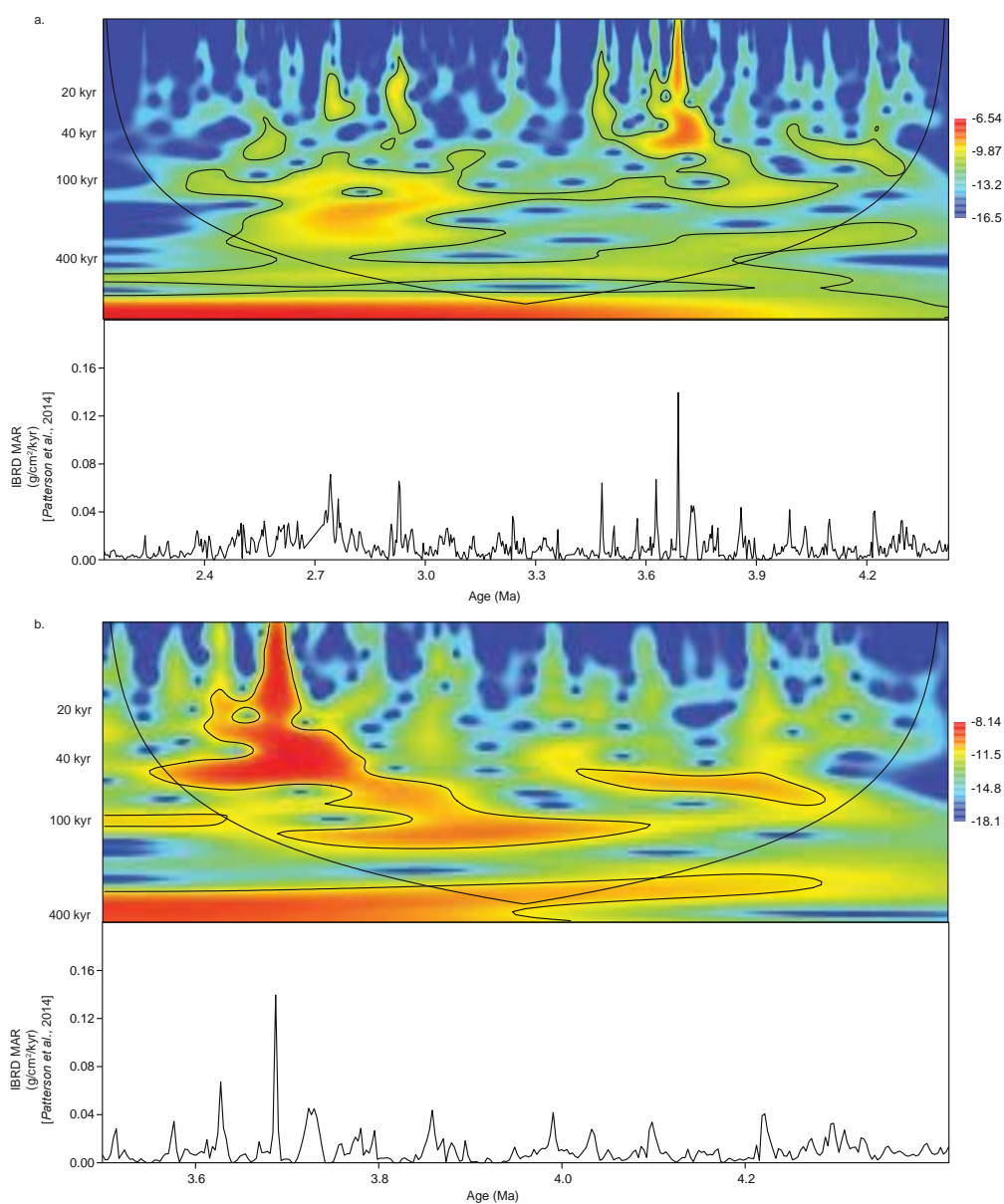


**Figure B3.** Morlet wavelet plots for the time series based on an untuned age model of Site U1361 [Patterson et al., 2014]. The IBRD MAR is based on the raw sieve data [Robert McKay, pers. comm, 2015], excluding any detrending procedures. The upper plot shows the full time series. The lower plot indicates the result for the interval below a condensed section, dated at 3.5-3.3 Ma.

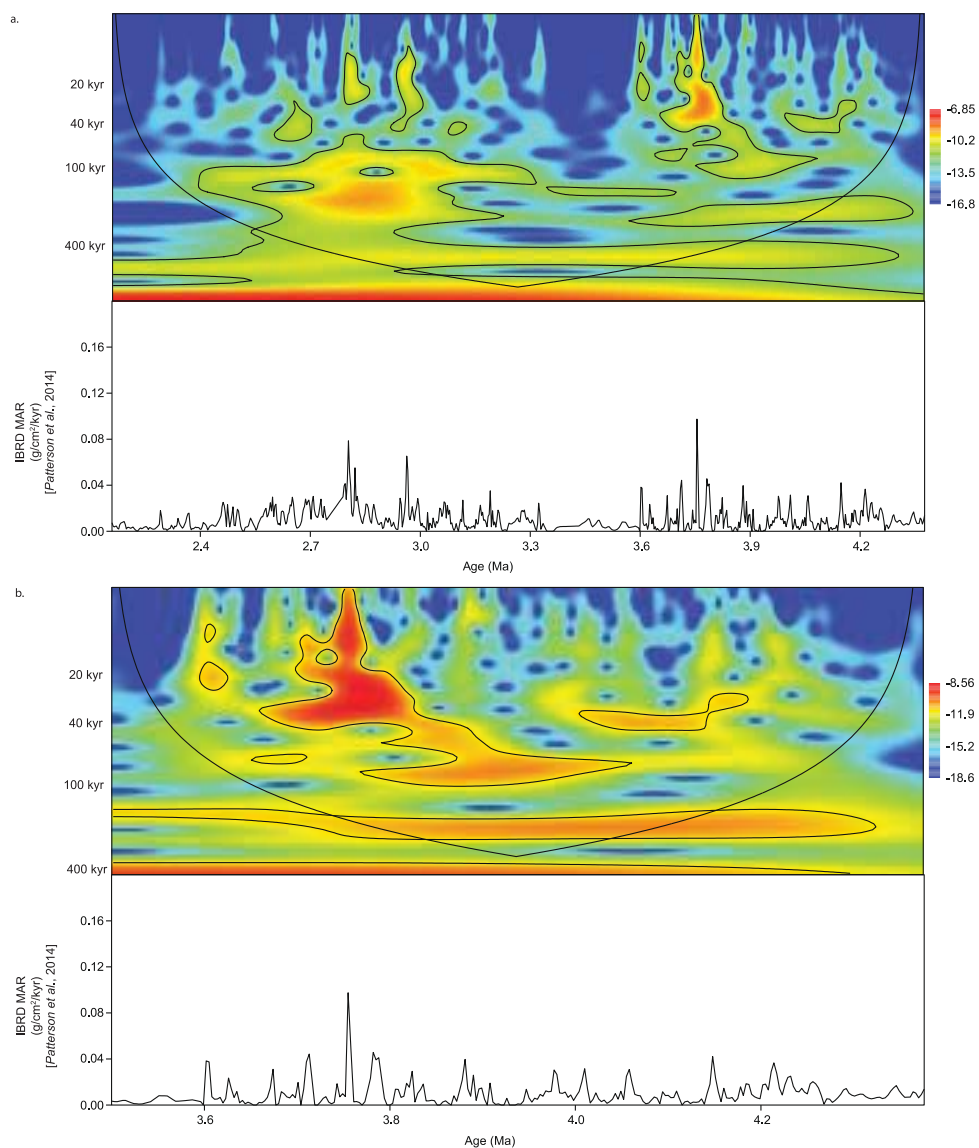


**Figure B4.** Morlet wavelet plots for the time series based on a tuned age model of Site U1361 [Patterson et al., 2014]. The IBRD MAR is based on the raw sieve data [Robert McKay, pers. comm, 2015] excluding any detrending procedures. The upper plot shows the full time series. The lower plot indicates the result for the interval below a condensed section, dated at 3.5-3.3 Ma. Significant obliquity is expressed in short intervals between approx. 3.6 and 4.1 Ma.

**Data Set ds01.** Summary of data used to calculate IRD MAR (Displayed in Figure 2-2) and encompass both Holes A and B.

<u>Sample ID</u>	<u>Depth (mcd)</u>	<u>Depth (mbsf-A)</u>	<u>Age (Ma)</u>	<u>IRD (cm<sup>3</sup>/cm<sup>3</sup>)</u>	<u>LSR (cm/kyr)</u>	<u>Opal (g/g)</u>	<u>TERR (g/g)</u>	<u>DBD (g/cm<sup>3</sup>)</u>	<u>IRD.MAR (g/cm<sup>2</sup>/kyr)</u>	<u>% Silt</u>	<u>% Clay</u>	<u>Sorting</u>
U1359A-9H-1-W-0-2	67.17	67.11	3.28	0.04	3.52	0.22	0.78	1.00	0.12	63.76	31.76	1.75
U1359A-9H-1-W-45-47	67.62	67.56	3.29	0.03	3.52	0.20	0.80	1.07	0.09	78.15	18.77	1.94
U1359A-9H-1-W-90-92	68.07	68.01	3.30	0.02	3.52	0.19	0.81	1.13	0.08	77.27	20.25	1.90
U1359A-9H-1-W-135-137	68.52	68.46	3.32	0.01	3.52	0.18	0.82	1.18	0.05	75.10	23.45	1.79
U1359A-9H-2-W-15-17	68.82	68.76	3.33	0.04	3.52	0.17	0.83	1.22	0.14	80.18	15.86	1.93
U1359A-9H-2-W-60-62	69.27	69.21	3.43	0.04	0.34	0.16	0.84	1.19	0.01	75.97	20.31	1.57
U1359A-9H-2-W-75-77	69.42	69.36	3.48	0.06	0.34	0.16	0.84	1.17	0.02	73.84	20.30	1.92
U1359A-9H-2-W-90-92	69.57	69.51	3.52	0.08	0.34	0.16	0.84	1.16	0.03	78.25	13.70	1.68

<u>Sample ID</u>	<u>Depth (mcd)</u>	<u>Depth (mbsf-A)</u>	<u>Age (Mia)</u>	<u>IRD (cm<sup>3</sup>/cm<sup>3</sup>)</u>	<u>LSR (cm/kyr)</u>	<u>Opal (g/g)</u>	<u>TERR (g/g)</u>	<u>DBD (g/cm<sup>3</sup>)</u>	<u>IRD MAR (g/cm<sup>2</sup>/kyr)</u>	<u>% Silt</u>	<u>% Clay</u>	<u>Sorting</u>
U1359A -9H-2- W-105- 107	69.72	69.66	3.57	0.12	0.34	0.16	0.84	1.15	0.04	76.08	11.76	1.81
U1359A -9H-2- W-120- 122	69.87	69.81	3.60	0.08	4.54	0.16	0.84	1.14	0.33	76.01	16.34	1.81
U1359A -9H-2- W-135- 137	70.02	69.96	3.60	0.06	4.54	0.15	0.85	1.13	0.28	74.06	19.53	1.70
U1359A -9H-2- W-148- 150	70.15	70.09	3.60	0.03	4.54	0.15	0.85	1.12	0.12	78.71	18.44	1.52
U1359A -9H-3- W-0-2	70.17	70.11	3.61	0.04	4.54	0.15	0.85	1.11	0.16	65.39	30.91	1.62
U1359A -9H-3- W-15-17	70.32	70.26	3.61	0.04	4.54	0.15	0.85	1.10	0.16	71.42	24.75	1.53
U1359A -9H-3- W-30-32	70.47	70.41	3.61	0.03	4.54	0.15	0.85	1.09	0.15	85.80	10.71	1.61
U1359A -9H-3- W-45-47	70.62	70.56	3.61	0.07	4.54	0.14	0.86	1.08	0.28	69.84	23.60	1.80

<u>Sample ID</u>	<u>Depth (mcd)</u>	<u>Depth (mbsf-A)</u>	<u>Age (Ma)</u>	<u>IRD (cm<sup>3</sup>/cm<sup>3</sup>)</u>	<u>LSR (cm/kyr)</u>	<u>Opal (g/g)</u>	<u>TERR (g/g)</u>	<u>DBD (g/cm<sup>3</sup>)</u>	<u>IRD_MAR (g/cm<sup>2</sup>/kyr)</u>	<u>% Silt</u>	<u>% Clay</u>	<u>Sorting</u>
U1359A-9H-3-W-60-62	70.77	70.71	3.62	0.05	4.54	0.13	0.87	1.07	0.23	64.38	30.21	1.54
U1359A-9H-3-W-75-77	70.92	70.86	3.62	0.03	4.54	0.12	0.88	1.05	0.11	62.12	35.20	1.57
U1359A-9H-3-W-90-92	71.07	71.01	3.62	0.04	4.54	0.11	0.89	1.04	0.15	74.52	21.81	1.73
U1359A-9H-3-W-105-107	71.22	71.16	3.63	0.04	4.54	0.10	0.90	1.03	0.17	78.98	17.10	1.86
U1359A-9H-3-W-120-122	71.37	71.31	3.63	0.03	4.54	0.09	0.91	1.02	0.11	69.22	28.07	1.77
U1359A-9H-3-W-135-137	71.52	71.46	3.63	0.02	4.54	0.08	0.92	1.02	0.08	74.46	23.57	1.72
U1359A-9H-3-W-148-150	71.65	71.59	3.64	0.03	4.54	0.07	0.93	1.04	0.11	58.57	38.88	1.66
U1359A-9H-4-W-0-2	71.67	71.61	3.64	0.01	4.54	0.07	0.93	1.04	0.06	59.03	39.69	1.67

<u>Sample ID</u>	<u>Depth (mcd)</u>	<u>Depth (mbsf-A)</u>	<u>Age (Ma)</u>	<u>IRD (cm<sup>3</sup>/cm<sup>3</sup>)</u>	<u>LSR (cm/kyr)</u>	<u>Opal (g/g)</u>	<u>TERR (g/g)</u>	<u>DBD (g/cm<sup>3</sup>)</u>	<u>IRD_MAR (g/cm<sup>2</sup>/kyr)</u>	<u>% Silt</u>	<u>% Clay</u>	<u>Sorting</u>
U1359A-9H-4-W-15-17	71.82	71.76	3.64	0.04	4.54	0.06	0.94	1.06	0.18	70.34	25.75	1.68
U1359A-9H-4-W-30-32	71.97	71.91	3.64	0.01	4.54	0.05	0.95	1.07	0.04	56.51	42.60	1.60
U1359A-9H-4-W-45-47	72.12	72.06	3.65	0.03	4.54	0.06	0.94	1.09	0.13	63.41	33.89	1.63
U1359A-9H-4-W-60-62	72.27	72.21	3.65	0.05	4.54	0.06	0.94	1.10	0.23	59.56	35.45	1.88
U1359A-9H-4-W-75-77	72.42	72.36	3.65	0.01	4.54	0.07	0.93	1.12	0.06	69.78	29.01	1.58
U1359A-9H-4-W-90-92	72.57	72.51	3.66	0.03	4.54	0.07	0.93	1.13	0.14	67.07	29.94	1.65
U1359A-9H-4-W-105-107	72.72	72.66	3.66	0.09	4.54	0.08	0.92	1.14	0.42	73.58	17.59	1.93
U1359A-9H-4-W-120-122	72.87	72.81	3.66	0.03	4.54	0.08	0.92	1.16	0.12	76.58	20.90	1.66
U1359A-9H-4-W-135-137	73.02	72.96	3.67	0.00	4.54	0.09	0.91	1.17	0.01	53.33	46.45	1.54

<u>Sample ID</u>	<u>Depth (mcd)</u>	<u>Depth (mbsf-A)</u>	<u>Age (Ma)</u>	<u>IRD (cm<sup>3</sup>/cm<sup>3</sup>)</u>	<u>LSR (cm/kvr)</u>	<u>Opal (g/g)</u>	<u>TERR (g/g)</u>	<u>DBD (g/cm<sup>3</sup>)</u>	<u>IRD/MAR (g/cm<sup>2</sup>/kvr)</u>	<u>% Silt</u>	<u>% Clay</u>	<u>Sorting</u>
U1359A-9H-4-W-148-150	73.15	73.09	3.67	0.03	4.54	0.09	0.91	1.18	0.16	62.43	34.20	1.85
U1359A-9H-5-W-0-2	73.17	73.11	3.67	0.01	4.54	0.09	0.91	1.18	0.05	59.63	39.40	1.80
U1359A-9H-5-W-15-17	73.32	73.26	3.67	0.02	4.54	0.10	0.90	1.19	0.09	54.01	44.09	1.86
U1359A-9H-5-W-30-32	73.47	73.41	3.68	0.04	4.54	0.10	0.90	1.20	0.19	68.33	27.86	1.64
U1359A-9H-5-W-45-47	73.62	73.56	3.68	0.01	4.54	0.11	0.89	1.21	0.06	63.91	34.87	1.74
U1359A-9H-5-W-60-62	73.77	73.71	3.68	0.05	4.54	0.12	0.88	1.22	0.26	73.67	21.04	1.87
U1359A-9H-5-W-75-77	73.92	73.86	3.68	0.03	4.54	0.12	0.88	1.23	0.14	70.16	26.91	1.69
U1359A-9H-5-W-90-92	74.07	74.01	3.69	0.03	4.54	0.13	0.87	1.25	0.16	71.38	25.28	1.76
U1359A-9H-5-W-105-107	74.22	74.16	3.69	0.01	4.54	0.14	0.86	1.21	0.04	68.95	30.27	1.71



<u>Sample ID</u>	<u>Depth (mcd)</u>	<u>Depth (mbsf-A)</u>	<u>Age (Ma)</u>	<u>IRD (cm<sup>3</sup>/cm<sup>3</sup>)</u>	<u>LSR (cm/kyr)</u>	<u>Opal (g/g)</u>	<u>TERR (g/g)</u>	<u>DBD (g/cm<sup>3</sup>)</u>	<u>IRD MAR (g/cm<sup>2</sup>/kyr)</u>	<u>% Silt</u>	<u>% Clay</u>	<u>Sorting</u>
U1359A-9H-5-W-120-122	74.37	74.31	3.69	0.00	4.54	0.15	0.85	1.18	0.01	74.25	25.43	1.69
U1359A-9H-5-W-135-137	74.52	74.46	3.70	0.02	4.54	0.15	0.85	1.14	0.07	68.13	30.21	1.75
U1359A-9H-5-W-148-150	74.65	74.59	3.70	0.01	4.54	0.16	0.84	1.10	0.04	80.64	18.35	1.58
U1359A-9H-6-W-0-2	74.67	74.61	3.70	0.02	4.54	0.16	0.84	1.10	0.06	74.11	24.34	1.74
U1359A-9H-6-W-15-17	74.82	74.76	3.70	0.02	4.54	0.17	0.83	1.06	0.06	67.32	31.06	1.79
U1359A-9H-6-W-32-34	74.99	74.93	3.71	0.03	4.54	0.17	0.83	1.02	0.11	86.01	11.01	1.67
U1359A-9H-6-W-45-47	75.12	75.06	3.71	0.02	4.54	0.16	0.84	0.98	0.07	64.43	33.62	1.76
U1359A-9H-6-W-60-62	75.27	75.21	3.71	0.00	4.54	0.16	0.84	0.96	0.00	57.65	42.25	1.70
U1359A-9H-6-W-70-72	75.37	75.31	3.72	0.00	4.54	0.15	0.85	0.97	0.00	52.39	47.48	1.66

<u>Sample ID</u>	<u>Depth (mcd)</u>	<u>Depth (mbsf-A)</u>	<u>Age (Mia)</u>	<u>IRD (cm<sup>3</sup>/cm<sup>3</sup>)</u>	<u>LSR (cm/kvr)</u>	<u>Opal (g/g)</u>	<u>TERR (g/g)</u>	<u>DBD (g/cm<sup>3</sup>)</u>	<u>IRD.MAR (g/cm<sup>2</sup>/kvr)</u>	<u>% Silt</u>	<u>% Clay</u>	<u>Sorting</u>
U1359A-9H-6-W-90-92	75.57	75.51	3.72	0.05	4.54	0.14	0.86	0.98	0.20	58.01	36.90	1.58
U1359A-9H-6-W-105-107	75.72	75.66	3.72	0.00	4.54	0.13	0.87	0.99	0.00	55.48	44.52	1.53
U1359A-10H-1-W-0-2	77.26	76.61	3.76	0.05	4.54	0.05	0.95	1.10	0.26	64.51	30.05	1.66
U1359A-10H-1-W-0-2	77.26	76.61	3.76	0.04	4.54	0.05	0.95	1.10	0.21	59.36	36.29	1.70
U1359A-10H-1-W-15-17	77.41	76.76	3.76	0.03	4.54	0.04	0.96	1.11	0.15	58.44	38.49	1.43
U1359A-10H-1-W-30-32	77.56	76.91	3.76	0.02	4.54	0.04	0.96	1.12	0.09	57.87	40.29	1.41
U1359A-10H-1-W-45-47	77.71	77.06	3.76	0.01	4.54	0.05	0.95	1.14	0.04	64.56	34.59	1.52
U1359A-10H-1-W-45-47	77.71	77.06	3.76	0.02	4.54	0.05	0.95	1.14	0.11	59.89	37.82	1.61
U1359A-10H-1-W-60-62	77.86	77.21	3.77	0.00	4.54	0.06	0.94	1.15	0.00	78.05	21.87	1.60

<u>Sample ID</u>	<u>Depth (mcd)</u>	<u>Depth (mbsf-A)</u>	<u>Age (Ma)</u>	<u>IRD (cm<sup>3</sup>/cm<sup>3</sup>)</u>	<u>LSR (cm/kyr)</u>	<u>Opal (g/g)</u>	<u>TERR (g/g)</u>	<u>DBD (g/cm<sup>3</sup>)</u>	<u>IRD.MAR (g/cm<sup>2</sup>/kyr)</u>	<u>% Silt</u>	<u>% Clay</u>	<u>Sorting</u>
U1359A -10H-1- W-75-77	78.01	77.36	3.77	0.02	4.54	0.07	0.93	1.16	0.09	81.30	16.80	1.59
U1359A -10H-1- W-90-92	78.16	77.51	3.77	0.03	4.54	0.07	0.93	1.17	0.13	71.38	26.01	1.74
U1359A -10H-1- W-105- 107	78.31	77.66	3.78	0.02	4.54	0.08	0.92	1.16	0.10	67.49	30.44	1.45
U1359A -10H-1- W-120- 122	78.46	77.81	3.78	0.00	4.54	0.09	0.91	1.15	0.00	67.29	32.71	1.47
U1359A -10H-1- W-135- 137	78.61	77.96	3.78	0.04	4.54	0.10	0.90	1.13	0.20	60.55	35.19	1.45
U1359A -10H-1- W-148- 150	78.74	78.09	3.79	0.02	4.54	0.11	0.89	1.12	0.11	64.31	33.34	1.42
U1359A -10H-2- W-0-2	78.76	78.11	3.79	0.00	4.54	0.11	0.89	1.12	0.00	67.47	32.53	1.39
U1359A -10H-2- W-15-17	78.91	78.26	3.79	0.03	4.54	0.12	0.88	1.11	0.11	66.55	30.87	1.86

<u>Sample ID</u>	<u>Depth (mcd)</u>	<u>Depth (mbsf-A)</u>	<u>Age (Mia)</u>	<u>IRD (cm<sup>3</sup>/cm<sup>3</sup>)</u>	<u>LSR (cm/kyr)</u>	<u>Opal (g/g)</u>	<u>TERR (g/g)</u>	<u>DBD (g/cm<sup>3</sup>)</u>	<u>IRD.MAR (g/cm<sup>2</sup>/kyr)</u>	<u>% Silt</u>	<u>% Clay</u>	<u>Sorting</u>
U1359A -10H-2- W-30-32	79.06	78.41	3.79	0.00	4.54	0.12	0.88	1.09	0.01	58.71	41.17	1.69
U1359A -10H-2- W-45-47	79.21	78.56	3.80	0.03	4.54	0.12	0.88	1.08	0.14	78.06	18.70	1.64
U1359A -10H-2- W-60-62	79.36	78.71	3.80	0.03	4.54	0.11	0.89	1.07	0.13	65.52	31.39	1.56
U1359A -10H-2- W-75-77	79.51	78.86	3.80	0.05	4.54	0.11	0.89	1.05	0.21	62.22	32.83	1.69
U1359A -10H-2- W-90-92	79.66	79.01	3.81	0.02	4.54	0.10	0.90	1.06	0.07	70.03	28.24	1.80
U1359A -10H-2- W-105- 107	79.81	79.16	3.81	0.01	4.54	0.10	0.90	1.07	0.05	71.15	27.79	1.76
U1359A -10H-2- W-120- 122	79.96	79.31	3.81	0.02	4.54	0.09	0.91	1.09	0.10	69.61	28.24	1.52
U1359A -10H-2- W-135- 137	80.11	79.46	3.82	0.01	4.54	0.09	0.91	1.10	0.03	66.16	33.13	1.39

<u>Sample ID</u>	<u>Depth (mcd)</u>	<u>Depth (mbsf-A)</u>	<u>Age (Ma)</u>	<u>IRD (cm<sup>3</sup>/cm<sup>3</sup>)</u>	<u>LSR (cm/kvr)</u>	<u>Opal (g/g)</u>	<u>TERR (g/g)</u>	<u>DBD (g/cm<sup>3</sup>)</u>	<u>IRD.MAR (g/cm<sup>2</sup>/kvr)</u>	<u>% Silt</u>	<u>% Clay</u>	<u>Sorting</u>
U1359A -10H-2- W-148- 150	80.24	79.59	3.82	0.02	4.54	0.08	0.92	1.11	0.10	83.91	13.81	1.76
U1359A -10H-3- W-0-2	80.26	79.61	3.82	0.02	4.54	0.08	0.92	1.11	0.10	81.03	16.71	1.82
U1359A -10H-3- W-15-17	80.41	79.76	3.82	0.00	4.54	0.08	0.92	1.12	0.00	61.11	38.89	1.52
U1359A -10H-3- W-30-32	80.56	79.91	3.83	0.03	4.54	0.08	0.92	1.13	0.13	58.87	38.45	1.53
U1359A -10H-3- W-45-47	80.71	80.06	3.83	0.00	4.54	0.08	0.92	1.14	0.00	63.51	36.49	1.50
U1359A -10H-3- W-60-62	80.86	80.21	3.83	0.01	4.54	0.09	0.91	1.15	0.07	63.48	35.09	1.60
U1359A -10H-3- W-75-77	81.01	80.36	3.83	0.03	4.54	0.09	0.91	1.16	0.14	61.09	35.96	1.52
U1359A -10H-3- W-90-92	81.16	80.51	3.84	0.02	4.54	0.10	0.90	1.16	0.08	68.81	29.43	1.60
U1359A -10H-3- W-105- 107	81.31	80.66	3.84	0.00	4.54	0.10	0.90	1.15	0.00	66.38	33.61	1.51

<u>Sample ID</u>	<u>Depth (mcd)</u>	<u>Depth (mbsf-A)</u>	<u>Age (Ma)</u>	<u>IRD (cm<sup>3</sup>/cm<sup>3</sup>)</u>	<u>LSR (cm/kyr)</u>	<u>Opal (g/g)</u>	<u>TERR (g/g)</u>	<u>DBD (g/cm<sup>3</sup>)</u>	<u>IRD.MAR (g/cm<sup>2</sup>/kyr)</u>	<u>% Silt</u>	<u>% Clay</u>	<u>Sorting</u>
U1359A -10H-3- W-120- 122	81.46	80.81	3.84	0.03	4.54	0.11	0.89	1.15	0.16	65.47	31.16	1.59
U1359A -10H-3- W-135- 137	81.61	80.96	3.85	0.03	4.54	0.11	0.89	1.14	0.13	74.40	22.79	1.74
U1359A -10H-3- W-148- 150	81.74	81.09	3.85	0.10	4.54	0.12	0.88	1.14	0.46	79.65	10.31	1.72
U1359A -10H-4- W-0-2	81.76	81.11	3.85	0.02	4.54	0.12	0.88	1.14	0.07	81.87	16.60	1.69
U1359A -10H-4- W-15-17	81.91	81.26	3.85	0.02	4.54	0.13	0.87	1.13	0.09	77.42	20.61	1.79
U1359A -10H-4- W-30-32	82.06	81.41	3.86	0.05	4.54	0.13	0.87	1.12	0.23	71.56	23.25	1.75
U1359A -10H-4- W-45-47	82.21	81.56	3.86	0.07	4.54	0.12	0.88	1.12	0.29	77.79	15.71	2.03
U1359A -10H-4- W-60-62	82.36	81.71	3.86	0.01	4.54	0.12	0.88	1.12	0.07	79.50	19.05	1.78
U1359A -10H-4- W-75-77	82.51	81.86	3.87	0.02	4.54	0.11	0.89	1.11	0.09	88.11	9.95	1.47

<u>Sample ID</u>	<u>Depth (mcd)</u>	<u>Depth (mbsf-A)</u>	<u>Age (Ma)</u>	<u>IRD (cm<sup>3</sup>/cm<sup>3</sup>)</u>	<u>LSR (cm/kvr)</u>	<u>Opal (g/g)</u>	<u>TERR (g/g)</u>	<u>DBD (g/cm<sup>3</sup>)</u>	<u>IRD.MAR (g/cm<sup>2</sup>/kvr)</u>	<u>% Silt</u>	<u>% Clay</u>	<u>Sorting</u>
U1359A -10H-4- W-90-92	82.66	82.01	3.87	0.01	4.54	0.10	0.90	1.11	0.05	74.31	24.60	1.81
U1359A -10H-4- W-105- 107	82.81	82.16	3.87	0.00	4.54	0.10	0.90	1.11	0.01	67.21	32.49	1.80
U1359A -10H-4- W-120- 122	82.96	82.31	3.88	0.00	4.54	0.09	0.91	1.10	0.00	74.53	25.45	1.67
U1359A -10H-4- W-135- 137	83.11	82.46	3.88	0.00	4.54	0.09	0.91	1.10	0.02	76.17	23.35	1.54
U1359A -10H-4- W-148- 150	83.24	82.59	3.88	0.02	4.54	0.08	0.92	1.10	0.08	73.99	24.26	1.65
U1359A -10H-5- W-0-2	83.26	82.61	3.88	0.02	4.54	0.08	0.92	1.10	0.09	69.85	28.26	1.49
U1359A -10H-5- W-15-17	83.41	82.76	3.89	0.04	4.54	0.07	0.93	1.10	0.20	74.16	21.54	1.90
U1359A -10H-5- W-30-32	83.56	82.91	3.89	0.00	4.54	0.07	0.93	1.09	0.01	61.45	38.25	1.73

<u>Sample ID</u>	<u>Depth (mcd)</u>	<u>Depth (mbsf-A)</u>	<u>Age (Mia)</u>	<u>IRD (cm<sup>3</sup>/cm<sup>3</sup>)</u>	<u>LSR (cm/kyr)</u>	<u>Opal (g/g)</u>	<u>TERR (g/g)</u>	<u>DBD (g/cm<sup>3</sup>)</u>	<u>IRD_MAR (g/cm<sup>2</sup>/kyr)</u>	<u>% Silt</u>	<u>% Clay</u>	<u>Sorting</u>
U1359A -10H-5- W-45-47	83.71	83.06	3.89	0.01	4.54	0.08	0.92	1.09	0.05	64.30	34.66	1.78
U1359A -10H-5- W-60-62	83.86	83.21	3.90	0.07	4.54	0.09	0.91	1.09	0.32	72.19	20.74	1.82
U1359A -10H-5- W-75-77	84.01	83.36	3.90	0.03	4.54	0.10	0.90	1.08	0.15	65.96	30.59	1.77
U1359A -10H-5- W-90-92	84.16	83.51	3.90	0.01	4.54	0.11	0.89	1.08	0.05	67.56	31.40	1.62
U1359A -10H-5- W-105- 107	84.31	83.66	3.90	0.00	4.54	0.12	0.88	1.08	0.02	57.54	42.05	1.78
U1359A -10H-5- W-120- 122	84.46	83.81	3.91	0.01	4.54	0.12	0.88	1.08	0.06	57.99	40.56	1.77
U1359A -10H-5- W-135- 137	84.61	83.96	3.91	0.01	4.54	0.13	0.87	1.08	0.04	63.83	35.23	1.59
U1359A -10H-5- W-148- 150	84.74	84.09	3.91	0.07	4.54	0.14	0.86	1.07	0.28	57.28	35.95	1.81



<u>Sample ID</u>	<u>Depth (mcd)</u>	<u>Depth (mbsf-A)</u>	<u>Age (Mia)</u>	<u>IRD (cm<sup>3</sup>/cm<sup>3</sup>)</u>	<u>LSR (cm/kyr)</u>	<u>Opal (g/g)</u>	<u>TERR (g/g)</u>	<u>DBD (g/cm<sup>3</sup>)</u>	<u>IRD_MAR (g/cm<sup>2</sup>/kyr)</u>	<u>% Silt</u>	<u>% Clay</u>	<u>Sorting</u>
U1359A -10H-6- W-0-2	84.76	84.11	3.91	0.01	4.54	0.14	0.86	1.07	0.06	68.23	30.32	1.73
U1359A -10H-6- W-15-17	84.91	84.26	3.92	0.03	4.54	0.15	0.85	1.07	0.11	55.22	42.15	1.82
U1359A -10H-6- W-30-32	85.06	84.41	3.92	0.01	4.54	0.16	0.84	1.07	0.03	79.68	19.49	1.61
U1359A -10H-6- W-45-47	85.21	84.56	3.92	0.01	4.54	0.16	0.84	1.07	0.04	59.38	39.68	1.58
U1359A -10H-6- W-60-62	85.36	84.71	3.93	0.01	4.54	0.16	0.84	1.07	0.06	79.87	18.70	1.79
U1359A -10H-6- W-75-77	85.51	84.86	3.93	0.14	4.54	0.16	0.84	1.07	0.59	65.79	19.76	2.07
U1359A -10H-6- W-90-92	85.66	85.01	3.93	0.02	4.54	0.16	0.84	1.07	0.09	69.21	28.65	1.75
U1359A -10H-6- W-105- 107	85.81	85.16	3.94	0.01	4.54	0.16	0.84	1.08	0.05	77.56	21.18	1.70
U1359A -10H-6- W-120- 122	85.96	85.31	3.94	0.02	4.54	0.16	0.84	1.08	0.10	61.74	35.80	1.68

<u>Sample ID</u>	<u>Depth (mcd)</u>	<u>Depth (mbsf-A)</u>	<u>Age (Ma)</u>	<u>IRD (cm<sup>3</sup>/cm<sup>3</sup>)</u>	<u>LSR (cm/kyr)</u>	<u>Opal (g/g)</u>	<u>TERR (g/g)</u>	<u>DBD (g/cm<sup>3</sup>)</u>	<u>IRD MAR (g/cm<sup>2</sup>/kyr)</u>	<u>% Silt</u>	<u>% Clay</u>	<u>Sorting</u>
U1359A -10H-6- W-135- 137	86.11	85.46	3.94	0.02	4.54	0.16	0.84	1.09	0.07	69.48	28.96	1.76
U1359A -10H-6- W-148- 150	86.24	85.59	3.95	0.05	4.54	0.16	0.84	1.09	0.23	58.80	35.79	1.91
U1359A -10H-7- W-0-2	86.26	85.61	3.95	0.03	4.54	0.16	0.84	1.10	0.13	56.17	40.69	1.71
U1359A -10H-7- W-15-17	86.41	85.76	3.95	0.01	4.54	0.16	0.84	1.10	0.06	85.82	12.78	1.62
U1359A -10H-7- W-30-32	86.56	85.91	3.95	0.02	4.54	0.16	0.84	1.11	0.09	71.25	26.62	1.80
U1359A -10H-7- W-45-47	86.71	86.06	3.96	0.03	4.54	0.17	0.83	1.11	0.11	75.70	21.77	1.83
U1359A -10H-7- W-60-62	86.86	86.21	3.96	0.01	4.54	0.19	0.81	1.09	0.04	85.55	13.46	1.75
U1359A -11H-1- W-3-5	88.58	86.14	4.00	0.00	4.54	0.34	0.66	0.89	0.01	61.66	37.87	1.56
U1359A -11H-1- W-18-20	88.73	86.29	4.00	0.21	4.54	0.36	0.64	0.88	0.53	64.93	14.26	2.10

<u>Sample ID</u>	<u>Depth (mcd)</u>	<u>Depth (mbsf-A)</u>	<u>Age (Ma)</u>	<u>IRD (cm<sup>3</sup>/cm<sup>3</sup>)</u>	<u>LSR (cm/kyr)</u>	<u>Opal (g/g)</u>	<u>TERR (g/g)</u>	<u>DBD (g/cm<sup>3</sup>)</u>	<u>IRD_MAR (g/cm<sup>2</sup>/kyr)</u>	<u>% Silt</u>	<u>% Clay</u>	<u>Sorting</u>
U1359A -11H-1- W-33-35	88.88	86.44	4.00	0.07	4.54	0.37	0.63	0.86	0.18	80.77	11.77	1.45
U1359A -11H-1- W-48-50	89.03	86.59	4.00	0.06	4.54	0.38	0.62	0.84	0.15	78.37	15.47	1.47
U1359A -11H-1- W-63-65	89.18	86.74	4.01	0.04	4.54	0.39	0.61	0.82	0.09	80.17	16.02	1.47
U1359A -11H-1- W-78-80	89.33	86.89	4.01	0.18	4.54	0.40	0.60	0.82	0.40	65.15	16.74	2.03
U1359A -11H-1- W-93-95	89.48	87.04	4.01	0.09	4.54	0.40	0.60	0.83	0.21	75.98	14.80	1.79
U1359A -11H-1- W-108- 110	89.63	87.19	4.02	0.07	4.54	0.36	0.64	0.83	0.18	77.59	15.05	1.45
U1359A -11H-1- W-123- 125	89.78	87.34	4.02	0.17	4.54	0.32	0.68	0.84	0.45	71.74	11.04	1.89
U1359A -11H-1- W-138- 140	89.93	87.49	4.02	0.06	4.54	0.28	0.72	0.85	0.17	76.86	16.86	1.55
U1359A -11H-2- W-3-5	90.08	87.64	4.03	0.12	4.54	0.24	0.76	0.86	0.34	77.71	10.68	1.58

<u>Sample ID</u>	<u>Depth (mcd)</u>	<u>Depth (mbsf-A)</u>	<u>Age (Ma)</u>	<u>IRD (cm<sup>3</sup>/cm<sup>3</sup>)</u>	<u>LSR (cm/kyr)</u>	<u>Opal (g/g)</u>	<u>TERR (g/g)</u>	<u>DBD (g/cm<sup>3</sup>)</u>	<u>IRD_MAR (g/cm<sup>2</sup>/kyr)</u>	<u>% Silt</u>	<u>% Clay</u>	<u>Sorting</u>
U1359A -11H-2- W-18-20	90.23	87.79	4.03	0.07	4.54	0.20	0.80	0.86	0.22	74.09	19.00	1.64
U1359A -11H-2- W-33-35	90.38	87.94	4.03	0.06	4.54	0.17	0.83	0.87	0.21	79.31	14.33	1.65
U1359A -11H-2- W-48-50	90.53	88.09	4.04	0.04	4.54	0.17	0.83	0.88	0.15	80.63	14.92	1.48
U1359A -11H-2- W-63-65	90.68	88.24	4.04	0.06	4.54	0.17	0.83	0.88	0.22	64.48	29.05	1.61
U1359A -11H-2- W-78-80	90.83	88.39	4.04	0.28	4.54	0.17	0.83	0.89	0.93	60.62	11.63	1.96
U1359A -11H-2- W-93-95	90.98	88.54	4.05	0.11	4.54	0.17	0.83	0.89	0.37	67.08	21.89	1.62
U1359A -11H-2- W-108- 110	91.13	88.69	4.05	0.11	4.54	0.17	0.83	0.89	0.38	80.15	8.54	1.73
U1359A -11H-2- W-123- 125	91.28	88.84	4.05	0.15	4.54	0.17	0.83	0.89	0.50	73.87	11.17	1.68
U1359A -11H-2- W-138- 140	91.43	88.99	4.06	0.13	4.54	0.17	0.83	0.89	0.44	75.89	11.04	1.72

<u>Sample ID</u>	<u>Depth (mcd)</u>	<u>Depth (mbsf-A)</u>	<u>Age (Ma)</u>	<u>IRD (cm<sup>3</sup>/cm<sup>3</sup>)</u>	<u>LSR (cm/kyr)</u>	<u>Opal (g/g)</u>	<u>TERR (g/g)</u>	<u>DBD (g/cm<sup>3</sup>)</u>	<u>IRD MAR (g/cm<sup>2</sup>/kyr)</u>	<u>% Silt</u>	<u>% Clay</u>	<u>Sorting</u>
U1359A -11H-3- W-3-5	91.58	89.14	4.06	0.06	4.54	0.16	0.84	0.88	0.19	79.28	15.19	1.57
U1359A -11H-3- W-18-20	91.73	89.29	4.06	0.26	4.54	0.16	0.84	0.88	0.89	63.44	10.30	1.89
U1359A -11H-3- W-33-35	91.88	89.44	4.07	0.03	4.54	0.16	0.84	0.88	0.12	84.49	12.07	1.62
U1359A -11H-3- W-48-50	92.03	89.59	4.07	0.05	4.54	0.17	0.83	0.88	0.17	83.97	10.97	1.54
U1359A -11H-3- W-63-65	92.18	89.74	4.07	0.07	4.54	0.18	0.82	0.89	0.23	81.06	11.97	1.61
U1359A -11H-3- W-78-80	92.33	89.89	4.07	0.10	4.54	0.19	0.81	0.92	0.34	80.06	9.74	1.76
U1359A -11H-3- W-93-95	92.48	90.04	4.08	0.17	4.54	0.19	0.81	0.94	0.58	69.56	13.68	1.89
U1359A -11H-3- W-108- 110	92.63	90.19	4.08	0.29	4.54	0.18	0.82	0.97	1.05	62.20	8.77	1.74
U1359A -11H-3- W-123- 125	92.78	90.34	4.08	0.43	4.54	0.16	0.84	1.00	1.62	46.48	10.91	2.01

<u>Sample ID</u>	<u>Depth (mcd)</u>	<u>Depth (mbsf-A)</u>	<u>Age (Ma)</u>	<u>IRD (cm<sup>3</sup>/cm<sup>3</sup>)</u>	<u>LSR (cm/kyr)</u>	<u>Opal (g/g)</u>	<u>TERR (g/g)</u>	<u>DBD (g/cm<sup>3</sup>)</u>	<u>IRD.MAR (g/cm<sup>2</sup>/kyr)</u>	<u>% Silt</u>	<u>% Clay</u>	<u>Sorting</u>
U1359A -11H-4- W-3-5	93.08	90.64	4.09	0.01	4.54	0.12	0.88	1.05	0.04	68.78	30.31	1.76
U1359A -11H-4- W-18-20	93.23	90.79	4.09	0.06	4.54	0.11	0.89	1.08	0.25	77.55	16.74	1.81
U1359A -11H-4- W-33-35	93.38	90.94	4.10	0.06	4.54	0.09	0.91	1.10	0.28	69.05	24.85	2.03
U1359A -11H-4- W-48-50	93.53	91.09	4.10	0.01	4.54	0.08	0.92	1.13	0.04	67.23	31.92	1.66
U1359A -11H-4- W-63-65	93.68	91.24	4.10	0.03	4.54	0.08	0.92	1.16	0.14	61.00	36.19	1.68
U1359A -11H-4- W-78-80	93.83	91.39	4.11	0.08	4.54	0.07	0.93	1.18	0.39	57.11	35.09	1.56
U1359A -11H-4- W-93-95	93.98	91.54	4.11	0.03	4.54	0.06	0.94	1.17	0.16	63.05	33.83	1.63
U1359A -11H-4- W-108- 110	94.13	91.69	4.11	0.04	4.54	0.07	0.93	1.17	0.20	73.89	22.10	1.71
U1359A -11H-4- W-123- 125	94.28	91.84	4.12	0.03	4.54	0.07	0.93	1.16	0.12	73.52	23.94	1.57

<u>Sample ID</u>	<u>Depth (mcd)</u>	<u>Depth (mbsf-A)</u>	<u>Age (Ma)</u>	<u>IRD (cm<sup>3</sup>/cm<sup>3</sup>)</u>	<u>LSR (cm/kvr)</u>	<u>Opal (g/g)</u>	<u>TERR (g/g)</u>	<u>DBD (g/cm<sup>3</sup>)</u>	<u>IRD.MAR (g/cm<sup>2</sup>/kvr)</u>	<u>% Silt</u>	<u>% Clay</u>	<u>Sorting</u>
U1359A -11H-4- W-138- 140	94.43	91.99	4.12	0.00	4.54	0.08	0.92	1.16	0.01	55.53	44.30	1.74
U1359A -11H-5- W-3-5	94.58	92.14	4.12	0.12	4.54	0.09	0.91	1.15	0.59	67.15	20.55	2.00
U1359A -11H-5- W-18-20	94.73	92.29	4.13	0.08	4.54	0.09	0.91	1.14	0.36	64.24	28.21	1.61
U1359A -11H-5- W-33-35	94.88	92.44	4.13	0.00	4.54	0.10	0.90	1.14	0.02	63.25	36.34	1.57
U1359A -11H-5- W-48-50	95.03	92.59	4.13	0.01	4.54	0.09	0.91	1.13	0.03	73.89	25.50	1.67
U1359A -11H-5- W-63-65	95.18	92.74	4.14	0.15	4.54	0.08	0.92	1.13	0.71	59.28	25.58	1.99
U1359A -11H-5- W-78-80	95.33	92.89	4.14	0.00	4.54	0.07	0.93	1.13	0.00	52.28	47.72	1.43
U1359A -11H-5- W-93-95	95.48	93.04	4.14	0.06	4.54	0.06	0.94	1.13	0.27	59.63	34.65	1.70
U1359A -11H-5- W-108- 110	95.63	93.19	4.14	0.15	4.54	0.06	0.94	1.13	0.74	54.70	29.94	1.91

<u>Sample ID</u>	<u>Depth (mcd)</u>	<u>Depth (mbsf-A)</u>	<u>Age (Ma)</u>	<u>IRD (cm<sup>3</sup>/cm<sup>3</sup>)</u>	<u>LSR (cm/kyr)</u>	<u>Opal (g/g)</u>	<u>TERR (g/g)</u>	<u>DBD (g/cm<sup>3</sup>)</u>	<u>IRD MAR (g/cm<sup>2</sup>/kyr)</u>	<u>% Silt</u>	<u>% Clay</u>	<u>Sorting</u>
U1359A -11H-5- W-123- 125	95.78	93.34	4.15	0.01	4.54	0.06	0.94	1.13	0.03	60.56	38.77	1.50
U1359A -11H-5- W-138- 140	95.93	93.49	4.15	0.43	4.54	0.06	0.94	1.14	2.10	44.88	11.82	2.16
U1359A -11H-6- W-3-5	96.08	93.64	4.15	0.04	4.54	0.06	0.94	1.14	0.21	69.86	25.77	1.66
U1359A -11H-6- W-18-20	96.23	93.79	4.16	0.03	4.54	0.06	0.94	1.14	0.14	59.67	37.45	1.83
U1359A -11H-6- W-33-35	96.38	93.94	4.16	0.22	4.54	0.06	0.94	1.14	1.06	55.55	22.66	2.25
U1359A -11H-6- W-48-50	96.53	94.09	4.16	0.17	4.54	0.06	0.94	1.15	0.82	63.50	19.79	1.90
U1359A -11H-6- W-63-65	96.68	94.24	4.17	0.02	4.54	0.06	0.94	1.15	0.10	62.34	35.61	1.45
U1359A -11H-6- W-78-80	96.83	94.39	4.17	0.01	4.54	0.06	0.94	1.14	0.03	66.08	33.36	1.56
U1359A -11H-6- W-93-95	96.98	94.54	4.17	0.02	4.54	0.06	0.94	1.14	0.11	76.22	21.59	1.58



<u>Sample ID</u>	<u>Depth (mcd)</u>	<u>Depth (mbsf-A)</u>	<u>Age (Mia)</u>	<u>IRD (cm<sup>3</sup>/cm<sup>3</sup>)</u>	<u>LSR (cm/kyr)</u>	<u>Opal (g/g)</u>	<u>TERR (g/g)</u>	<u>DBD (g/cm<sup>3</sup>)</u>	<u>IRD MAR (g/cm<sup>2</sup>/kyr)</u>	<u>% Silt</u>	<u>% Clay</u>	<u>Sorting</u>
U1359A -11H-6- W-108- 110	97.13	94.69	4.18	0.00	4.54	0.06	0.94	1.14	0.00	51.63	48.37	1.48
U1359A -11H-6- W-123- 125	97.28	94.84	4.18	0.00	4.54	0.06	0.94	1.13	0.00	54.31	45.69	1.47
U1359A -12H-1- W-3-5	97.78	95.64	4.19	0.00	4.54	0.06	0.94	1.12	0.01	59.51	40.23	1.64
U1359A -12H-1- W-18-20	97.93	95.79	4.19	0.03	4.54	0.07	0.93	1.12	0.15	60.98	35.92	1.58
U1359A -12H-1- W-33-35	98.08	95.94	4.20	0.04	4.54	0.07	0.93	1.12	0.21	59.72	35.83	1.70
U1359A -12H-1- W-48-50	98.23	96.09	4.20	0.00	4.54	0.09	0.91	1.11	0.00	63.43	36.57	1.44
U1359A -12H-1- W-63-65	98.38	96.24	4.20	0.00	4.54	0.11	0.89	1.11	0.01	66.59	33.24	1.59
U1359A -12H-1- W-78-80	98.53	96.39	4.21	0.02	4.54	0.12	0.88	1.11	0.08	55.20	42.99	1.82
U1359A -12H-1- W-93-95	98.68	96.54	4.21	0.05	4.54	0.14	0.86	1.10	0.20	74.80	20.47	2.06

<u>Sample ID</u>	<u>Depth (mcd)</u>	<u>Depth (mbsf-A)</u>	<u>Age (Ma)</u>	<u>IRD (cm<sup>3</sup>/cm<sup>3</sup>)</u>	<u>LSR (cm/kyr)</u>	<u>Opal (g/g)</u>	<u>TERR (g/g)</u>	<u>DBD (g/cm<sup>3</sup>)</u>	<u>IRD MAR (g/cm<sup>2</sup>/kyr)</u>	<u>% Silt</u>	<u>% Clay</u>	<u>Sorting</u>
U1359A -12H-1- W-108- 110	98.83	96.69	4.21	0.16	4.54	0.15	0.85	1.10	0.68	62.07	21.93	2.32
U1359A -12H-1- W-123- 125	98.98	96.84	4.22	0.16	4.54	0.15	0.85	1.10	0.68	70.29	13.76	2.04
U1359A -12H-1- W-138- 140	99.13	96.99	4.22	0.01	4.54	0.16	0.84	1.10	0.04	74.96	23.98	1.74
U1359A -12H-2- W-3-5	99.28	97.14	4.22	0.01	4.54	0.16	0.84	1.10	0.03	79.89	19.30	1.61
U1359A -12H-2- W-18-20	99.43	97.29	4.23	0.00	4.54	0.16	0.84	1.10	0.01	82.05	17.62	1.54
U1359A -12H-2- W-33-35	99.58	97.44	4.23	0.01	4.54	0.17	0.83	1.09	0.06	78.76	19.79	1.67
U1359A -12H-2- W-48-50	99.73	97.59	4.23	0.06	4.54	0.15	0.85	1.09	0.25	69.28	24.80	2.05
U1359A -12H-2- W-63-65	99.88	97.74	4.23	0.00	4.54	0.13	0.87	1.09	0.00	56.25	43.75	1.62
U1359A -12H-2- W-78-80	100.03	97.89	4.24	0.03	4.54	0.11	0.89	1.09	0.12	51.39	45.76	1.65

<u>Sample ID</u>	<u>Depth (mcd)</u>	<u>Depth (mbsf-A)</u>	<u>Age (Ma)</u>	<u>IRD (cm<sup>3</sup>/cm<sup>3</sup>)</u>	<u>LSR (cm/kvr)</u>	<u>Opal (g/g)</u>	<u>TERR (g/g)</u>	<u>DBD (g/cm<sup>3</sup>)</u>	<u>IRD.MAR (g/cm<sup>2</sup>/kvr)</u>	<u>% Silt</u>	<u>% Clay</u>	<u>Sorting</u>
U1359A -12H-2- W-93-95	100.18	98.04	4.24	0.02	4.54	0.10	0.90	1.09	0.08	61.39	36.82	1.88
U1359A -12H-2- W-108- 110	100.33	98.19	4.24	0.02	4.54	0.11	0.89	1.09	0.10	89.47	8.31	1.50
U1359A -12H-2- W-123- 125	100.48	98.34	4.25	0.00	4.54	0.11	0.89	1.09	0.02	56.66	42.98	1.86
U1359A -12H-2- W-138- 140	100.63	98.49	4.25	0.11	4.54	0.12	0.88	1.08	0.46	68.70	20.75	2.12
U1359A -12H-3- W-3-5	100.78	98.64	4.25	0.16	4.54	0.13	0.87	1.08	0.68	61.58	22.58	2.36
U1359A -12H-3- W-18-20	100.93	98.79	4.26	0.06	4.54	0.13	0.87	1.08	0.23	70.72	23.75	2.05
U1359A -12H-3- W-33-35	101.08	98.94	4.26	0.05	4.54	0.14	0.86	1.08	0.19	76.42	19.08	1.89
U1359A -12H-3- W-48-50	101.23	99.09	4.26	0.03	4.54	0.13	0.87	1.08	0.12	61.77	35.52	1.81
U1359A -12H-3- W-63-65	101.38	99.24	4.27	0.01	4.54	0.12	0.88	1.06	0.04	66.87	32.24	1.84

<u>Sample ID</u>	<u>Depth (mcd)</u>	<u>Depth (mbsf-A)</u>	<u>Age (Ma)</u>	<u>IRD (cm<sup>3</sup>/cm<sup>3</sup>)</u>	<u>LSR (cm/kyr)</u>	<u>Opal (g/g)</u>	<u>TERR (g/g)</u>	<u>DBD (g/cm<sup>3</sup>)</u>	<u>IRD.MAR (g/cm<sup>2</sup>/kyr)</u>	<u>% Silt</u>	<u>% Clay</u>	<u>Sorting</u>
U1359A -12H-3- W-78-80	101.53	99.39	4.27	0.01	4.54	0.11	0.89	1.02	0.05	76.51	22.30	1.77
U1359A -12H-3- W-93-95	101.68	99.54	4.27	0.04	4.54	0.12	0.88	0.99	0.15	72.82	23.48	1.87
U1359A -12H-3- W-108- 110	101.83	99.69	4.28	0.00	4.54	0.16	0.84	0.95	0.01	62.89	36.80	1.84
U1359A -12H-3- W-123- 125	101.98	99.84	4.28	0.05	4.54	0.20	0.80	0.92	0.17	72.50	22.27	1.70
U1359A -12H-3- W-138- 140	102.13	99.99	4.28	0.09	4.54	0.24	0.76	0.88	0.26	75.34	16.00	1.75
U1359A -12H-4- W-3-5	102.28	100.14	4.29	0.36	4.54	0.29	0.71	0.85	0.99	54.25	9.52	2.11
U1359A -12H-4- W-18-20	102.43	100.29	4.29	0.11	4.54	0.33	0.67	0.81	0.26	73.28	16.21	1.87
U1359A -12H-4- W-33-35	102.58	100.44	4.29	0.07	4.54	0.36	0.64	0.78	0.17	78.36	14.22	1.60
U1359A -12H-4- W-48-50	102.73	100.59	4.30	0.20	4.54	0.37	0.63	0.75	0.43	70.12	9.74	1.83

<u>Sample ID</u>	<u>Depth (mcd)</u>	<u>Depth (mbsf-A)</u>	<u>Age (Ma)</u>	<u>IRD (cm<sup>3</sup>/cm<sup>3</sup>)</u>	<u>LSR (cm/kyr)</u>	<u>Opal (g/g)</u>	<u>TERR (g/g)</u>	<u>DBD (g/cm<sup>3</sup>)</u>	<u>IRD/MAR (g/cm<sup>2</sup>/kyr)</u>	<u>% Silt</u>	<u>% Clay</u>	<u>Sorting</u>
U1359A -12H-4- W-63-65	102.88	100.74	4.30	0.06	4.54	0.38	0.62	0.76	0.13	75.81	18.07	1.65
U1359A -12H-4- W-78-80	103.03	100.89	4.30	0.05	4.54	0.39	0.61	0.77	0.12	74.11	20.43	1.65
U1359A -12H-4- W-93-95	103.18	101.04	4.30	0.05	4.54	0.40	0.60	0.78	0.10	68.55	26.63	1.66
U1359A -12H-4- W-108- 110	103.33	101.19	4.31	0.09	4.54	0.39	0.61	0.79	0.19	74.23	17.25	1.67
U1359A -12H-4- W-123- 125	103.48	101.34	4.31	0.08	4.54	0.38	0.62	0.80	0.17	72.42	19.86	1.78
U1359A -12H-4- W-138- 140	103.63	101.49	4.31	0.07	4.54	0.37	0.63	0.81	0.16	78.88	14.01	1.68
U1359A -12H-5- W-3-5	103.78	101.64	4.32	0.05	4.54	0.37	0.63	0.82	0.13	81.58	13.06	1.43
U1359A -12H-5- W-18-20	103.93	101.79	4.32	0.11	4.54	0.36	0.64	0.83	0.27	69.40	19.48	1.88
U1359A -12H-5- W-33-35	104.08	101.94	4.32	0.11	4.54	0.35	0.65	0.84	0.28	75.16	13.42	1.76

<u>Sample ID</u>	<u>Depth (mcd)</u>	<u>Depth (mbsf-A)</u>	<u>Age (Ma)</u>	<u>IRD (cm<sup>3</sup>/cm<sup>3</sup>)</u>	<u>LSR (cm/kyr)</u>	<u>Opal (g/g)</u>	<u>TERR (g/g)</u>	<u>DBD (g/cm<sup>3</sup>)</u>	<u>IRD MAR (g/cm<sup>2</sup>/kyr)</u>	<u>% Silt</u>	<u>% Clay</u>	<u>Sorting</u>
U1359A -12H-5- W-48-50	104.23	102.09	4.33	0.30	4.54	0.34	0.66	0.85	0.77	62.65	6.85	1.79
U1359B -12H-1- W-3-5	104.29	102.15	4.33	0.05	4.54	0.34	0.66	0.85	0.13	79.70	15.08	1.67
U1359A -12H-5- W-63-65	104.38	102.24	4.33	0.07	4.54	0.33	0.67	0.86	0.17	85.81	7.65	1.47
U1359B -12H-1- W-18-20	104.44	102.3	4.33	0.03	4.54	0.33	0.67	0.86	0.09	71.27	25.23	1.76
U1359A -12H-5- W-78-80	104.53	102.39	4.33	0.04	4.54	0.32	0.68	0.86	0.10	73.92	22.26	1.63
U1359B -12H-1- W-33-35	104.59	102.45	4.33	0.11	4.54	0.32	0.68	0.86	0.28	77.66	11.83	1.79
U1359A -12H-5- W-93-95	104.68	102.54	4.34	0.15	4.54	0.32	0.68	0.86	0.40	76.78	8.33	1.70
U1359B -12H-1- W-48-50	104.74	102.6	4.34	0.19	4.54	0.31	0.69	0.86	0.51	73.07	8.04	1.78
U1359A -12H-5- W-108- 110	104.83	102.69	4.34	0.18	4.54	0.31	0.69	0.86	0.50	71.03	10.49	1.85

<u>Sample ID</u>	<u>Depth (mcd)</u>	<u>Depth (mbsf-A)</u>	<u>Age (Mia)</u>	<u>IRD (cm<sup>3</sup>/cm<sup>3</sup>)</u>	<u>LSR (cm/kyr)</u>	<u>Opal (g/g)</u>	<u>TERR (g/g)</u>	<u>DBD (g/cm<sup>3</sup>)</u>	<u>IRD MAR (g/cm<sup>2</sup>/kyr)</u>	<u>% Silt</u>	<u>% Clay</u>	<u>Sorting</u>
U1359B -12H-1- W-63-65	104.89	102.75	4.34	0.44	4.54	0.31	0.69	0.87	1.19	49.27	6.96	2.22
U1359A -12H-5- W-123- 125	104.98	102.84	4.34	0.09	4.54	0.31	0.69	0.87	0.25	78.77	12.16	1.62
U1359B -12H-1- W-78-80	105.04	102.9	4.34	0.04	4.54	0.30	0.70	0.87	0.10	77.65	18.82	1.67
U1359A -12H-5- W-138- 140	105.13	102.99	4.35	0.11	4.54	0.30	0.70	0.87	0.31	79.54	9.39	1.63
U1359B -12H-1- W-93-95	105.19	103.05	4.35	0.12	4.54	0.30	0.70	0.87	0.32	80.72	7.73	1.64
U1359A -12H-6- W-3-5	105.28	103.14	4.35	0.09	4.54	0.30	0.70	0.87	0.24	78.18	13.18	1.62
U1359B -12H-1- W-108- 110	105.34	103.2	4.35	0.07	4.54	0.30	0.70	0.87	0.21	68.77	23.87	1.73
U1359A -12H-6- W-18-20	105.43	103.29	4.35	0.06	4.54	0.29	0.71	0.87	0.18	85.77	7.99	1.62

<u>Sample ID</u>	<u>Depth (mcd)</u>	<u>Depth (mbsf-A)</u>	<u>Age (Ma)</u>	<u>IRD (cm<sup>3</sup>/cm<sup>3</sup>)</u>	<u>LSR (cm/kyr)</u>	<u>Opal (g/g)</u>	<u>TERR (g/g)</u>	<u>DBD (g/cm<sup>3</sup>)</u>	<u>IRD MAR (g/cm<sup>2</sup>/kyr)</u>	<u>% Silt</u>	<u>% Clay</u>	<u>Sorting</u>
U1359B -12H-1- W-122- 124	105.48	103.34	4.35	0.05	4.54	0.29	0.71	0.87	0.15	79.63	14.97	1.65
U1359A -12H-6- W-33-35	105.58	103.44	4.36	0.13	4.54	0.29	0.71	0.88	0.36	69.87	17.51	1.86
U1359B -12H-1- W-138- 140	105.64	103.5	4.36	0.14	4.54	0.29	0.71	0.88	0.39	70.49	15.81	1.94
U1359A -12H-6- W-48-50	105.73	103.59	4.36	0.08	4.54	0.28	0.72	0.88	0.23	83.96	7.95	1.53
U1359B -12H-2- W-3-5	105.79	103.65	4.36	0.11	4.54	0.28	0.72	0.88	0.31	75.76	13.40	1.82
U1359A -12H-6- W-63-65	105.88	103.74	4.36	0.06	4.54	0.28	0.72	0.88	0.18	84.37	9.57	1.61
U1359B -12H-2- W-18-20	105.94	103.8	4.36	0.04	4.54	0.28	0.72	0.88	0.11	71.42	24.91	1.73
U1359A -12H-6- W-78-80	106.03	103.89	4.37	0.04	4.54	0.27	0.73	0.88	0.11	82.09	13.97	1.57
U1359B -12H-2- W-33-35	106.09	103.95	4.37	0.01	4.54	0.27	0.73	0.88	0.03	71.81	27.09	1.75



<u>Sample ID</u>	<u>Depth (mcd)</u>	<u>Depth (mbsf-A)</u>	<u>Age (Ma)</u>	<u>IRD (cm<sup>3</sup>/cm<sup>3</sup>)</u>	<u>LSR (cm/kyr)</u>	<u>Opal (g/g)</u>	<u>TERR (g/g)</u>	<u>DBD (g/cm<sup>3</sup>)</u>	<u>IRD_MAR (g/cm<sup>2</sup>/kyr)</u>	<u>% Silt</u>	<u>% Clay</u>	<u>Sorting</u>
U1359A -12H-6- W-93-95	106.18	104.04	4.37	0.04	4.54	0.26	0.74	0.87	0.11	78.29	17.97	1.61
U1359B -12H-2- W-48-50	106.24	104.1	4.37	0.02	4.54	0.26	0.74	0.87	0.07	72.94	24.59	1.67
U1359A -12H-6- W-108- 110	106.33	104.19	4.37	0.03	4.54	0.24	0.76	0.87	0.09	83.76	13.29	1.62
U1359B -12H-2- W-63-65	106.39	104.25	4.37	0.07	4.54	0.23	0.77	0.86	0.21	77.98	15.15	1.65
U1359A -12H-6- W-123- 125	106.48	104.34	4.37	0.02	4.54	0.22	0.78	0.86	0.06	86.23	11.86	1.49
U1359B -12H-2- W-78-80	106.54	104.4	4.38	0.09	4.54	0.21	0.79	0.86	0.26	82.91	8.58	1.57
U1359A -12H-6- W-138- 140	106.63	104.49	4.38	0.05	4.54	0.20	0.80	0.86	0.15	86.11	8.92	1.62
U1359B -12H-2- W-93-95	106.69	104.55	4.38	0.04	4.54	0.19	0.81	0.85	0.12	58.41	37.63	1.76

<u>Sample ID</u>	<u>Depth (mcd)</u>	<u>Depth (mbsf-A)</u>	<u>Age (Ma)</u>	<u>IRD (cm<sup>3</sup>/cm<sup>3</sup>)</u>	<u>LSR (cm/kyr)</u>	<u>Opal (g/g)</u>	<u>TERR (g/g)</u>	<u>DBD (g/cm<sup>3</sup>)</u>	<u>IRD.MAR (g/cm<sup>2</sup>/kyr)</u>	<u>% Silt</u>	<u>% Clay</u>	<u>Sorting</u>
U1359B -12H-2- W-108- 110	106.84	104.7	4.38	0.07	4.54	0.17	0.83	0.85	0.22	75.99	17.07	1.65
U1359B -12H-2- W-122- 124	106.98	104.84	4.39	0.02	4.54	0.15	0.85	0.84	0.06	71.47	26.74	1.71
U1359B -12H-2- W-138- 140	107.14	105	4.39	0.03	4.54	0.13	0.87	0.83	0.11	60.04	36.55	1.73
U1359B -12H-3- W-3-5	107.29	105.15	4.39	0.05	4.54	0.11	0.89	0.83	0.18	75.66	18.92	1.63
U1359B -12H-3- W-18-20	107.44	105.3	4.40	0.02	4.54	0.09	0.91	0.82	0.05	67.89	30.56	1.72
U1359B -12H-3- W-33-35	107.59	105.45	4.40	0.05	4.54	0.07	0.93	0.82	0.16	70.03	25.43	1.71
U1359B -12H-3- W-48-50	107.74	105.6	4.40	0.04	4.54	0.12	0.88	0.81	0.12	70.44	25.84	1.74
U1359B -12H-3- W-63-65	107.89	105.75	4.40	0.05	4.54	0.18	0.82	0.80	0.15	65.74	29.12	1.76
U1359B -12H-3- W-78-80	108.04	105.9	4.41	0.05	4.54	0.24	0.76	0.80	0.14	69.96	24.81	1.73

<u>Sample ID</u>	<u>Depth (mcd)</u>	<u>Depth (mbsf-A)</u>	<u>Age (Ma)</u>	<u>IRD (cm<sup>3</sup>/cm<sup>3</sup>)</u>	<u>LSR (cm/kyr)</u>	<u>Opal (g/g)</u>	<u>TERR (g/g)</u>	<u>DBD (g/cm<sup>3</sup>)</u>	<u>IRD.MAR (g/cm<sup>2</sup>/kyr)</u>	<u>% Silt</u>	<u>% Clay</u>	<u>Sorting</u>
U1359B -12H-3- W-93-95	108.19	106.05	4.41	0.27	4.54	0.31	0.69	0.81	0.70	57.36	15.19	2.08
U1359B -12H-3- W-108- 110	108.34	106.2	4.41	0.08	4.54	0.29	0.71	0.84	0.22	77.96	13.93	1.76
U1359B -12H-3- W-122- 124	108.48	106.34	4.42	0.05	4.54	0.26	0.74	0.87	0.13	87.24	8.25	1.55
U1359B -12H-3- W-138- 140	108.64	106.5	4.42	0.03	4.54	0.23	0.77	0.90	0.10	77.01	19.69	1.59
U1359B -12H-4- W-3-5	108.79	106.65	4.42	0.03	4.54	0.19	0.81	0.93	0.11	66.30	30.37	1.73
U1359B -12H-4- W-18-20	108.94	106.8	4.43	0.05	4.54	0.16	0.84	0.96	0.16	64.90	30.59	1.78
U1359B -12H-4- W-33-35	109.09	106.95	4.43	0.01	4.54	0.13	0.87	0.99	0.04	72.67	26.29	1.61
U1359B -12H-4- W-48-50	109.24	107.1	4.43	0.01	4.54	0.15	0.85	1.02	0.04	74.89	24.02	1.74
U1359B -12H-4- W-63-65	109.39	107.25	4.44	0.02	4.54	0.18	0.82	1.03	0.09	74.59	23.13	1.64

<u>Sample ID</u>	<u>Depth (mcd)</u>	<u>Depth (mbsf-A)</u>	<u>Age (Ma)</u>	<u>IRD (cm<sup>3</sup>/cm<sup>3</sup>)</u>	<u>LSR (cm/kyr)</u>	<u>Opal (g/g)</u>	<u>TERR (g/g)</u>	<u>DBD (g/cm<sup>3</sup>)</u>	<u>IRD.MAR (g/cm<sup>2</sup>/kyr)</u>	<u>% Silt</u>	<u>% Clay</u>	<u>Sorting</u>
U1359B -12H-4 W-78-80	109.54	107.4	4.44	0.02	4.54	0.22	0.78	1.01	0.07	75.71	22.33	1.69
U1359B -12H-4 W-93-95	109.69	107.55	4.44	0.08	4.54	0.25	0.75	0.98	0.26	71.91	20.27	1.79
U1359B -12H-4 W-108-110	109.84	107.7	4.45	0.27	4.54	0.26	0.74	0.96	0.87	57.14	16.17	1.76
U1359B -12H-4 W-122-124	109.98	107.84	4.45	0.06	4.54	0.25	0.75	0.94	0.20	71.82	21.97	1.64
U1359B -12H-4 W-138-140	110.14	108	4.45	0.09	4.54	0.25	0.75	0.92	0.28	67.95	23.22	1.74
U1359B -12H-5 W-3-5	110.29	108.15	4.46	0.09	4.54	0.24	0.76	0.90	0.27	69.99	21.32	1.70
U1359B -12H-5 W-18-20	110.44	108.3	4.46	0.06	4.54	0.24	0.76	0.88	0.19	71.69	22.01	1.63
U1359B -12H-5 W-33-35	110.59	108.45	4.46	0.08	4.54	0.23	0.77	0.86	0.25	72.26	19.56	1.60
U1359B -12H-5 W-48-50	110.74	108.6	4.47	0.07	4.54	0.27	0.73	0.84	0.19	73.06	20.13	1.68

<u>Sample ID</u>	<u>Depth (mcd)</u>	<u>Depth (mbsf-A)</u>	<u>Age (Ma)</u>	<u>IRD (cm<sup>3</sup>/cm<sup>3</sup>)</u>	<u>LSR (cm/kyr)</u>	<u>Opal (g/g)</u>	<u>TERR (g/g)</u>	<u>DBD (g/cm<sup>3</sup>)</u>	<u>IRD MAR (g/cm<sup>2</sup>/kyr)</u>	<u>% Silt</u>	<u>% Clay</u>	<u>Sorting</u>
U1359B-12H-5-W-63-65	110.89	108.75	4.47	0.10	4.54	0.32	0.68	0.81	0.25	75.88	14.39	1.76
U1359B-12H-5-W-78-80	111.04	108.9	4.47	0.14	4.54	0.37	0.63	0.81	0.32	68.70	17.52	2.02
U1359B-12H-5-W-93-95	111.19	109.05	4.47	0.17	4.54	0.42	0.58	0.80	0.36	70.13	12.92	1.94
U1359B-12H-5-W-108-110	111.34	109.2	4.48	0.08	4.54	0.41	0.59	0.79	0.17	76.95	15.01	1.72
U1359B-12H-5-W-122-124	111.48	109.34	4.48	0.10	4.54	0.39	0.61	0.79	0.23	67.65	21.97	1.83
U1359B-12H-5-W-138-140	111.64	109.5	4.48	0.17	4.54	0.36	0.64	0.78	0.38	66.15	17.04	1.94
U1359B-12H-6-W-3-5	111.79	109.65	4.49	0.04	4.54	0.34	0.66	0.78	0.10	72.04	23.86	1.64
U1359B-12H-6-W-18-20	111.94	109.8	4.49	0.09	4.54	0.32	0.68	0.77	0.22	71.14	19.65	1.86
U1359B-12H-6-W-33-35	112.09	109.95	4.49	0.04	4.54	0.29	0.71	0.77	0.10	71.54	24.46	1.72

<u>Sample ID</u>	<u>Depth (mcd)</u>	<u>Depth (mbsf-A)</u>	<u>Age (Ma)</u>	<u>IRD (cm<sup>3</sup>/cm<sup>3</sup>)</u>	<u>LSR (cm/kyr)</u>	<u>Opal (g/g)</u>	<u>TERR (g/g)</u>	<u>DBD (g/cm<sup>3</sup>)</u>	<u>IRD_MAR (g/cm<sup>2</sup>/kyr)</u>	<u>% Silt</u>	<u>% Clay</u>	<u>Sorting</u>
U1359B-12H-6-W-48-50	112.24	110.1	4.50	0.06	4.54	0.27	0.73	0.76	0.16	80.62	13.05	1.66
U1359B-12H-6-W-63-65	112.39	110.25	4.50	0.06	4.54	0.25	0.75	0.77	0.17	69.20	24.52	1.74
U1359B-12H-6-W-78-80	112.54	110.4	4.50	0.05	4.54	0.22	0.78	0.79	0.15	70.47	24.33	1.74
U1359B-12H-6-W-93-95	112.69	110.55	4.51	0.14	4.54	0.20	0.80	0.81	0.41	74.98	11.22	1.82
U1359B-12H-6-W-108-110	112.84	110.7	4.51	0.10	4.54	0.19	0.81	0.83	0.32	70.97	18.66	1.65
U1359B-12H-6-W-122-124	112.98	110.84	4.51	0.15	4.54	0.19	0.81	0.85	0.48	68.84	15.89	1.89
U1359B-12H-6-W-138-140	113.14	111	4.52	0.06	4.54	0.18	0.82	0.87	0.18	78.13	16.34	1.55
U1359B-12H-7-W-3-5	113.2	111.06	4.52	0.11	4.54	0.18	0.82	0.88	0.36	72.40	16.65	1.58
U1359B-12H-7-W-18-20	113.35	111.21	4.52	0.06	4.54	0.18	0.82	0.90	0.20	61.84	32.11	1.69

<u>Sample ID</u>	<u>Depth (mcd)</u>	<u>Depth (mbsf-A)</u>	<u>Age (Ma)</u>	<u>IRD (cm<sup>3</sup>/cm<sup>3</sup>)</u>	<u>LSR (cm/kyr)</u>	<u>Opal (g/g)</u>	<u>TERR (g/g)</u>	<u>DBD (g/cm<sup>3</sup>)</u>	<u>IRD_MAR (g/cm<sup>2</sup>/kyr)</u>	<u>% Silt</u>	<u>% Clay</u>	<u>Sorting</u>
U1359B-12H-7-W-33-35	113.5	111.36	4.52	0.03	4.54	0.17	0.83	0.93	0.09	59.59	37.85	1.64
U1359B-12H-7-W-48-50	113.65	111.51	4.53	0.12	4.54	0.17	0.83	0.95	0.42	59.59	28.58	1.92
U1359B-13H-1-W-3-5	113.79	111.57	4.53	0.23	4.54	0.16	0.84	0.97	0.85	65.78	11.14	2.05
U1359B-12H-7-W-63-65	113.8	111.66	4.53	0.09	4.54	0.16	0.84	0.97	0.34	57.22	33.72	1.83
U1359B-13H-1-W-18-20	113.94	111.72	4.53	0.10	4.54	0.15	0.85	0.99	0.40	69.26	20.26	2.13
U1359B-13H-1-W-33-35	114.09	111.87	4.54	0.19	4.54	0.14	0.86	1.00	0.72	52.88	28.60	2.05
U1359B-13H-1-W-48-50	114.24	112.02	4.54	0.08	4.54	0.13	0.87	1.01	0.33	68.79	22.83	1.82
U1359B-13H-1-W-63-65	114.39	112.17	4.54	0.28	4.54	0.13	0.87	1.02	1.11	50.34	21.86	2.27
U1359B-13H-1-W-78-80	114.54	112.32	4.55	0.09	4.54	0.13	0.87	1.03	0.35	55.50	35.86	2.16
U1359B-13H-1-W-93-95	114.69	112.47	4.55	0.00	4.54	0.13	0.87	1.04	0.00	73.23	26.77	1.63

<u>Sample ID</u>	<u>Depth (mcd)</u>	<u>Depth (mbsf-A)</u>	<u>Age (Ma)</u>	<u>IRD (cm<sup>3</sup>/cm<sup>3</sup>)</u>	<u>LSR (cm/kyr)</u>	<u>Opal (g/g)</u>	<u>TERR (g/g)</u>	<u>DBD (g/cm<sup>3</sup>)</u>	<u>IRD MAR (g/cm<sup>2</sup>/kyr)</u>	<u>% Silt</u>	<u>% Clay</u>	<u>Sorting</u>
U1359B -13H-1- W-108- 110	114.84	112.62	4.55	0.08	4.54	0.13	0.87	1.05	0.33	47.35	44.67	1.65
U1359B -13H-1- W-122- 124	114.98	112.76	4.56	0.19	4.54	0.13	0.87	1.06	0.77	58.20	23.21	1.82
U1359B -13H-1- W-138- 140	115.14	112.92	4.56	0.08	4.54	0.13	0.87	1.07	0.35	62.34	29.41	1.82
U1359B -13H-2- W-3-5	115.29	113.07	4.56	0.11	4.54	0.11	0.89	1.08	0.46	68.48	20.85	1.98
U1359B -13H-2- W-18-20	115.44	113.22	4.56	0.54	4.54	0.09	0.91	1.08	2.43	41.03	4.76	2.20
U1359B -13H-2- W-33-35	115.59	113.37	4.57	0.01	4.54	0.07	0.93	1.09	0.06	89.71	8.93	1.43
U1359B -13H-2- W-48-50	115.74	113.52	4.57	0.01	4.54	0.05	0.95	1.10	0.03	87.16	12.31	1.38
U1359B -13H-2- W-63-65	115.89	113.67	4.57	0.18	4.54	0.05	0.95	1.10	0.87	58.86	22.87	2.31
U1359B -13H-2- W-78-80	116.04	113.82	4.58	0.06	4.54	0.05	0.95	1.09	0.29	61.60	32.26	2.09



<u>Sample ID</u>	<u>Depth (mcd)</u>	<u>Depth (mbsf-A)</u>	<u>Age (Ma)</u>	<u>IRD (cm<sup>3</sup>/cm<sup>3</sup>)</u>	<u>LSR (cm/kvr)</u>	<u>Opal (g/g)</u>	<u>TERR (g/g)</u>	<u>DBD (g/cm<sup>3</sup>)</u>	<u>IRD.MAR (g/cm<sup>2</sup>/kvr)</u>	<u>% Silt</u>	<u>% Clay</u>	<u>Sorting</u>
U1359B-13H-2-W-93-95	116.19	113.97	4.58	0.15	4.54	0.05	0.95	1.08	0.71	60.27	24.38	1.97
U1359B-13H-2-W-108-110	116.34	114.12	4.58	0.10	4.54	0.05	0.95	1.06	0.47	42.58	47.19	1.60
U1359B-13H-2-W-122-124	116.48	114.26	4.59	0.12	4.54	0.05	0.95	1.05	0.56	50.96	36.72	2.27
U1359B-13H-2-W-138-140	116.64	114.42	4.59	0.10	4.54	0.05	0.95	1.04	0.46	75.63	14.16	1.95
U1359B-13H-3-W-3-5	116.79	114.57	4.59	0.04	4.54	0.05	0.95	1.03	0.17	66.62	29.52	1.81
U1359B-13H-3-W-18-20	116.94	114.72	4.60	0.02	4.54	0.06	0.94	1.02	0.11	72.04	25.51	1.80
U1359B-13H-3-W-33-35	117.09	114.87	4.60	0.06	4.54	0.06	0.94	1.01	0.28	68.28	25.35	1.81
U1359B-13H-3-W-48-50	117.24	115.02	4.60	0.27	4.54	0.06	0.94	1.01	1.14	60.22	13.21	1.77
U1359B-13H-3-W-63-65	117.39	115.17	4.61	0.30	4.54	0.06	0.94	1.00	1.30	56.94	12.72	1.80

<u>Sample ID</u>	<u>Depth (mcd)</u>	<u>Depth (mbsf-A)</u>	<u>Age (Ma)</u>	<u>IRD (cm<sup>3</sup>/cm<sup>3</sup>)</u>	<u>LSR (cm/kyr)</u>	<u>Opal (g/g)</u>	<u>TERR (g/g)</u>	<u>DBD (g/cm<sup>3</sup>)</u>	<u>IRD.MAR (g/cm<sup>2</sup>/kyr)</u>	<u>% Silt</u>	<u>% Clay</u>	<u>Sorting</u>
U1359B-13H-3-W-78-80	117.54	115.32	4.61	0.05	4.54	0.06	0.94	1.00	0.22	80.27	14.64	1.73
U1359B-13H-3-W-93-95	117.69	115.47	4.61	0.33	4.54	0.07	0.93	0.99	1.37	57.58	9.78	2.08
U1359B-13H-3-W-108-110	117.84	115.62	4.62	0.08	4.54	0.07	0.93	0.98	0.32	69.16	23.08	1.77
U1359B-13H-3-W-122-124	117.98	115.76	4.62	0.52	4.54	0.07	0.93	0.98	2.13	43.23	5.12	2.15
U1359B-13H-3-W-138-140	118.14	115.92	4.62	0.07	4.54	0.08	0.92	0.97	0.29	71.17	21.74	1.65
U1359B-13H-4-W-3-5	118.29	116.07	4.63	0.14	4.54	0.08	0.92	0.96	0.56	61.63	24.44	1.56
U1359B-13H-4-W-18-20	118.44	116.22	4.63	0.08	4.54	0.08	0.92	0.96	0.31	70.78	21.51	1.72
U1359B-13H-4-W-33-35	118.59	116.37	4.63	0.10	4.54	0.08	0.92	0.95	0.40	72.98	16.88	2.19
U1359B-13H-4-W-48-50	118.74	116.52	4.63	0.19	4.54	0.09	0.91	0.94	0.76	65.96	14.69	1.82

<u>Sample ID</u>	<u>Depth (mcd)</u>	<u>Depth (mbsf-A)</u>	<u>Age (Ma)</u>	<u>IRD (cm<sup>3</sup>/cm<sup>3</sup>)</u>	<u>LSR (cm/kyr)</u>	<u>Opal (g/g)</u>	<u>TERR (g/g)</u>	<u>DBD (g/cm<sup>3</sup>)</u>	<u>IRD MAR (g/cm<sup>2</sup>/kyr)</u>	<u>% Silt</u>	<u>% Clay</u>	<u>Sorting</u>
U1359B-13H-4-W-63-65	118.89	116.67	4.64	0.16	4.54	0.09	0.91	0.94	0.62	67.66	16.41	1.77
U1359B-13H-4-W-78-80	119.04	116.82	4.64	0.26	4.54	0.09	0.91	0.93	1.02	61.92	11.62	1.71
U1359B-13H-4-W-93-95	119.19	116.97	4.64	0.12	4.54	0.09	0.91	0.93	0.45	66.99	21.30	2.30
U1359B-13H-4-W-108-110	119.34	117.12	4.65	0.05	4.54	0.10	0.90	0.92	0.19	72.76	22.19	1.90
U1359B-13H-4-W-122-124	119.48	117.26	4.65	0.17	4.54	0.10	0.90	0.91	0.63	69.01	14.21	1.80
U1359B-13H-4-W-138-140	119.64	117.42	4.65	0.07	4.54	0.10	0.90	0.91	0.25	70.08	23.28	2.01
U1359B-13H-5-W-3-5	119.79	117.57	4.66	0.07	4.54	0.11	0.89	0.90	0.25	65.09	28.00	1.87
U1359B-13H-5-W-18-20	119.94	117.72	4.66	0.02	4.54	0.11	0.89	0.89	0.08	65.84	31.99	1.77
U1359B-13H-5-W-33-35	120.09	117.87	4.66	0.60	4.54	0.11	0.89	0.89	2.15	32.01	7.97	1.66

<u>Sample ID</u>	<u>Depth (mcd)</u>	<u>Depth (mbsf-A)</u>	<u>Age (Ma)</u>	<u>IRD (cm<sup>3</sup>/cm<sup>3</sup>)</u>	<u>LSR (cm/kyr)</u>	<u>Opal (g/g)</u>	<u>TERR (g/g)</u>	<u>DBD (g/cm<sup>3</sup>)</u>	<u>IRD_MAR (g/cm<sup>2</sup>/kyr)</u>	<u>% Silt</u>	<u>% Clay</u>	<u>Sorting</u>
U1359A -14H-1- W-3-5	120.23	114.64	4.67	0.03	4.54	0.11	0.89	0.88	0.09	68.57	28.86	1.70
U1359B -13H-5- W-48-50	120.24	118.02	4.67	0.17	4.54	0.11	0.89	0.88	0.59	59.79	23.70	1.80
U1359A -14H-1- W-18-20	120.38	114.79	4.67	0.02	4.54	0.12	0.88	0.88	0.08	59.58	38.03	1.73
U1359B -13H-5- W-63-65	120.39	118.17	4.67	0.00	4.54	0.12	0.88	0.88	0.01	67.94	31.76	1.93
U1359A -14H-1- W-33-35	120.53	114.94	4.67	0.04	4.54	0.12	0.88	0.87	0.12	69.25	27.25	1.68
U1359B -13H-5- W-78-80	120.54	118.32	4.67	0.02	4.54	0.12	0.88	0.87	0.06	76.10	22.11	1.98
U1359A -14H-1- W-48-50	120.68	115.09	4.68	0.09	4.54	0.13	0.87	0.86	0.30	70.55	20.58	1.70
U1359B -13H-5- W-93-95	120.69	118.47	4.68	0.41	4.54	0.13	0.87	0.86	1.38	50.19	9.07	1.82
U1359B -13H-6- W-3-5	120.79	118.57	4.68	0.04	4.54	0.14	0.86	0.86	0.14	78.36	17.37	1.91
U1359A -14H-1- W-63-65	120.83	115.24	4.68	0.03	4.54	0.15	0.85	0.86	0.11	64.71	32.03	1.76

<u>Sample ID</u>	<u>Depth (mcd)</u>	<u>Depth (mbsf-A)</u>	<u>Age (Ma)</u>	<u>IRD (cm<sup>3</sup>/cm<sup>3</sup>)</u>	<u>LSR (cm/kyr)</u>	<u>Opal (g/g)</u>	<u>TERR (g/g)</u>	<u>DBD (g/cm<sup>3</sup>)</u>	<u>IRD_MAR (g/cm<sup>2</sup>/kyr)</u>	<u>% Silt</u>	<u>% Clay</u>	<u>Sorting</u>
U1359B -13H-6- W-18-20	120.94	118.72	4.68	0.03	4.54	0.16	0.84	0.86	0.09	86.43	10.83	1.68
U1359A -14H-1- W-78-80	120.98	115.39	4.68	0.05	4.54	0.16	0.84	0.86	0.16	68.75	26.49	1.55
U1359B -13H-6- W-33-35	121.09	118.87	4.68	0.35	4.54	0.17	0.83	0.86	1.13	58.31	6.91	1.87
U1359A -14H-1- W-93-95	121.13	115.54	4.69	0.29	4.54	0.17	0.83	0.86	0.94	54.20	16.99	1.87
U1359B -13H-6- W-48-50	121.24	119.02	4.69	0.01	4.54	0.17	0.83	0.86	0.04	54.02	44.66	1.81
U1359A -14H-1- W-108- 110	121.28	115.69	4.69	0.15	4.54	0.16	0.84	0.87	0.48	64.25	21.08	1.72
U1359B -13H-6- W-63-65	121.39	119.17	4.69	0.10	4.54	0.16	0.84	0.87	0.31	72.22	18.28	1.73
U1359A -14H-1- W-123- 125	121.43	115.84	4.69	0.11	4.54	0.16	0.84	0.87	0.37	68.96	19.78	1.68
U1359B -13H-6- W-78-80	121.54	119.32	4.69	0.02	4.54	0.16	0.84	0.87	0.07	63.56	34.39	1.81

<u>Sample ID</u>	<u>Depth (mcd)</u>	<u>Depth (mbsf-A)</u>	<u>Age (Ma)</u>	<u>IRD (cm<sup>3</sup>/cm<sup>3</sup>)</u>	<u>LSR (cm/kyr)</u>	<u>Opal (g/g)</u>	<u>TERR (g/g)</u>	<u>DBD (g/cm<sup>3</sup>)</u>	<u>IRD MAR (g/cm<sup>2</sup>/kyr)</u>	<u>% Silt</u>	<u>% Clay</u>	<u>Sorting</u>
U1359A -14H-1- W-138- 140	121.58	115.99	4.69	0.43	4.54	0.16	0.84	0.87	1.45	48.17	8.62	1.51
U1359A -14H-2- W-3-5	121.73	116.14	4.70	0.09	4.54	0.15	0.85	0.88	0.29	74.16	17.18	1.72
U1359A -14H-2- W-18-20	121.88	116.29	4.70	0.05	4.54	0.15	0.85	0.88	0.18	70.00	24.85	2.52
U1359A -14H-2- W-33-35	122.03	116.44	4.70	0.12	4.54	0.14	0.86	0.89	0.41	66.28	21.73	1.91
U1359A -14H-2- W-48-50	122.18	116.59	4.71	0.02	4.54	0.14	0.86	0.89	0.06	73.54	24.61	1.95
U1359A -14H-2- W-63-65	122.33	116.74	4.71	0.04	4.54	0.13	0.87	0.88	0.14	71.70	24.11	1.71
U1359A -14H-2- W-78-80	122.48	116.89	4.71	0.11	4.54	0.13	0.87	0.86	0.38	69.81	19.05	1.75
U1359A -14H-2- W-93-95	122.63	117.04	4.72	0.03	4.54	0.12	0.88	0.84	0.09	73.27	24.01	1.64
U1359A -14H-2- W-108- 110	122.78	117.19	4.72	0.06	4.54	0.13	0.87	0.82	0.20	71.77	22.17	1.71

<u>Sample ID</u>	<u>Depth (mcd)</u>	<u>Depth (mbsf-A)</u>	<u>Age (Ma)</u>	<u>IRD (cm<sup>3</sup>/cm<sup>3</sup>)</u>	<u>LSR (cm/kyr)</u>	<u>Opal (g/g)</u>	<u>TERR (g/g)</u>	<u>DBD (g/cm<sup>3</sup>)</u>	<u>IRD MAR (g/cm<sup>2</sup>/kyr)</u>	<u>% Silt</u>	<u>% Clay</u>	<u>Sorting</u>
U1359A -14H-2- W-123- 125	122.93	117.34	4.72	0.10	4.54	0.14	0.86	0.80	0.31	67.56	22.55	1.64
U1359A -14H-2- W-138- 140	123.08	117.49	4.73	0.05	4.54	0.15	0.85	0.78	0.14	70.02	25.25	2.04
U1359A -14H-3- W-3-5	123.23	117.64	4.73	0.07	4.54	0.16	0.84	0.77	0.20	71.58	21.53	1.67
U1359A -14H-3- W-18-20	123.38	117.79	4.73	0.07	4.54	0.17	0.83	0.75	0.20	71.07	21.95	1.91
U1359A -14H-3- W-35-37	123.55	117.96	4.74	0.09	4.54	0.18	0.82	0.73	0.26	73.12	17.43	1.71
U1359A -14H-3- W-48-50	123.68	118.09	4.74	0.06	4.54	0.18	0.82	0.71	0.15	76.78	17.70	1.64
U1359A -14H-3- W-63-65	123.83	118.24	4.74	0.05	4.54	0.19	0.81	0.70	0.14	75.28	19.37	1.75
U1359A -14H-3- W-78-80	123.98	118.39	4.75	0.04	4.54	0.20	0.80	0.71	0.11	73.96	21.62	2.00
U1359A -14H-3- W-93-95	124.13	118.54	4.75	0.04	4.54	0.21	0.79	0.72	0.10	73.31	22.96	1.78

<u>Sample ID</u>	<u>Depth (mcd)</u>	<u>Depth (mbsf-A)</u>	<u>Age (Ma)</u>	<u>IRD (cm<sup>3</sup>/cm<sup>3</sup>)</u>	<u>LSR (cm/kyr)</u>	<u>Opal (g/g)</u>	<u>TERR (g/g)</u>	<u>DBD (g/cm<sup>3</sup>)</u>	<u>IRD.MAR (g/cm<sup>2</sup>/kyr)</u>	<u>% Silt</u>	<u>% Clay</u>	<u>Sorting</u>
U1359A -14H-3- W-108- 110	124.28	118.69	4.75	0.06	4.54	0.21	0.79	0.73	0.17	69.14	24.37	1.65
U1359A -14H-3- W-123- 125	124.43	118.84	4.76	0.04	4.54	0.22	0.78	0.74	0.12	70.26	25.38	1.74
U1359A -14H-3- W-138- 140	124.58	118.99	4.76	0.12	4.54	0.22	0.78	0.75	0.32	66.71	21.07	1.74
U1359A -14H-4- W-3-5	124.73	119.14	4.76	0.04	4.54	0.23	0.77	0.76	0.12	67.48	28.06	1.68
U1359A -14H-4- W-18-20	124.88	119.29	4.76	0.05	4.54	0.23	0.77	0.77	0.12	64.83	30.56	1.55
U1359A -14H-4- W-33-35	125.03	119.44	4.77	0.07	4.54	0.23	0.77	0.78	0.18	62.10	31.18	1.68
U1359A -14H-4- W-48-50	125.18	119.59	4.77	0.06	4.54	0.22	0.78	0.78	0.16	63.93	30.45	1.70
U1359A -14H-4- W-63-65	125.33	119.74	4.77	0.08	4.54	0.22	0.78	0.79	0.22	64.82	27.45	1.70
U1359A -14H-4- W-78-80	125.48	119.89	4.78	0.04	4.54	0.21	0.79	0.81	0.13	67.09	28.47	1.65



<u>Sample ID</u>	<u>Depth (mcd)</u>	<u>Depth (mbsf-A)</u>	<u>Age (Ma)</u>	<u>IRD (cm<sup>3</sup>/cm<sup>3</sup>)</u>	<u>LSR (cm/kvr)</u>	<u>Opal (g/g)</u>	<u>TERR (g/g)</u>	<u>DBD (g/cm<sup>3</sup>)</u>	<u>IRD.MAR (g/cm<sup>2</sup>/kvr)</u>	<u>% Silt</u>	<u>% Clay</u>	<u>Sorting</u>
U1359A -14H-4- W-93-95	125.63	120.04	4.78	0.03	4.54	0.20	0.80	0.82	0.09	72.00	24.86	1.68
U1359A -14H-4- W-108- 110	125.78	120.19	4.78	0.03	4.54	0.20	0.80	0.83	0.08	70.80	26.59	1.71
U1359A -14H-4- W-123- 125	125.93	120.34	4.79	0.04	4.54	0.19	0.81	0.84	0.13	69.87	25.80	1.72
U1359A -14H-4- W-138- 140	126.08	120.49	4.79	0.09	4.54	0.19	0.81	0.86	0.27	71.86	19.61	1.80
U1359A -14H-5- W-3-5	126.23	120.64	4.79	0.06	4.54	0.18	0.82	0.87	0.20	72.02	21.83	1.77
U1359A -14H-5- W-18-20	126.38	120.79	4.80	0.07	4.54	0.18	0.82	0.88	0.24	71.41	21.19	1.84
U1359A -14H-5- W-33-35	126.53	120.94	4.80	0.04	4.54	0.18	0.82	0.89	0.12	67.84	28.56	1.73
U1359A -14H-5- W-48-50	126.68	121.09	4.80	0.04	4.54	0.18	0.82	0.90	0.12	67.26	29.05	1.72
U1359A -14H-5- W-63-65	126.83	121.24	4.81	0.04	4.54	0.18	0.82	0.92	0.13	69.15	26.98	1.78

<u>Sample ID</u>	<u>Depth (mcd)</u>	<u>Depth (mbsf-A)</u>	<u>Age (Ma)</u>	<u>IRD (cm<sup>3</sup>/cm<sup>3</sup>)</u>	<u>LSR (cm/kyr)</u>	<u>Opal (g/g)</u>	<u>TERR (g/g)</u>	<u>DBD (g/cm<sup>3</sup>)</u>	<u>IRD.MAR (g/cm<sup>2</sup>/kyr)</u>	<u>% Silt</u>	<u>% Clay</u>	<u>Sorting</u>
U1359A-14H-5-W-78-80	126.98	121.39	4.81	0.22	4.54	0.18	0.82	0.93	0.76	71.62	6.43	2.11
U1359A-14H-5-W-93-95	127.13	121.54	4.81	0.04	4.54	0.18	0.82	0.94	0.13	70.66	25.57	1.74
U1359A-14H-5-W-108-110	127.28	121.69	4.82	0.06	4.54	0.17	0.83	0.96	0.21	71.26	22.97	1.70
U1359A-14H-5-W-123-125	127.43	121.84	4.82	0.06	4.54	0.17	0.83	0.97	0.24	70.24	23.28	1.71
U1359A-14H-5-W-138-140	127.58	121.99	4.82	0.07	4.54	0.17	0.83	0.98	0.28	72.40	20.14	1.80
U1359A-14H-6-W-3-5	127.73	122.14	4.83	0.10	4.54	0.17	0.83	0.99	0.36	71.61	18.83	1.87
U1359A-14H-6-W-18-20	127.88	122.29	4.83	0.12	4.54	0.16	0.84	1.01	0.45	72.65	15.71	1.85
U1359A-14H-6-W-33-35	128.03	122.44	4.83	0.15	4.54	0.16	0.84	1.02	0.57	72.85	12.41	1.81
U1359A-14H-6-W-48-50	128.18	122.59	4.83	0.08	4.54	0.15	0.85	1.03	0.34	71.19	20.37	1.91

<u>Sample ID</u>	<u>Depth (mcd)</u>	<u>Depth (mbsf-A)</u>	<u>Age (Ma)</u>	<u>IRD (cm<sup>3</sup>/cm<sup>3</sup>)</u>	<u>LSR (cm/kyr)</u>	<u>Opal (g/g)</u>	<u>TERR (g/g)</u>	<u>DBD (g/cm<sup>3</sup>)</u>	<u>IRD_MAR (g/cm<sup>2</sup>/kyr)</u>	<u>% Silt</u>	<u>% Clay</u>	<u>Sorting</u>
U1359A -14H-6- W-63-65	128.33	122.74	4.84	0.07	4.54	0.13	0.87	1.05	0.28	66.81	26.34	1.78
U1359A -14H-6- W-78-80	128.48	122.89	4.84	0.15	4.54	0.13	0.87	1.07	0.61	66.00	19.47	2.12
U1359A -14H-6- W-93-95	128.63	123.04	4.84	0.01	4.54	0.14	0.86	1.09	0.06	66.49	32.14	1.71
U1359A -14H-7- W-3-5	128.73	123.14	4.85	0.15	4.54	0.14	0.86	1.11	0.64	69.06	16.03	2.10
U1359A -14H-7- W-18-20	128.88	123.29	4.85	0.12	4.54	0.15	0.85	1.14	0.52	71.26	16.80	2.01
U1359A -14H-7- W-33-35	129.03	123.44	4.85	0.06	4.54	0.16	0.84	1.16	0.29	72.62	20.89	1.90
U1359A -14H-7- W-48-50	129.18	123.59	4.86	0.06	4.54	0.16	0.84	1.17	0.25	71.47	22.97	1.83
U1359A -14H-7- W-63-65	129.33	123.74	4.86	0.06	4.54	0.16	0.84	1.17	0.26	71.94	22.18	1.91
U1359A -14H-7- W-78-80	129.48	123.89	4.86	0.29	4.54	0.16	0.84	1.18	1.29	54.97	16.39	2.24
U1359A -14H-7- W-91-93	129.61	124.02	4.87	0.04	4.54	0.16	0.84	1.18	0.18	77.49	18.59	1.80

<u>Sample ID</u>	<u>Depth (mcd)</u>	<u>Depth (mbsf-A)</u>	<u>Age (Ma)</u>	<u>IRD (cm<sup>3</sup>/cm<sup>3</sup>)</u>	<u>LSR (cm/kyr)</u>	<u>Opal (g/g)</u>	<u>TERR (g/g)</u>	<u>DBD (g/cm<sup>3</sup>)</u>	<u>IRD.MAR (g/cm<sup>2</sup>/kyr)</u>	<u>% Silt</u>	<u>% Clay</u>	<u>Sorting</u>
U1359A -15H-1- W-3-5	129.73	124.14	4.87	0.12	4.54	0.15	0.85	1.18	0.54	74.00	14.01	2.04
U1359A -15H-1- W-18-20	129.88	124.29	4.87	0.16	4.54	0.15	0.85	1.18	0.72	69.41	14.82	2.04
U1359A -15H-1- W-33-35	130.03	124.44	4.87	0.58	4.54	0.15	0.85	1.18	2.66	35.68	6.08	2.52
U1359A -15H-1- W-48-50	130.18	124.59	4.88	0.19	4.54	0.15	0.85	1.19	0.88	64.45	16.18	2.10
U1359A -15H-1- W-63-65	130.33	124.74	4.88	0.55	4.54	0.15	0.85	1.19	2.51	38.73	6.36	2.13
U1359A -15H-1- W-78-80	130.48	124.89	4.88	0.15	4.54	0.15	0.85	1.19	0.70	68.31	16.47	1.94
U1359A -15H-1- W-93-95	130.63	125.04	4.89	0.59	4.54	0.16	0.84	1.18	2.68	35.99	4.80	2.28
U1359A -15H-1- W-108- 110	130.78	125.19	4.89	0.38	4.54	0.17	0.83	1.16	1.65	49.76	12.63	2.24
U1359A -15H-1- W-123- 125	130.93	125.34	4.89	0.55	4.54	0.18	0.82	1.14	2.33	36.89	7.90	2.48

<u>Sample ID</u>	<u>Depth (mcd)</u>	<u>Depth (mbsf-A)</u>	<u>Age (Ma)</u>	<u>IRD (cm<sup>3</sup>/cm<sup>3</sup>)</u>	<u>LSR (cm/kvr)</u>	<u>Opal (g/g)</u>	<u>TERR (g/g)</u>	<u>DBD (g/cm<sup>3</sup>)</u>	<u>IRD_MAR (g/cm<sup>2</sup>/kvr)</u>	<u>% Silt</u>	<u>% Clay</u>	<u>Sorting</u>
U1359A -15H-1- W-138- 140	131.08	125.49	4.90	0.27	4.54	0.19	0.81	1.11	1.09	63.59	9.58	2.15
U1359A -15H-2- W-3-5	131.23	125.64	4.90	0.06	4.54	0.21	0.79	1.09	0.24	70.09	23.83	1.79
U1359A -15H-2- W-18-20	131.38	125.79	4.90	0.03	4.54	0.22	0.78	1.07	0.13	70.00	26.62	1.84
U1359A -15H-2- W-33-35	131.53	125.94	4.91	0.03	4.54	0.23	0.77	1.05	0.10	73.05	24.24	1.77
U1359A -15H-2- W-48-50	131.68	126.09	4.91	0.01	4.54	0.24	0.76	1.04	0.03	76.51	22.56	1.71
U1359A -15H-2- W-63-65	131.83	126.24	4.91	0.08	4.54	0.24	0.76	1.03	0.27	79.08	13.40	1.96
U1359A -15H-2- W-78-80	131.98	126.39	4.92	0.01	4.54	0.25	0.75	1.02	0.05	71.96	26.72	1.75
U1359A -15H-2- W-93-95	132.13	126.54	4.92	0.01	4.54	0.25	0.75	1.01	0.03	69.42	29.64	1.76
U1359A -15H-2- W-108- 110	132.28	126.69	4.92	0.07	4.54	0.25	0.75	1.01	0.23	76.61	16.51	1.96

<u>Sample ID</u>	<u>Depth (mcd)</u>	<u>Depth (mbsf-A)</u>	<u>Age (Ma)</u>	<u>IRD (cm<sup>3</sup>/cm<sup>3</sup>)</u>	<u>LSR (cm/kyr)</u>	<u>Opal (g/g)</u>	<u>TERR (g/g)</u>	<u>DBD (g/cm<sup>3</sup>)</u>	<u>IRD_MAR (g/cm<sup>2</sup>/kyr)</u>	<u>% Silt</u>	<u>% Clay</u>	<u>Sorting</u>
U1359A -15H-2- W-123- 125	132.43	126.84	4.93	0.02	4.54	0.25	0.75	1.00	0.06	73.38	24.84	1.79
U1359A -15H-2- W-138- 140	132.58	126.99	4.93	0.02	4.54	0.25	0.75	0.99	0.08	83.83	13.71	1.84
U1359A -15H-3- W-3-5	132.73	127.14	4.93	0.02	4.54	0.25	0.75	0.98	0.07	75.27	22.51	1.69
U1359A -15H-3- W-18-20	132.88	127.29	4.93	0.02	4.54	0.25	0.75	0.97	0.06	72.96	25.15	1.69
U1359A -15H-3- W-33-35	133.03	127.44	4.94	0.05	4.54	0.26	0.74	0.96	0.17	75.99	18.84	1.88
U1359A -15H-3- W-48-50	133.18	127.59	4.94	0.07	4.54	0.26	0.74	0.96	0.24	74.87	17.70	1.92
U1359A -15H-3- W-63-65	133.33	127.74	4.94	0.08	4.54	0.26	0.74	0.95	0.25	74.81	17.29	1.74
U1359A -15H-3- W-78-80	133.48	127.89	4.95	0.28	4.54	0.27	0.73	0.94	0.87	61.66	10.57	2.01
U1359A -15H-3- W-93-95	133.63	128.04	4.95	0.22	4.54	0.27	0.73	0.95	0.69	65.88	12.31	1.92

<u>Sample ID</u>	<u>Depth (mcd)</u>	<u>Depth (mbsf-A)</u>	<u>Age (Ma)</u>	<u>IRD (cm<sup>3</sup>/cm<sup>3</sup>)</u>	<u>LSR (cm/kyr)</u>	<u>Opal (g/g)</u>	<u>TERR (g/g)</u>	<u>DBD (g/cm<sup>3</sup>)</u>	<u>IRD MAR (g/cm<sup>2</sup>/kyr)</u>	<u>% Silt</u>	<u>% Clay</u>	<u>Sorting</u>
U1359A -15H-3- W-108- 110	133.78	128.19	4.95	0.07	4.54	0.28	0.72	0.96	0.21	80.64	12.73	1.55
U1359A -15H-3- W-123- 125	133.93	128.34	4.96	0.01	4.54	0.29	0.71	0.98	0.02	73.84	25.52	1.65
U1359A -15H-3- W-138- 140	134.08	128.49	4.96	0.01	4.54	0.30	0.70	0.99	0.03	73.41	25.74	1.64
U1359A -15H-4- W-3-5	134.23	128.64	4.96	0.29	4.54	0.30	0.70	1.00	0.93	57.14	13.53	2.15
U1359A -15H-4- W-18-20	134.38	128.79	4.97	0.09	4.54	0.31	0.69	1.02	0.29	66.76	24.14	2.13
U1359A -15H-4- W-33-35	134.53	128.94	4.97	0.04	4.54	0.31	0.69	1.03	0.13	74.62	21.39	1.87
U1359A -15H-4- W-48-50	134.68	129.09	4.97	0.01	4.54	0.25	0.75	1.04	0.04	64.34	34.67	1.75
U1359A -15H-4- W-63-65	134.83	129.24	4.98	0.06	4.54	0.18	0.82	1.06	0.22	74.86	19.48	2.01
U1359A -15H-4- W-78-80	134.98	129.39	4.98	0.09	4.54	0.12	0.88	1.07	0.39	68.41	22.35	1.94

<u>Sample ID</u>	<u>Depth (mcd)</u>	<u>Depth (mbsf-A)</u>	<u>Age (Ma)</u>	<u>IRD (cm<sup>3</sup>/cm<sup>3</sup>)</u>	<u>LSR (cm/kvr)</u>	<u>Opal (g/g)</u>	<u>TERR (g/g)</u>	<u>DBD (g/cm<sup>3</sup>)</u>	<u>IRD MAR (g/cm<sup>2</sup>/kvr)</u>	<u>% Silt</u>	<u>% Clay</u>	<u>Sorting</u>
U1359A -15H-4- W-93-95	135.13	129.54	4.98	0.05	4.54	0.07	0.93	1.08	0.25	63.91	30.65	1.69
U1359A -15H-4- W-108- 110	135.28	129.69	4.99	0.01	4.54	0.07	0.93	1.09	0.06	73.32	25.26	1.65
U1359A -15H-4- W-123- 125	135.43	129.84	4.99	0.06	4.54	0.08	0.92	1.09	0.27	83.93	10.18	1.68
U1359A -15H-4- W-138- 140	135.58	129.99	4.99	0.01	4.54	0.08	0.92	1.08	0.05	69.55	29.44	1.63
U1359A -15H-5- W-3-5	135.73	130.14	4.99	0.12	4.54	0.08	0.92	1.08	0.54	61.48	26.67	2.00
U1359A -15H-5- W-18-20	135.88	130.29	5.00	0.01	4.54	0.08	0.92	1.08	0.05	62.43	36.56	1.54
U1359A -15H-5- W-33-35	136.03	130.44	5.00	0.01	4.54	0.09	0.91	1.08	0.03	60.58	38.79	1.55
U1359A -15H-5- W-48-50	136.18	130.59	5.00	0.01	4.54	0.12	0.88	1.08	0.05	63.81	35.13	1.54
U1359A -15H-5- W-63-65	136.33	130.74	5.01	0.15	4.54	0.15	0.85	1.08	0.64	73.22	11.40	2.25



<u>Sample ID</u>	<u>Depth (mcd)</u>	<u>Depth (mbsf-A)</u>	<u>Age (Ma)</u>	<u>IRD (cm<sup>3</sup>/cm<sup>3</sup>)</u>	<u>LSR (cm/kyr)</u>	<u>Opal (g/g)</u>	<u>TERR (g/g)</u>	<u>DBD (g/cm<sup>3</sup>)</u>	<u>IRD.MAR (g/cm<sup>2</sup>/kyr)</u>	<u>% Silt</u>	<u>% Clay</u>	<u>Sorting</u>
U1359A -15H-5- W-78-80	136.48	130.89	5.01	0.04	4.54	0.18	0.82	1.07	0.16	72.40	23.59	2.02
U1359A -15H-5- W-93-95	136.63	131.04	5.01	0.06	4.54	0.21	0.79	1.06	0.22	82.16	12.15	1.82
U1359A -15H-5- W-108- 110	136.78	131.19	5.02	0.17	4.54	0.19	0.81	1.05	0.66	73.94	9.14	1.84
U1359A -15H-5- W-123- 125	136.93	131.34	5.02	0.02	4.54	0.17	0.83	1.04	0.06	62.38	36.07	1.63
U1359A -15H-5- W-138- 140	137.08	131.49	5.02	0.03	4.54	0.16	0.84	1.04	0.10	65.71	31.68	1.63
U1359A -15H-6- W-3-5	137.23	131.64	5.03	0.00	4.54	0.14	0.86	1.03	0.01	67.65	32.08	1.56
U1359A -15H-6- W-18-20	137.38	131.79	5.03	0.01	4.54	0.12	0.88	1.02	0.04	62.58	36.55	1.53
U1359A -15H-6- W-33-35	137.53	131.94	5.03	0.01	4.54	0.11	0.89	1.01	0.03	65.83	33.40	1.61
U1359A -15H-6- W-48-50	137.68	132.09	5.04	0.01	4.54	0.13	0.87	1.01	0.03	70.22	29.02	1.61

<u>Sample ID</u>	<u>Depth (mcd)</u>	<u>Depth (mbsf-A)</u>	<u>Age (Ma)</u>	<u>IRD (cm<sup>3</sup>/cm<sup>3</sup>)</u>	<u>LSR (cm/kyr)</u>	<u>Opal (g/g)</u>	<u>TERR (g/g)</u>	<u>DBD (g/cm<sup>3</sup>)</u>	<u>IRD_MAR (g/cm<sup>2</sup>/kyr)</u>	<u>% Silt</u>	<u>% Clay</u>	<u>Sorting</u>
U1359A -15H-6- W-63-65	137.83	132.24	5.04	0.05	4.54	0.15	0.85	1.00	0.18	76.20	19.25	1.79
U1359A -15H-6- W-78-80	137.98	132.39	5.04	0.03	4.54	0.16	0.84	0.99	0.13	77.11	19.43	1.71
U1359A -15H-6- W-93-95	138.13	132.54	5.05	0.03	4.54	0.17	0.83	1.00	0.10	82.93	14.29	1.60
U1359A -15H-6- W-108- 110	138.28	132.69	5.05	0.04	4.54	0.16	0.84	1.02	0.15	78.64	17.40	1.77
U1359A -15H-6- W-123- 125	138.43	132.84	5.05	0.01	4.54	0.16	0.84	1.03	0.03	61.93	37.29	1.59
U1359A -15H-6- W-128- 130	138.48	132.89	5.05	0.02	4.54	0.15	0.85	1.04	0.08	64.00	34.05	1.62
U1359A -15H-7- W-3-5	138.55	132.96	5.05	0.04	4.54	0.15	0.85	1.04	0.16	60.96	34.98	1.69
U1359A -15H-7- W-18-20	138.7	133.11	5.06	0.03	4.54	0.14	0.86	1.06	0.11	64.71	32.58	1.91
U1359A -15H-7- W-33-35	138.85	133.26	5.06	0.04	4.54	0.13	0.87	1.06	0.17	65.05	30.85	1.74

<u>Sample ID</u>	<u>Depth (mcd)</u>	<u>Depth (mbsf-A)</u>	<u>Age (Ma)</u>	<u>IRD (cm<sup>3</sup>/cm<sup>3</sup>)</u>	<u>LSR (cm/kvr)</u>	<u>Opal (g/g)</u>	<u>TERR (g/g)</u>	<u>DBD (g/cm<sup>3</sup>)</u>	<u>IRD.MAR (g/cm<sup>2</sup>/kvr)</u>	<u>% Silt</u>	<u>% Clay</u>	<u>Sorting</u>
U1359A -15H-7- W-48-50	139	133.41	5.06	0.01	4.54	0.13	0.87	1.06	0.05	63.91	34.91	1.51
U1359A -15H-7- W-63-65	139.15	133.56	5.07	0.03	4.54	0.12	0.88	1.07	0.14	86.50	10.12	1.71

## References:

- Blott, S. J., & K. Pye (2001). GRADISTAT: a grain size distribution and statistics package for the analysis of unconsolidated sediments. *Earth surface processes and Landforms*, 26(11), 1237-1248.
- Cook, C. P., T. van de Flierdt, T. Williams, S.R. Hemming, M. Iwai, M. Kobayashi, F.J. Jimenez-Espejo, C. Escutia, J.J. González, B.K. Khim, R.M. McKay, S. Passchier, S.M. Bohaty, C.R. Riesselman, L. Tauxe, S. Sugisaki, A.L. Galindo, M.O. Patterson, F. Sangiorgi, E.L. Pierce, H. Brinkhuis & IODP Expedition 318 Scientists (2013). Dynamic behaviour of the East Antarctic ice sheet during Pliocene warmth. *Nature Geoscience*, 6(9), 765-769.
- Expedition 318 Scientists (2011). Wilkes Land Glacial History: Cenozoic East Antarctic Ice Sheet evolution from Wilkes Land margin sediments. *IODP Prel. Rept.*, 318.
- Folk, R. L., & W.C. Ward (1957). Brazos River bar: a study in the significance of grain size parameters. *Journal of Sedimentary Research*, 27(1).
- Gradstein, F. M., J.G. Ogg, & A.G. Smith (Eds.). (2004). *A geologic time scale 2004* (Vol. 86). Cambridge University Press.
- Patterson, M. O., R. McKay, T. Naish, C. Escutia, F.J. Jimenez-Espejo, M.E. Raymo, S.R. Meyers, L. Tauxe, H. Brinkhuis & IODP Expedition 318 Scientists (2014). Orbital forcing of the East Antarctic ice sheet during the Pliocene and Early Pleistocene. *Nature Geoscience*, 7(11), 841-847.

Tauxe, L., C.E. Stickley, S. Sugisaki, P.K. Bijl, S.M. Bohaty, H. Brinkhuis, C. Escutia, J.A. Flores, A.J.P. Houben, M. Iwai, F. Jiménez-Espejo, R. McKay, S. Passchier, J. Pross, C.R. Riesselman, U. Röhl, F. Sangiorgi, K. Welsh, A. Klaus, A. Fehr, J.A.P. Bendle, R. Dunbar, J. González, T. Hayden, K. Katsuki, M.P. Olney, S.F. Pekar, P.K. Shrivastava, T. van de Flierdt, T. Williams, & M. Yamane (2012). Chronostratigraphic framework for the IODP Expedition 318 cores from the Wilkes Land Margin: constraints for paleoceanographic reconstruction. *Paleoceanography*, 27(2).

## APPENDIX C

### C.1: Quartz Microtexture Methodology and Raw Data

#### *Preparation*

Grains were wet sieved with Millipore water using a 63-micron mesh. (The fine fraction was separately collected and stored). Grains were washed with water (not with SnCl as per Strand et al. (2003) and others) or acids, in order to preserve surface features. They were then dried in a drying oven at 75°C and stored in a labeled vial. Forty quartz grains were randomly selected as representatives for each sample for SEM analysis using fine tweezers under magnification and mounted on an aluminum stub using double sided-tape adhesive. The stubs were then gold coated.

#### *Data Generation*

Grains were analyzed for microtexture using a Hitachi S-3400N scanning electron microscope with an accelerating voltage of 12 kV to 15 kV as per Strand et al. (2003) and Helland et al. (1997). Microtexture classifications were derived from Mahaney et al. (1996), and Mahaney (2002). Frequency and presence of microtextures were ranked according to Newsome and Ladd (1999) and quantified into grain types using a system similar to Damiani et al. (2006). Roundness and shape of individual particles were qualified using the Powers (1953) scale.

Composition of grains was also measured using a Bruker X-Flash energy dispersive x-ray spectrometer. Generated spectra were compared to known examples of spectra as presented in Reed (2005). These spectra were subsequently used to differentiate non-quartz grains in the analysis.

### *Analysis*

Sand grains retain signatures of mechanical and chemical alterations from transport processes and can be used to better understand the dynamics of the ice sheet (Hansen, 2011). The abundance of certain microtextures will yield evidence of glacial crushing or abrasion intensity during glacial transport. Grain crushing and abrasion during glacial transport generate various mechanical textures such as arcuate steps and conchoidal fractures while subaqueous sedimentary processes generate chemical textures such as solution pits and overgrowths (Strand et al., 2003). Changes in the roundness of the particles can be influenced by fluctuations in the ice margin. For example, a glaciomarine environment will have current reworking causing edge abrasion and lower numbers of angular grains whereas in an ice-contact environment the angular outline is better preserved.

Frequency of grain surface features were based on an assigned value of 1 (<2% or absent), 2 (2-25%), 3 (25-75%), or 4 (>75%). Each grain was also assigned a grain type of Type 1 (Glacial), Type 2 (glacial and low-energy subaqueous), Type 3 (glacial and high-energy subaqueous), Type 4 (marine), Type 5 (eolian), and Type 6 (diagenetic) based on the Damiani et al. (2006) scale. A summary showing the total number of grains, frequency of textures, and grain types are shown in Tables C1-C7.

Ice-contact environments produce greater abundance of angular outlines and glaciomarine environments produce a lower number of angular grains due to edge abrasion from current (Strand et al., 2003). The outline of the grains were assigned angular, subangular, subrounded, or rounded and shed light on the origin of the grains,

where more angular outlines indicate a lack of underlying meltwater and sub-angular to sub-rounded outlines attributed to edge abrasion indicate the presence of meltwater (Hansen, 2011).

Grain relief ranged from low to high and is based on Mahaney (2002). The degree of relief is related to transport processes and something. More extensive crushing and fracturing of grains creates a higher relief as opposed to a more passive environment producing a lower relief. Relief is the degree of topographic irregularities on a grain's surface, defined as low relief (nearly smooth), medium relief (semi-smooth), and high relief (irregular). Glacial grains are described as having medium to high relief. High relief is result of heavy fracturing and abrasion.

## C2. Barite Investigation

### *Preparation*

Bulk sediment was lightly powdered using a mortar and pestle to lightly tap out larger clumps before being dispersed evenly onto an aluminum stub with a carbon sticker. Each sample was then gold coated and viewed on the Hitachi S-3400N Scanning Electron Microscope (SEM) with a Bruker-AXS X-flash Energy Dispersive X-ray spectrometer (EDX) operating at 15 kV.

### *Data Generation*

Barite grain identification was performed first by using the mapping feature on the Bruker X-Flash EDX to identify areas containing the elements Barium and Sulfur, which make up marine barite ( $\text{BaSO}_4$ ). Once the elements were identified, individual



grain spectra were captured and an image taken of the grain. The generated spectra were compared to a known example of barite presented in Riedinger et al. (2006).

**References:**

- Damiani, D., Giorgetti, G., & Turbanti, I. M. (2006). Clay mineral fluctuations and surface textural analysis of quartz grains in Pliocene–Quaternary marine sediments from Wilkes Land continental rise (East-Antarctica): paleoenvironmental significance. *Marine geology*, 226(3), 281-295.
- Hansen, M. (2011). *Determining Middle Miocene Through Pliocene Changes in Provenance and Basal Ice Conditions Through Sedimentological Analyses of Subglacial Diamictites in AND-2A, Ross Sea, Antarctica* (Master's thesis). Montclair State University, Montclair, NJ.
- Helland, P. E., Huang, P. H., & Diffendal Jr, R. F. (1997). SEM analysis of quartz sand grain surface textures indicates alluvial/colluvial origin of the Quaternary “glacial” boulder clays at Huangshan (Yellow Mountain), East-Central China. *Quaternary research*, 48(2), 177-186.
- Mahaney, W. C., Claridge, G., & Campbell, I. (1996). Microtextures on quartz grains in tills from Antarctica. *Palaeogeography, Palaeoclimatology, Palaeoecology*, 121(1), 89-103.
- Mahaney, W. C. (2002). *Atlas of sand grain surface textures and applications*. Oxford University Press.
- Newsome, D., & Ladd, P. (1999). The use of quartz grain microtextures in the study of the origin of sand terrains in Western Australia. *Catena*, 35(1), 1-17.
- Powers, M. C. (1953). A new roundness scale for sedimentary particles. *Journal of Sedimentary Research*, 23(2), 117-119.

- Reed, S. J. B. (2005). *Electron microprobe analysis and scanning electron microscopy in geology* (Vol. 158). Cambridge: Cambridge University Press.
- Riedinger, N., Kasten, S., Gröger, J., Franke, C., & Pfeifer, K. (2006). Active and buried authigenic barite fronts in sediments from the Eastern Cape Basin. *Earth and Planetary Science Letters*, 241(3), 876-887.
- Strand, K., Passchier, S., & Näsi, J. (2003). Implications of quartz grain microtextures for onset Eocene/Oligocene glaciation in Prydz Bay, ODP Site 1166, Antarctica. *Palaeogeography, Palaeoclimatology, Palaeoecology*, 198(1), 101-111.

Figure C1. Examples of Microtextures

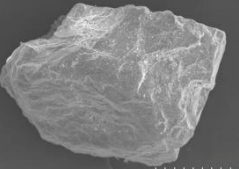
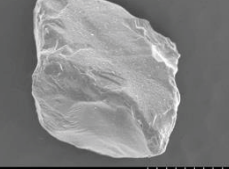
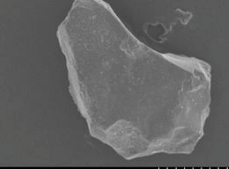
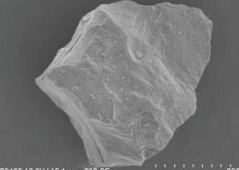
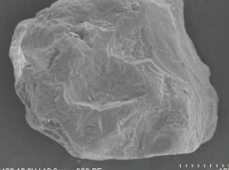
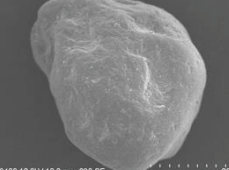
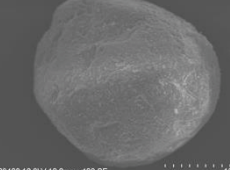
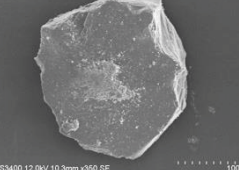
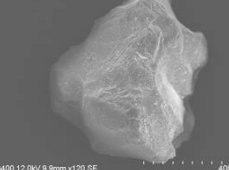
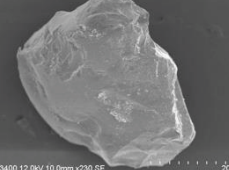
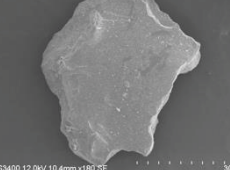
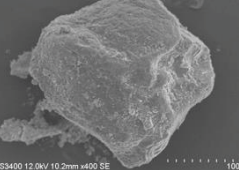
 <p>S3400 12.0kV 10.2mm x230 SE 200um</p>	 <p>S3400 12.0kV 10.2mm x230 SE 200um</p>	 <p>S3400 12.0kV 10.3mm x210 SE 200um</p>	
<p>High-Relief U1359B-13H-3W- 122-124 Grain 16</p>	<p>Medium-Relief U1359A-11H-3W- 123-125 Grain 1</p>	<p>Low-Relief U1359A-11H-3W- 123-125 Grain 25</p>	
 <p>S3400 12.0kV 10.1mm x230 SE 200um</p>	 <p>S3400 12.0kV 10.3mm x200 SE 100um</p>	 <p>S3400 12.0kV 10.0mm x230 SE 200um</p>	 <p>S3400 12.0kV 10.2mm x400 SE 100um</p>
<p>Angular U1359B-13H-3W- 122-124 Grain 27</p>	<p>Subangular U1359B-13H-3W- 122-124 Grain 29</p>	<p>Subrounded U1359A-12H-1W- 108-110 Grain 3</p>	<p>Rounded U1359A-15H-1W- 93-95 Grain 7</p>
 <p>S3400 12.0kV 10.3mm x350 SE 100um</p>	 <p>S3400 12.0kV 9.8mm x120 SE 400um</p>	 <p>S3400 12.0kV 10.0mm x230 SE 200um</p>	 <p>S3400 12.0kV 10.4mm x180 SE 300um</p>
<p>Fresh Surface U1359A-15H-1W- 63-65 Grain 33</p>	<p>Grooves U1359A-15H-1W- 93-95 Grain 2</p>	<p>Conchoidal Frac. U1359A-15H-1W- 33-35 Grain 2</p>	<p>Adhering Particles U1359A-15H-1W- 33-35 Grain 15</p>
 <p>S3400 12.0kV 10.2mm x400 SE 100um</p> <p>Silica Precipitation U1359A-15H-1W- 93-95 Grain 21</p>			

Figure C2. Micrographs of Grain types under Damiani et al. (2006) Classification

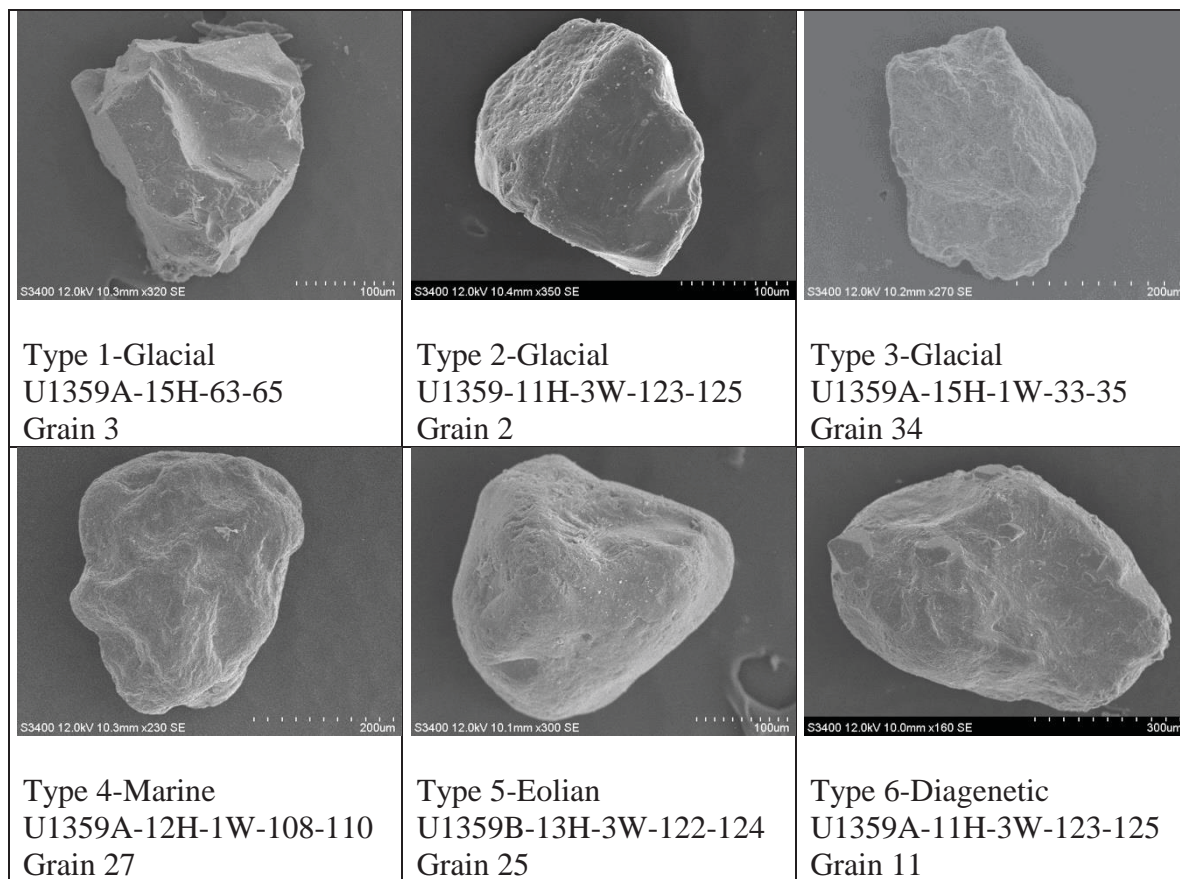


Figure C3. Barite Particles micrographs and associated spectra

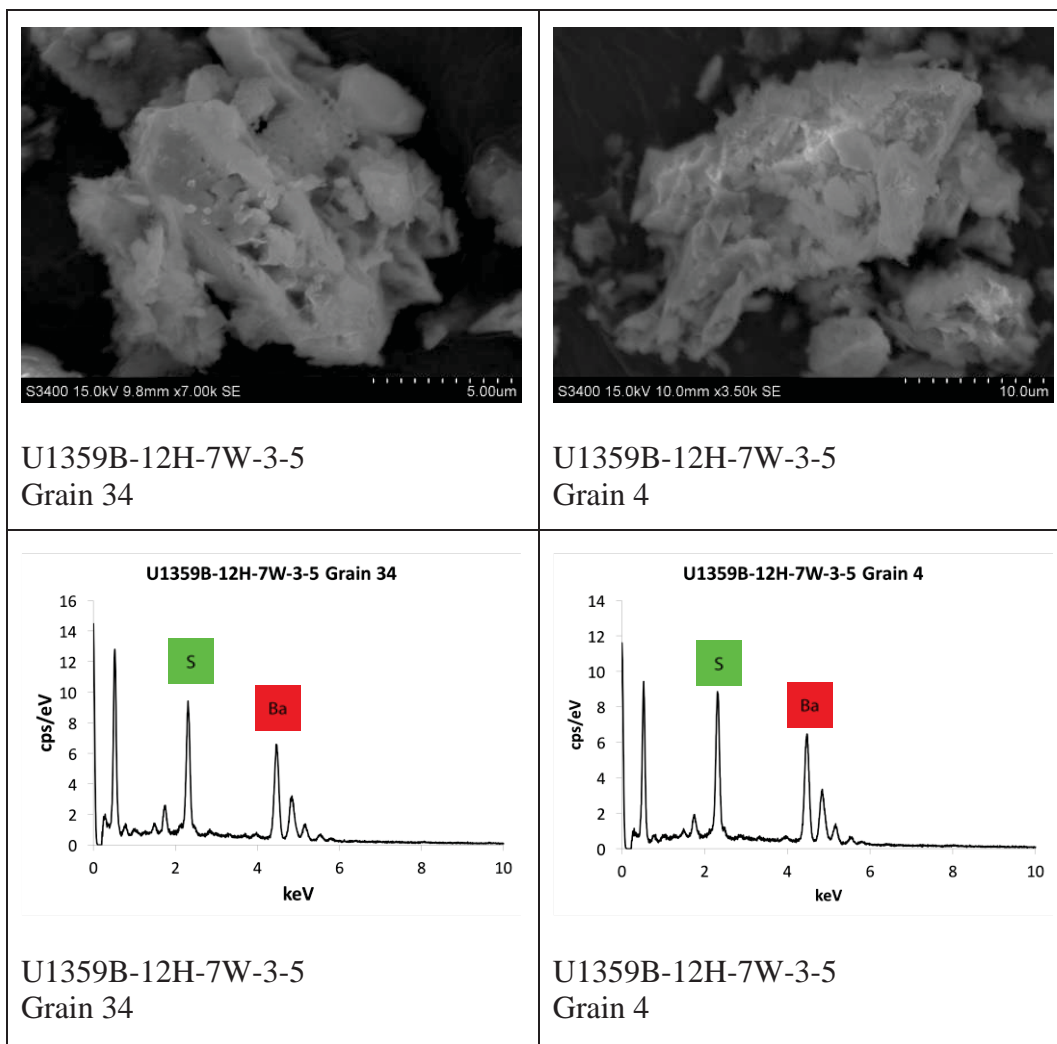


Figure C3. (Cont'd) Barite Particles micrographs and associated spectra

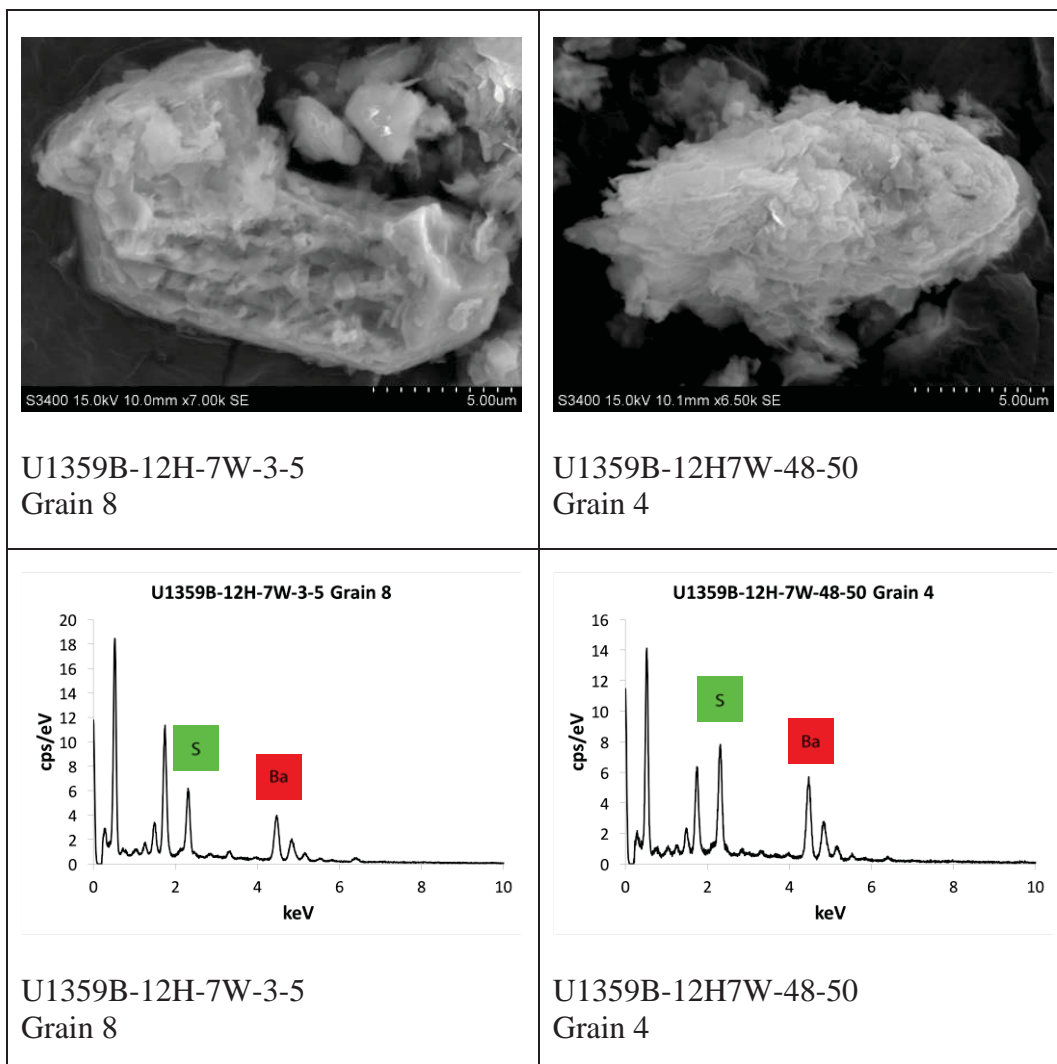


Figure C3. (Cont'd) Barite Particles micrographs and associated spectra

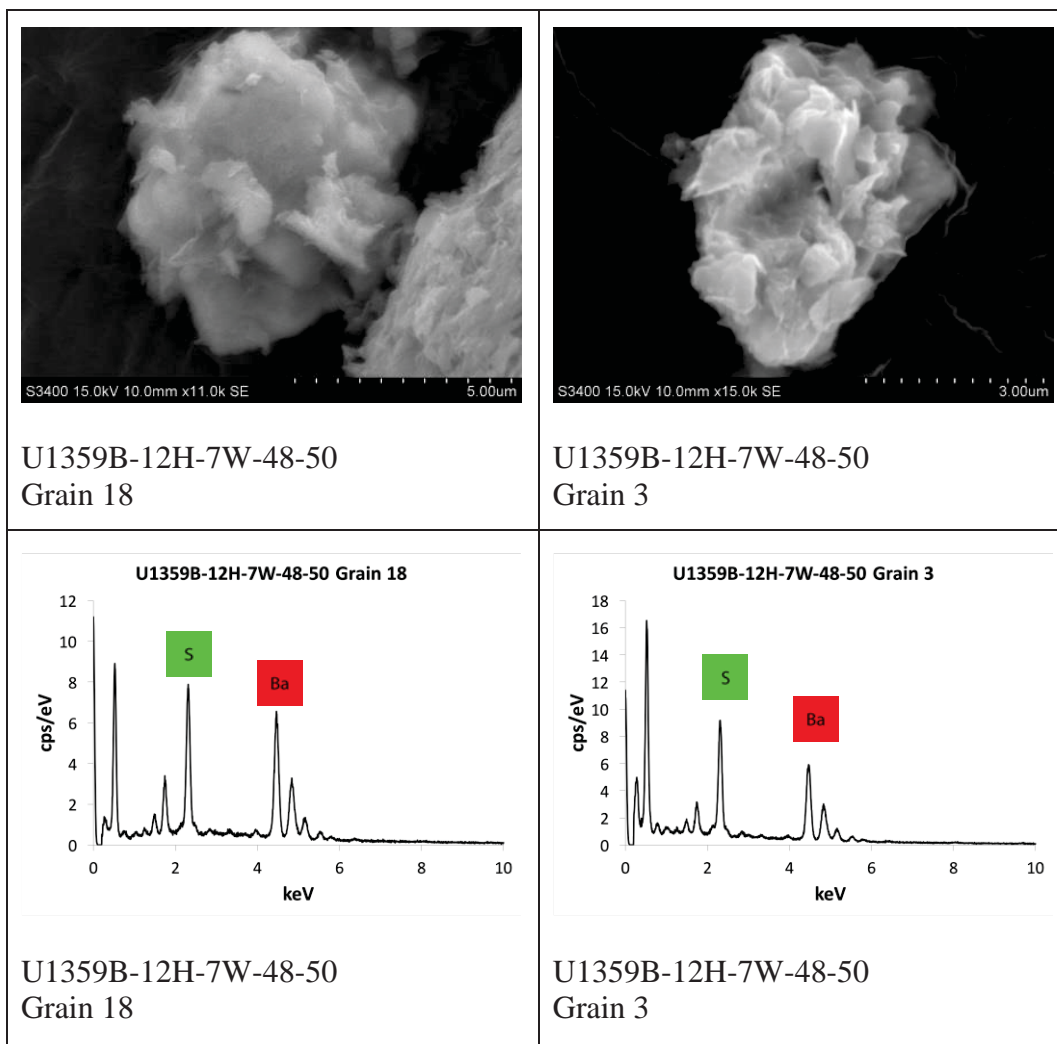




Table C1. U1359A-11H-3W-123-125

1		High-Relief	Y	Medium-Relief		Low-Relief		Angular		Sub-Angular		Sub-Rounded		Rounded	Fresh Surface	Impact Craters	Saw-tooth Fractures	Fracture Faces (Fresh)	Sub-parallel Linear	Conchoidal Fractures	Straight Grooves	Curved Grooves	Sharp Angular Features	Chatter Marks	Linear Steps	Arcuate Steps	Mech. Upturned Plates	Abrasion Features	Cracked Grains	Rounded Edges	Pre-weathered Surface	Chem. Weathered Surface	Adhering Particles (AP)	Silica Precipitation (SP)	Overgrowths (OG)		
2			Y							Y		Y			1	2	1	3	2	2	2	1	1	1	1	2	1	1	1	1	1	1	3	2	1		
3	Y									Y					2	3	2	1	1	1	1	1	1	1	1	1	3	2	3	3	3	1	3	1			
4			Y							Y					1	1	1	2	2	2	1	1	1	1	1	2	1	1	3	2	1	1	1	3	1		
5				Y							Y				2	3	1	1	1	1	1	1	1	1	1	1	1	1	3	2	1	1	1	3	2	1	
6			Y							Y					2	2	1	3	1	3	1	1	1	2	1	2	2	1	1	1	1	1	1	1	3	2	1
7	Y							Y							2	3	1	1	1	1	1	1	2	1	1	1	2	1	2	3	3	1	2	3	3	1	
8			Y								Y				1	3	2	1	2	2	1	1	1	1	1	1	2	1	3	3	1	1	1	3	3	1	
9			Y											Y	1	3	1	1	1	1	1	1	1	1	1	1	1	3	1	2	2	2	2	2	2	1	
10			Y								Y				1	4	1	2	1	1	1	2	1	1	1	1	1	1	2	3	1	2	1	2	3	1	
11			Y								Y				1	2	1	1	2	1	1	1	1	1	1	1	1	3	1	2	4	2	2	2	4	2	
12			Y								Y				1	3	1	1	1	1	1	1	1	2	1	1	1	2	2	3	1	2	2	2	3	1	
13			Y								Y				1	2	1	3	2	1	1	1	1	1	2	1	2	2	2	1	2	2	2	2	2	2	1
14			Y								Y				2	2	1	1	1	2	1	1	1	1	1	1	2	2	1	2	2	1	1	2	2	2	1
15	Y							Y							1	2	1	1	1	1	1	1	1	2	1	1	1	2	1	2	3	1	1	2	3	1	
16			Y					Y							1	3	1	1	1	1	1	2	2	2	2	2	3	3	1	2	1	1	1	1	3	2	1
17			Y							Y					1	2	1	1	2	1	2	2	2	2	1	2	3	3	1	1	1	1	1	3	2	2	1



	High-Relief	Medium-Relief	Low-Relief	Angular	Sub-Angular	Sub-Rounded	Rounded	Fresh Surface	Impact Craters	Saw-tooth Fractures	Fracture Faces (Fresh)	Sub-parallel Linear	Conchoidal Fractures	Straight Grooves	Curved Grooves	Sharp Angular Features	Chatter Marks	Linear Steps	Arcuate Steps	Mech. Upturned Plates	Abrasion Features	Cracked Grains	Rounded Edges	Pre-weathered Surface	Chem. Weathered Surface	Adhering Particles (AP)	Silica Precipitation (SP)	Overgrowths (OG)
37		Y				Y		2	1	2	1	1	2	1	1	1	1	1	1	1	2	2	1	1	2	1	1	1
38	Y				Y			1	2	1	1	1	2	1	1	2	1	1	1	1	1	1	2	1	1	3	3	1
39	Y			Y				1	2	2	1	2	2	1	1	2	2	1	1	1	1	1	1	1	1	2	2	1
40		Y			Y			1	2	1	1	1	1	2	1	1	1	1	1	2	1	1	2	1	1	3	3	1

Table C2. U1359B-13H-3W-122-124

	High-Relief	Medium-Relief	Low-Relief	Angular	Sub-Angular	Sub-Rounded	Rounded	Fresh Surface	Impact Craters	Saw-tooth Fractures	Fracture Faces (Fresh)	Sub-parallel Linear	Conchoidal Fractures	Straight Grooves	Curved Grooves	Sharp Angular Features	Chatter Marks	Linear Steps	Arcuate Steps	Mech. Upturned Plates	Abrasion Features	Cracked Grains	Rounded Edges	Pre-weathered Surface	Chem. Weathered Surface	Adhering Particles (AP)	Silica Precipitation (SP)	Overgrowths (OG)
1		Y		Y				2	2	1	2	1	2	1	2	1	1	1	1	1	1	1	1	1	1	2	1	1
2	Y			Y				1	2	1	1	1	1	2	1	1	2	1	1	1	2	1	1	1	1	1	2	1
3		Y			Y			1	2	1	1	2	2	1	2	1	2	1	2	1	1	1	3	1	1	1	2	1
4		Y			Y			1	2	2	1	2	2	1	1	1	2	1	1	1	2	1	2	2	1	2	3	2
5	Y			Y				1	2	2	1	1	2	1	2	2	2	1	2	2	1	2	1	1	1	1	2	2
6		Y				Y		1	2	1	1	1	2	1	1	1	2	1	1	2	1	1	3	1	1	1	2	2
7		Y			Y			2	2	2	1	1	2	2	1	1	2	1	1	2	1	1	2	1	1	1	1	1
8	Y			Y				1	1	1	1	2	2	2	2	2	2	1	2	1	2	1	1	1	1	2	1	1
9			Y	Y				3	1	1	1	2	1	2	1	2	1	1	1	2	2	2	1	1	1	1	1	1
10		Y			Y			1	2	1	2	2	2	2	2	1	2	1	2	2	1	1	2	2	1	1	3	1
11	Y			Y				2	3	1	1	2	2	2	2	1	1	2	2	1	1	1	1	1	1	2	1	2
12	Y				Y			1	2	1	1	2	1	2	1	1	2	1	1	1	2	1	2	1	1	1	2	2
13		Y			Y			1	1	2	2	1	1	2	2	1	2	1	1	1	1	1	2	1	1	2	1	2
14	Y				Y			1	2	2	1	1	2	1	2	1	2	1	2	1	1	1	2	1	1	1	3	2
15			Y			Y		1	1	1	1	1	2	1	1	1	2	1	1	1	2	1	3	1	1	1	1	1
16	Y			Y				1	2	2	1	1	3	1	2	1	1	1	2	2	2	1	1	1	1	2	1	1
17		Y			Y			1	2	1	1	1	1	1	2	1	2	1	1	1	2	1	2	2	1	1	3	2



37	Y	High-Relief	Medium-Relief	Low-Relief	Angular	Sub-Angular	Sub-Rounded	Rounded	Fresh Surface	Impact Craters	Saw-tooth Fractures	Fracture Faces (Fresh	Sub-parallel Linear	Conchoidal Fractures	Straight Grooves	Curved Grooves	Sharp Angular Features	Chatter Marks	Linear Steps	Arcuate Steps	Mech. Upturned Plates	Abrasion Features	Cracked Grains	Rounded Edges	Pre-weathered Surface	Chem. Weathered Surface	Adhering Particles (AP)	Silica Precipitation (SP)	Overgrowths (OG)
38		Y			Y		Y		1	2	1	1	1	1	1	1	1	1	1	1	1	2	2	3	1	1	1	1	1
39		Y	Y		Y				2	1	1	1	2	2	2	2	1	2	1	1	2	1	1	1	1	1	1	2	1
40	Y					Y			3	1	1	2	1	2	2	2	1	1	1	2	1	1	2	2	1	1	2	1	1

Table C3. U1359A-12H-1W-108-110

	High-Relief	Medium-Relief	Low-Relief	Angular	Sub-Angular	Sub-Rounded	Rounded	Fresh Surface	Impact Craters	Saw-tooth Fractures	Fracture Faces (Fresh)	Sub-parallel Linear	Conchoidal Fractures	Straight Grooves	Curved Grooves	Sharp Angular Features	Chatter Marks	Linear Steps	Arcuate Steps	Mech. Upturned Plates	Abrasion Features	Cracked Grains	Rounded Edges	Pre-weathered Surface	Chem. Weathered Surface	Adhering Particles (AP)	Silica Precipitation (SP)	Overgrowths (OG)
1	Y			Y				1	1	1	2	1	2	1	1	1	1	1	1	1	2	1	1	1	1	2	3	1
2		Y			Y			2	2	1	1	1	1	1	1	1	1	1	1	2	1	2	1	1	1	2	3	1
3	Y					Y		1	2	1	2	1	1	1	1	1	1	1	1	1	2	1	3	2	1	2	4	1
4		Y				Y		1	2	1	1	1	1	1	1	1	2	1	1	1	2	1	4	1	1	1	3	1
5		Y				Y		1	2	1	1	1	1	1	1	1	2	1	1	1	2	1	1	2	1	2	3	1
6	Y							1	2	1	2	1	2	2	2	1	2	1	2	1	1	1	1	1	1	3	2	1
7		Y				Y		1	2	2	1	1	2	1	1	2	1	1	1	1	1	1	2	1	1	3	3	1
8	Y							2	2	1	2	2	1	2	1	1	1	1	1	2	1	2	2	2	2	1	2	2
9		Y				Y		1	2	1	1	1	1	2	2	1	2	1	1	1	1	1	2	1	1	2	2	1
10	Y							1	1	1	1	1	2	1	2	1	1	1	1	1	1	1	2	1	1	2	2	1
11	Y							2	1	1	2	1	1	1	1	1	1	1	1	1	1	1	1	2	1	1	2	1
12		Y				Y		1	1	1	1	1	2	1	1	2	1	1	1	1	1	1	4	2	1	3	2	1
13	Y					Y		1	2	1	1	1	1	1	1	1	1	1	1	1	1	1	4	2	1	3	3	1
14		Y				Y		2	1	1	2	1	2	1	1	2	1	1	1	1	1	1	2	1	1	3	1	1
15		Y				Y		1	2	1	2	2	1	1	1	1	2	1	1	1	1	3	1	1	1	2	1	1
16		Y				Y		1	1	1	1	1	1	1	1	1	1	1	1	1	1	2	1	1	1	2	3	1
17	Y					Y		1	2	2	1	1	2	1	1	1	2	1	1	1	1	2	1	1	1	1	2	1





	High-Relief	Medium-Relief	Low-Relief	Angular	Sub-Angular	Sub-Rounded	Rounded	Fresh Surface	Impact Craters	Saw-tooth Fractures	Fracture Faces (Fresh)	Sub-parallel Linear	Conchoidal Fractures	Straight Grooves	Curved Grooves	Sharp Angular Features	Chatter Marks	Linear Steps	Arcuate Steps	Mech. Upturned Plates	Abrasion Features	Cracked Grains	Rounded Edges	Pre-weathered Surface	Chem. Weathered Surface	Adhering Particles (AP)	Silica Precipitation (SP)	Overgrowths (OG)	
36	Y			Y				2	2	1	2	1	3	2	1	2	1	2	2	1	1	1	1	1	1	1	1	1	1
37		Y			Y			1	2	1	1	1	2	2	2	1	2	1	1	1	1	1	1	1	1	2	2	1	
38		Y			Y			2	1	1	2	1	2	1	1	1	1	1	1	2	1	1	2	1	1	1	1	1	
39	Y				Y			2	1	1	2	1	2	2	2	1	1	1	1	2	2	2	1	1	1	2	1	1	
40	Y					Y		1	2	1	2	1	2	1	1	1	1	1	1	1	1	1	1	1	1	2	2	1	

Table C4. U1359A-15H-1W-33-35

	High-Relief	Medium-Relief	Low-Relief	Angular	Sub-Angular	Sub-Rounded	Rounded	Fresh Surface	Impact Craters	Saw-tooth Fractures	Fracture Faces (Fresh)	Sub-parallel Linear	Conchoidal Fractures	Straight Grooves	Curved Grooves	Sharp Angular Features	Chatter Marks	Linear Steps	Arcuate Steps	Mech. Upturned Plates	Abrasion Features	Cracked Grains	Rounded Edges	Pre-weathered Surface	Chem. Weathered Surface	Adhering Particles (AP)	Silica Precipitation (SP)	Overgrowths (OG)	
1	Y			Y				1	2	1	2	1	2	1	1	2	1	1	1	1	2	1	1	1	2	3	2	1	
2	Y			Y				1	2	2	2	2	3	2	1	2	1	1	2	2	2	2	1	2	1	3	1	1	
3	Y			Y				1	2	2	2	3	3	2	2	2	1	1	2	2	2	2	1	2	1	3	2	1	
4		Y				Y		1	2	1	1	1	1	1	2	1	1	1	1	1	1	1	4	2	1	3	3	2	
5		Y				Y		1	2	1	1	1	2	1	1	1	1	1	1	1	1	1	3	2	1	4	1	1	
6		Y			Y			3	1	1	2	2	2	1	1	2	1	1	2	1	1	1	2	1	1	3	1	1	
7	Y					Y		1	2	1	1	1	2	2	2	1	1	1	1	1	1	2	1	4	2	1	3	1	1
8		Y			Y			1	1	2	1	1	2	1	1	2	1	1	1	1	1	1	1	1	1	1	1	4	1
9	Y			Y				1	2	2	2	2	2	2	2	3	1	1	2	1	1	1	1	1	1	2	2	1	
10	Y			Y				1	2	1	2	1	2	2	2	2	2	1	2	1	1	1	1	2	1	2	2	1	
11		Y				Y		2	2	2	2	1	1	1	1	1	2	1	1	1	1	2	1	3	1	1	3	2	1
12	Y					Y		1	2	1	1	2	1	2	2	2	2	2	1	1	1	2	1	3	1	1	4	1	2
13		Y				Y		1	2	1	2	1	2	2	1	1	2	1	1	1	1	2	1	2	1	2	2	2	2
14		Y				Y		2	2	1	1	1	2	2	1	2	2	1	1	1	1	2	1	3	1	1	2	1	1
15		Y		Y				1	1	1	1	1	2	2	1	2	1	1	1	1	1	2	1	1	1	4	2	1	1
16		Y				Y		1	2	1	1	1	2	2	1	2	2	1	1	1	1	1	1	1	1	3	2	2	2
17		Y				Y		1	1	2	1	2	2	1	1	1	1	1	1	1	1	1	3	1	1	2	3	1	1





Table C5. U1359A-15H-1W-93-95

	High-Relief	Medium-Relief	Low-Relief	Angular	Sub-Angular	Sub-Rounded	Rounded	Fresh Surface	Impact Craters	Saw-tooth Fractures	Fracture Faces (Fresh)	Sub-parallel Linear	Conchoidal Fractures	Straight Grooves	Curved Grooves	Sharp Angular Features	Chatter Marks	Linear Steps	Arcuate Steps	Mech. Upturned Plates	Abrasion Features	Cracked Grains	Rounded Edges	Pre-weathered Surface	Chem. Weathered Surface	Adhering Particles (AP)	Silica Precipitation (SP)	Overgrowths (OG)
1		Y					Y	1	2	1	1	1	1	1	1	1	2	1	1	1	2	2	4	2	1	2	2	2
2	Y			Y				1	1	1	2	2	2	3	2	2	1	2	1	2	2	1	1	1	1	3	1	2
3	Y			Y				1	2	1	1	1	2	2	1	1	2	1	1	2	2	2	1	1	1	3	2	2
4	Y				Y			2	2	1	1	1	2	2	2	1	1	1	1	2	1	2	3	2	1	3	3	2
5		Y			Y			1	1	1	1	1	1	2	1	1	2	1	1	1	1	1	2	1	1	2	2	2
6	Y			Y				1	2	1	1	2	1	1	1	1	1	1	1	1	1	1	1	1	2	2	1	2
7			Y				Y	1	2	1	1	1	1	1	1	1	2	1	1	1	1	2	4	2	1	1	4	1
8	Y			Y				2	2	2	1	1	2	2	1	2	1	1	1	2	1	2	1	1	1	2	2	2
9		Y		Y				1	2	1	1	2	2	2	1	2	1	1	1	2	1	2	1	1	1	3	1	1
10		Y		Y				2	1	2	1	1	2	2	1	2	2	1	2	1	1	1	1	1	1	3	1	2
11	Y			Y				1	1	1	2	1	1	1	2	1	1	1	1	1	1	1	1	1	1	2	1	1
12		Y				Y		1	1	1	1	1	1	1	1	1	1	1	1	1	2	2	2	2	1	2	3	1
13	Y				Y			2	1	1	1	1	2	2	1	1	2	1	2	1	2	1	1	1	1	2	1	1
14		Y		Y				1	1	1	1	1	1	2	1	1	2	1	1	1	1	2	2	2	1	3	1	1
15		Y		Y				1	2	1	1	1	1	2	1	1	1	1	1	1	1	2	1	1	1	2	3	1
16		Y				Y		1	1	1	1	1	1	1	1	1	1	2	1	2	1	2	2	2	2	3	2	1
17		Y				Y		2	1	1	1	2	1	2	1	1	1	1	1	1	1	2	2	2	2	3	1	3

	High-Relief	Medium-Relief	Low-Relief	Angular	Sub-Angular	Sub-Rounded	Rounded	Fresh Surface	Impact Craters	Saw-tooth Fractures	Fracture Faces (Fresh)	Sub-parallel Linear	Conchoidal Fractures	Straight Grooves	Curved Grooves	Sharp Angular Features	Chatter Marks	Linear Steps	Arcuate Steps	Mech. Upturned Plates	Abrasion Features	Cracked Grains	Rounded Edges	Pre-weathered Surface	Chem. Weathered Surface	Adhering Particles (AP)	Silica Precipitation (SP)	Overgrowths (OG)	
18			Y	Y				1	1	1	1	2	2	1	2	1	1	1	1	1	1	1	1	1	1	4	1	1	
19		Y			Y			1	2	1	1	1	1	2	1	2	2	1	1	1	1	1	3	1	1	2	2	1	
20	Y		Y				2	2	1	1	1	2	2	2	1	2	2	1	1	1	2	2	2	1	1	1	3	1	1
21			Y		Y		1	1	2	1	1	1	1	1	1	1	1	1	1	2	2	2	3	2	1	2	4	1	
22			Y		Y		1	1	1	1	1	1	1	2	1	1	1	1	1	1	2	2	3	2	1	2	4	1	
23		Y			Y		1	1	2	1	2	1	2	2	1	2	2	1	1	1	1	1	2	1	1	3	2	1	
24	Y				Y		1	1	2	1	1	1	2	2	1	1	2	1	1	1	1	1	3	1	1	2	2	2	
25	Y			Y			1	1	1	1	1	1	1	1	1	1	2	1	1	2	2	1	2	2	2	1	2	4	2
26	Y			Y			2	2	2	1	2	2	2	2	1	2	1	1	2	2	2	2	2	1	1	2	1	2	2
27	Y		Y				1	1	2	1	1	2	1	1	1	1	2	1	1	2	2	1	2	1	1	2	3	2	2
28		Y	Y	Y			1	1	1	1	2	2	2	1	1	2	1	2	1	2	1	1	1	1	1	4	1	1	1
29	Y		Y	Y			1	1	2	1	1	1	1	1	1	1	1	1	1	2	1	2	1	1	1	2	4	1	1
30	Y		Y	Y			2	2	2	1	1	1	1	2	1	2	1	1	1	2	1	2	1	2	1	3	2	1	1
31	Y				Y		1	1	2	1	2	1	1	1	1	1	1	1	1	2	2	2	3	2	1	3	3	2	2
32	Y		Y				2	2	3	1	2	1	2	1	1	2	1	1	1	2	2	2	1	1	2	3	1	1	1
33		Y	Y	Y			2	2	2	2	2	1	2	1	2	2	1	1	2	2	2	2	1	1	1	2	1	2	2
34	Y		Y	Y			1	1	2	1	1	1	1	1	2	1	1	1	1	2	2	2	1	1	1	2	2	2	2
35		Y		Y			2	1	1	1	1	1	1	1	1	1	1	1	1	2	1	2	2	2	1	3	3	1	1
36	Y		Y	Y			2	2	2	2	1	1	2	2	1	2	2	1	1	1	1	2	1	2	2	2	2	2	1

37	High-Relief	Medium-Relief	Low-Relief	Angular	Sub-Angular	Sub-Rounded	Rounded	Fresh Surface	Impact Craters	Saw-tooth Fractures	Fracture Faces (Fresh)	Sub-parallel Linear	Conchoidal Fractures	Straight Grooves	Curved Grooves	Sharp Angular Features	Chatter Marks	Linear Steps	Arcuate Steps	Mech. Upturned Plates	Abrasion Features	Cracked Grains	Rounded Edges	Pre-weathered Surface	Chem. Weathered Surface	Adhering Particles (AP)	Silica Precipitation (SP)	Overgrowths (OG)
38	Y					Y		1	2	1	2	2	1	2	2	1	2	1	1	2	1	1	3	2	1	2	1	2
39	Y			Y				2	2	1	2	1	2	2	1	2	1	1	2	1	2	1	1	1	1	3	1	1
40	Y			Y				2	2	1	1	2	2	2	1	1	2	1	1	2	1	2	1	1	1	3	2	1

Table C6. U1359A-15H-1W-63-65

1		High-Relief	Y	Medium-Relief		Low-Relief		Angular		Sub-Angular		Sub-Rounded		Rounded	Fresh Surface	Impact Craters	Saw-tooth Fractures	Fracture Faces (Fresh)	Sub-parallel Linear	Conchoidal Fractures	Straight Grooves	Curved Grooves	Sharp Angular Features	Chatter Marks	Linear Steps	Arcuate Steps	Mech. Upturned Plates	Abrasion Features	Cracked Grains	Rounded Edges	Pre-weathered Surface	Chem. Weathered Surface	Adhering Particles (AP)	Silica Precipitation (SP)	Overgrowths (OG)	
2		Y	Y					Y		Y					1	2	1	1	1	1	2	1	1	1	1	1	1	2	1	2	2	1	4	2	1	
3	Y														1	1	2	1	1	2	2	1	2	2	1	1	2	1	1	1	1	2	1	3	2	
4		Y	Y					Y		Y					1	2	1	1	1	1	2	2	1	2	1	1	2	2	2	2	1	2	1	2	1	
5		Y	Y					Y							2	2	2	2	2	2	2	2	2	2	2	1	2	2	1	1	1	3	1	1		
6	Y									Y					1	1	2	2	2	2	2	3	1	2	1	1	2	2	2	2	2	1	2	1	1	
7	Y							Y							2	2	1	1	1	1	2	1	1	1	1	1	1	2	1	2	1	2	1	2	4	1
8		Y	Y					Y							1	2	1	1	1	1	1	1	1	1	1	1	2	2	2	2	1	2	1	3	3	1
9		Y	Y							Y					1	1	1	2	1	1	2	1	1	1	2	1	1	1	1	2	1	1	2	3	1	
10		Y	Y							Y					1	2	1	1	1	2	1	1	1	2	1	1	1	2	2	2	2	2	2	3	3	1
11	Y							Y							1	2	1	1	1	2	2	1	2	2	1	1	2	1	1	1	1	2	3	2	2	
12		Y	Y					Y							1	1	1	2	1	2	2	1	1	2	1	1	1	1	1	1	1	4	2	1	1	
13	Y							Y							1	1	1	1	1	2	1	1	1	1	1	1	3	1	2	1	1	4	1	1	1	
14	Y							Y							1	2	2	1	1	2	2	2	2	2	2	1	2	2	2	1	1	3	2	2	2	
15	Y							Y							2	2	2	1	2	2	2	1	2	2	1	1	2	2	2	1	1	2	1	1	1	
16	Y							Y							1	2	1	1	1	2	1	2	2	2	1	1	2	1	1	1	1	2	3	1	1	
17	Y							Y							2	2	2	1	1	2	1	2	2	2	1	1	2	1	1	1	3	2	2	1		



18	Y	High-Relief		Medium-Relief	Low-Relief	Angular	Sub-Angular	Sub-Rounded	Rounded	Fresh Surface	Impact Craters	Saw-tooth Fractures	Fracture Faces (Fresh)	Sub-parallel Linear	Conchoidal Fractures	Straight Grooves	Curved Grooves	Sharp Angular Features	Chatter Marks	Linear Steps	Arcuate Steps	Mech. Upturned Plates	Abrasion Features	Cracked Grains	Rounded Edges	Pre-weathered Surface	Chem. Weathered Surface	Adhering Particles (AP)	Silica Precipitation (SP)	Overgrowths (OG)	
19	Y						Y	Y		1	2	1	1	1	2	2	1	1	1	1	1	2	1	2	3	2	2	2	3	2	
20	Y				Y					1	2	2	1	1	2	3	2	1	1	2	1	1	1	1	2	1	1	2	2	1	
21				Y				Y		1	2	1	1	1	2	2	1	1	1	2	1	1	1	1	1	3	1	1	2	4	1
22				Y				Y		2	2	1	1	1	2	1	2	1	1	2	1	1	1	2	1	3	1	1	2	1	1
23	Y					Y				1	1	1	1	1	2	2	2	2	2	1	1	1	2	2	1	1	1	1	3	1	1
24				Y		Y				2	2	1	1	2	2	2	1	2	2	1	1	1	1	1	1	1	1	1	2	1	1
25	Y					Y				1	2	1	1	1	2	1	1	1	1	1	1	1	1	2	2	1	2	1	2	3	2
26	Y					Y				1	2	2	1	1	2	2	1	2	2	2	1	1	2	2	2	1	1	1	2	2	1
27	Y					Y				2	2	2	1	2	2	2	1	2	2	2	1	1	2	2	2	1	1	1	2	2	1
28					Y	Y				3	1	1	1	3	2	1	1	2	1	2	1	1	1	1	1	1	1	1	2	1	1
29	Y						Y			2	2	1	1	1	3	2	1	2	2	1	1	1	2	2	1	2	1	1	3	1	1
30	Y					Y				1	1	1	1	2	2	2	2	2	2	1	1	1	1	1	1	1	1	1	3	2	1
31	Y						Y			1	1	2	1	1	2	2	1	2	1	1	1	1	2	1	2	1	2	3	3	2	2
32				Y		Y				1	2	2	1	1	2	1	1	1	1	2	1	2	2	1	2	1	2	1	2	3	2
33				Y	Y					3	1	2	1	1	2	2	2	2	2	1	1	2	1	1	1	1	1	1	2	1	1
34				Y			Y			1	1	1	1	1	2	1	1	1	1	2	1	1	1	1	1	1	1	1	2	4	2
35				Y				Y		1	2	2	2	1	1	1	2	1	1	1	1	1	2	2	2	3	1	1	2	1	1
36				Y		Y				1	2	2	1	2	2	2	1	2	1	1	1	1	2	2	1	1	1	1	3	1	1

		High-Relief	Medium-Relief	Low-Relief	Angular	Sub-Angular	Sub-Rounded	Rounded	Fresh Surface	Impact Craters	Saw-tooth Fractures	Fracture Faces (Fresh	Sub-parallel Linear	Conchoidal Fractures	Straight Grooves	Curved Grooves	Sharp Angular Features	Chatter Marks	Linear Steps	Arcuate Steps	Mech. Upturned Plates	Abrasion Features	Cracked Grains	Rounded Edges	Pre-weathered Surface	Chem. Weathered Surface	Adhering Particles (AP)	Silica Precipitation (SP)	Overgrowths (OG)	
37			Y			Y			1	1	1	1	2	2	2	1	1	1	1	1	1	1	1	1	1	1	1	3	1	2
38	Y					Y			1	1	1	1	1	2	1	1	1	1	1	1	2	1	2	1	2	2	2	4	2	2
39		Y				Y			1	2	2	1	1	2	1	2	1	1	1	1	1	2	2	2	2	2	3	3	2	2
40		Y				Y			1	2	1	1	2	2	2	1	1	1	1	1	2	2	2	3	1	1	4	1	1	1

Table C7. U1359B-13H-5W-33-35

1		High-Relief	Y	Medium-Relief		Low-Relief	Y	Angular		Sub-Angular		Sub-Rounded		Rounded	Fresh Surface	Impact Craters	Saw-tooth Fractures	Fracture Faces (Fresh Break)	Sub-parallel Linear Fractures	Conchoidal Fractures	Straight Grooves	Curved Grooves	Sharp Angular Features	Chatter Marks	Linear Steps	Arcuate Steps	Mech. Upturned Plates	Abrasion Features	Cracked Grains	Rounded Edges	Pre-weathered Surface	Chem. Weathered Surface	Adhering Particles (AP)	Silica Precipitation (SP)	Overgrowths (OG)	
2					Y										2	2	1	1	2	1	2	2	1	1	2	1	2	1	2	1	1	1	1	2	2	1
3	Y								Y		Y				3	2	1	1	2	1	1	1	1	1	1	1	2	2	1	3	2	1	1	2	4	2
4			Y					Y							1	2	1	1	2	1	2	1	1	1	2	2	2	1	2	2	2	1	1	2	3	1
5	Y				Y										1	2	2	2	2	2	2	2	2	2	1	2	2	2	1	1	1	1	2	1	1	
6	Y								Y			Y			2	2	1	1	2	2	2	1	1	1	1	1	2	1	2	2	1	1	1	3	1	2
7									Y			Y			1	2	1	1	1	1	1	1	1	1	1	1	1	1	1	4	1	1	1	1	3	2
8	Y				Y			Y							1	1	1	2	2	2	1	1	2	1	1	1	1	1	1	1	1	1	3	1	2	2
9				Y						Y					1	2	2	1	2	1	2	2	1	2	1	1	1	2	2	2	2	2	1	3	2	2
10			Y								Y				1	1	1	1	2	1	2	1	1	1	1	1	1	2	1	1	3	1	1	3	1	2
11	Y						Y								1	1	1	1	2	1	2	1	1	1	1	2	1	1	1	1	1	2	3	2	2	2
12	Y								Y			Y			1	2	1	1	2	1	2	1	1	1	1	1	1	2	1	3	1	1	1	2	3	1
13	Y								Y			Y			1	2	2	1	1	1	1	1	1	2	1	1	1	1	3	2	1	2	3	3	1	1
14			Y												1	2	1	2	2	2	1	1	1	1	2	1	1	1	1	1	1	1	1	2	2	2
15	Y				Y				Y						1	2	2	2	3	1	2	1	2	1	1	1	1	3	1	2	1	1	1	2	1	2
16	Y				Y			Y							1	1	2	1	1	1	2	1	1	1	1	1	1	2	2	1	1	1	1	1	2	2

17	Y	High-Relief	Medium-Relief	Low-Relief	Angular	Sub-Angular	Sub-Rounded	Rounded	Fresh Surface	Impact Craters	Saw-tooth Fractures	Fracture Faces (Fresh Break)	Sub-parallel Linear Fractures	Conchoidal Fractures	Straight Grooves	Curved Grooves	Sharp Angular Features	Chatter Marks	Linear Steps	Arcuate Steps	Mech. Upturned Plates	Abrasion Features	Cracked Grains	Rounded Edges	Pre-weathered Surface	Chem. Weathered Surface	Adhering Particles (AP)	Silica Precipitation (SP)	Overtgrowths (OG)	
18	Y				Y				1	1	1	1	2	2	1	1	1	1	1	1	2	1	1	1	1	1	2	2	1	
19			Y		Y				1	1	2	1	1	1	2	1	1	1	2	1	1	2	2	2	1	1	1	1	3	2
20	Y					Y			1	2	1	1	1	2	1	1	1	1	1	2	2	2	1	1	2	1	1	2	2	2
21			Y				Y		1	2	1	1	1	2	1	2	1	1	1	2	2	2	1	1	3	1	1	3	2	1
22				Y		Y			1	1	1	1	2	2	1	2	2	2	1	1	1	3	1	1	2	1	1	2	1	1
23	Y						Y		1	2	1	1	1	2	2	1	1	1	1	1	1	1	1	3	1	1	1	2	2	2
24			Y		Y				3	1	1	1	2	3	1	2	2	2	1	1	2	1	1	1	1	1	1	2	1	1
25	Y					Y			1	2	2	2	1	2	2	1	2	2	1	1	2	2	1	1	2	1	1	2	2	1
26			Y					Y	1	2	1	1	1	2	2	2	1	1	2	1	1	1	1	1	4	1	1	2	2	2
27	Y				Y				1	2	2	2	1	2	2	1	3	2	2	2	2	2	2	2	1	1	2	2	2	2
28	Y					Y			1	2	2	1	1	2	2	1	1	1	1	1	1	2	2	1	2	2	1	3	2	2
29			Y			Y			1	1	1	1	1	2	2	1	1	1	1	1	1	1	2	1	2	1	1	2	4	1
30	Y				Y				1	2	1	2	1	2	2	1	2	1	1	1	2	1	2	1	1	1	1	2	2	1
31	Y		Y		Y				2	2	2	1	1	2	2	2	2	2	1	1	2	1	1	1	1	1	1	2	1	2
32	Y						Y		1	2	1	1	1	1	1	1	1	1	1	1	1	2	1	2	3	2	2	2	3	2
33	Y				Y				1	2	1	1	1	2	1	1	1	1	1	1	1	2	1	1	1	1	1	1	3	2
34	Y					Y			1	2	1	1	1	2	1	1	2	1	1	1	2	2	2	1	2	1	1	3	1	1

35	High-Relief	Medium-Relief	Low-Relief	Angular	Sub-Angular	Sub-Rounded	Rounded	Fresh Surface	Impact Craters	Saw-tooth Fractures	Fracture Faces (Fresh Break)	Sub-parallel Linear Fractures	Conchoidal Fractures	Straight Grooves	Curved Grooves	Sharp Angular Features	Chatter Marks	Linear Steps	Arcuate Steps	Mech. Upturned Plates	Abrasion Features	Cracked Grains	Rounded Edges	Pre-weathered Surface	Chem. Weathered Surface	Adhering Particles (AP)	Silica Precipitation (SP)	Overgrowths (OG)			
36		Y		Y	Y			1	1	1	1	1	2	2	1	1	1	1	1	2	1	2	1	1	1	2	1	1	2	1	
37			Y		Y			2	2	1	1	1	1	1	1	1	2	1	1	2	2	1	2	1	1	2	1	1	1	1	
38	Y				Y			1	2	1	1	1	2	2	1	1	2	2	1	2	1	1	2	1	1	2	2	2	2	2	2
39	Y				Y			1	2	2	1	1	2	1	1	1	1	1	1	1	2	1	2	1	1	1	3	2	2	2	2
40		Y			Y			1	1	2	1	1	2	1	2	1	1	1	1	1	1	1	2	1	1	2	2	2	2	2	2

Table C8. Grain Type Classification based on Damiani et al. (2006)

	U1359A- 11H-3W- 123-125	U1359B- 13H-3W- 122-124	U1359A- 12H-1W- 108-110	U1359A- 15H-1W- 33-35	U1359A- 15H-1W- 93-95	U1350A- 15H-1W- 63-65	U1359B- 13H-5W- 33-35
1	2	1	3	3	5	2	1
2	2	2	6	1	1	2	1
3	6	5	5	1	1	1	6
4	2	3	5	2	2	3	2
5	2	2	5	2	3	1	3
6	1	5	2	1	2	1	2
7	4	2	3	2	5	3	5
8	5	2	2	1	1	2	2
9	5	1	3	2	1	5	6
10	6	2	2	1	1	3	1
11	6	1	6	2	1	6	2
12	5	4	5	2	3	1	3
13	2	2	3	5	1	1	5
14	2	3	1	1	3	1	1
15	6	5	2	1	2	1	1
16	2	1	3	2	3	3	6
17	1	5	3	3	3	1	1
18	5	5	1	1	1	1	6
19	4	1	5	2	3	3	2
20	1	1	5	1	1	1	3
21	2	2	2	1	3	3	2
22	1	3	1	3	3	1	1
23	6	2	1	1	2	1	3
24	2	5	5	2	2	1	1
25	1	5	5	1	6	6	3
26	2	3	1	1	1	1	5
27	2	2	4	1	2	1	1
28	1	6	1	1	1	1	3
29	1	2	5	1	6	1	2
30	3	1	2	1	2	2	1
31	3	1	6	1	6	3	1
32	5	1	3	2	1	3	3
33	4	5	3	6	1	1	3
34	3	3	2	3	1	3	1
35	1	3	2	3	3	2	1
36	2	3	1	3	1	1	2
37	2	1	2	3	2	1	2

	U1359A- 11H-3W- 123-125	U1359B- 13H-3W- 122-124	U1359A- 12H-1W- 108-110	U1359A- 15H-1W- 33-35	U1359A- 15H-1W- 93-95	U1350A- 15H-1W- 63-65	U1359B- 13H-5W- 33-35
38	2	5	1	3	1	3	2
39	1	1	1	1	1	3	3
40	2	1	2	1	2	1	3

**This Page Intentionally Left Blank**